4-13-2017

Finite Element Analysis of a Model of a Single-Level Degenerated Cervical Spine: Influence of Simulated Surgical Treatment Methods on Kinematics

Yuxin Qi

FINITE ELEMENT ANALYSIS OF A MODEL OF A SINGLE-LEVEL DEGENERATED CERVICAL SPINE: INFLUENCE OF SIMULATED SURGICALTREATMENT METHODS ON KINEMATICS

by

Yuxin Qi

A Dissertation

Submitted in Partial Fulfillment of the

Requirements for the Degree of

Doctor of Philosophy

Major: Mechanical Engineering

The University of Memphis

May 2017

ABSTRACT

Qi, Yuxin. Ph.D. The University of Memphis. May, 2017. Finite Element Analysis of a Model of a Single-Level Degenerated Cervical Spine: Influence of Simulated Surgical Treatment Methods on Kinematics. Major Professor: Gladius Lewis, Ph.D.

The most common pathology of the cervical spine is degenerative disc disease (DDD) and the surgical methods most often used to treat symptomatic cases of this condition are anterior cervical discectomy (ACD), anterior cervical discectomy followed by fusion (ACDF), and implantation of a total disc replacement (TDR). Although there are many literature reports on finite element analysis (FEA) of models of the cervical spine subjected to simulated surgical treatment(s), few modeled the full spine (C1-C7), very few analyzed a model in which degeneration was simulated at a disc, none compared all three of these popular surgical methods, and very few focused on kinematics of the spine. Since the performance of many activities of daily living involves the motion of cervical spine units, it is useful to determine the kinematic response of these units. The purpose of the present study was to determine the influence of these three popular surgical treatment methods on the rotation of motion at each of the functional units of a single-level degenerated cervical spine (C5-C6), under a series of clinically-relevant applied loadings. Thus, five FEA models were analyzed; namely, INTACT, DEGEN, ACD, ACDF, and TDR Models. With respect to the simulated surgical treatments, the principal finding was that rotation motion at the treatment level (C5-C6) as well as at each of the other levels of the spine model is best preserved when the TDR Model was used. This suggests that TDR is an attractive surgical option, but this can only be confirmed from the results of well-planned clinical trials.

TABLE OF CONTENTS

Contents Page

LIST OF TABLES

LIST OF FIGURES

CHAPTER 1

INTRODUCTION

The main function of the cervical spine is to support the weight of the head (about 74 N) [1]. The seven cervical vertebrae are numbered C1 to C7 [2], and muscles and ligaments work together to support the spine [3, 4]. The neck has the greatest range of motion because of two specialized vertebrae, the first of which is ring-shaped and is called the atlas (C1) and the second is peg-shaped and is called the axis (C2). C2 has a projection, called the odontoid, that the atlas pivots around. This atlanto-axial joint allows for the side-to-side or "no" motion of the head. Except for C1 and C2, between each of the other pairs of vertebral bodies there is a cushioning structure called an intervertebral disc (or, simply, disc). The outer region of the disc (the annulus fibrosus) is a cross-ply composite material comprised of a matrix called ground substance reinforced with elastic fibers, while the inner region (the nucleus pulposus) is soft. There are many pathologies of the cervical spine in which the disc is involved, examples being degenerative disc disease (DDD), herniated nucleus pulposus, and spinal stenosis [5]. For a given pathology condition, treatment method depends on the extent to which performance of activities of daily living are adversely affected by the pathology and the severity and duration of the associated pain. Thus, there are conservative methods, such as physical therapy, intermittent traction, and nonsteroidal anti-inflammatory medication in cases where the condition is mild, and surgical methods in cases where the condition is serious. The most common of these conditions

is DDD, and the most popular surgical methods for treating symptomatic DDD are anterior cervical discectomy (ACD), anterior cervical discectomy followed by fusion (ACDF), and implantation of a total disc replacement (TDR) [6-10].

There are many literature reports on finite element analysis (FEA) of models of the cervical spine subjected to simulated surgical treatment methods [11-29]. However, this body of literature has a number of shortcomings, such as there are very few studies in which a model of the full spine (C1-C7) was used, in very studies has a model of a degenerated spine been analyzed, all three of these popular surgical treatment methods have not been compared in any study, and kinematics results have been reported in very few studies even though many activities of daily living involve the motion of the cervical spine. The purpose of the present study was to determine influence of these three surgical methods on the range of motion of a model of the full cervical spine, under a series of clinically-relevant applied loadings. For this purpose, the results were compared to those obtained when an intact model. DDD is frequently reported to occur in the disc at the C5-C6 level; as such, in the degenerated spine and simulated surgical treatment models, characteristics of the C5-C6 were changed to reflect this clinical reality.

The thesis is organized into six chapters. Key aspects of all the background on the spine that is relevant to the study are presented in Chapter 2. These topics are anatomy and functions of the spine, anatomy of the cervical spine, pathological conditions that affect the cervical spine, and surgical methods for treating these conditions. A review of the literature on the application of the FEA method to models of the cervical spine subjected to simulated surgical treatment methods is

presented in Chapter 3. Details of the FEA of the five models used in the work are given in Chapter 4. These models are of the normal intact spine (INTACT Model), the spine in which it was considered that the patient has suffered a moderate degree of degeneration of the disc at one level (C5-C6) (DEGEN Model), the spine in which the surgical treatment method simulated is ACD (ACD Model), the spine in which the surgical treatment method simulated is ACDF (ACDF Model), and the spine in which the surgical treatment method simulated is implantation of a notional TDR design (TDR Model). For each model, the constraints and applied loadings were the same. The applied loadings, which are clinically relevant [18], are 1) 1 Nm sagittal plane (flexion) moment + 73.6 N axial compressive pre-load; 2) 1Nm sagittal plane (extension) moment +73.6 N axial compressive pre-load; 3) 1 Nm left lateral bending moment + 73.6 N axial compressive pre-load; 4) 1 Nm right lateral bending moment + 73.6 N axial compressive pre-load; 5) 1 Nm clockwise-acting axial torsional moment + 73.6 N axial compressive pre-load; and 6) 1 Nm counter-clockwise-acting axial torsional moment + 73.6 N axial compressive pre-load. For each of the models, the results under each of applied loadings, was the range of motion at each of the functional spinal units (for example, at C1-C2, C4-C5, and C6-C7). In the first part of Chapter 5, all of the results are presented and trends are described in terms of percentage change relative to the corresponding value obtained using INTACT Model. In the second part, these percentage results are discussed and comparisons are made between the present FEA results and those reported in relevant literature reports. Chapter 6 contains a statement of the study conclusions and recommendations for future study.

CHAPTER 2

THE SPINE AND THE CERVICAL SPINE

2.1. Anatomy and physiology of the spine

The spine is a curved column consisting of thirty-three vertebrae, with the upper twenty-four articulating and, as such, are separated from each other by an intervertebral disc (or, simply, disc), and the lower nine are fused, five in the sacrum and four in the coccyx or tailbone (Figure 2.1). The sacrum joins the upper end of the body to its lower end, via the pelvis. In modern mankind, the coccyx does not have a useful function. In a newborn baby, the spine is straight, and it is not until he/she begins to hold the weight of the head independently does the spine transform into a curved member. The articulating vertebrae are named according to their level in the spine; thus, there are seven cervical vertebrae, twelve thoracic vertebrae and five lumbar vertebrae. The vertebrae of the cervical, thoracic, and lumbar spines are independent bones, and, so, are different in configuration and size.

The spine surrounds the spinal cord, which travels within the spinal canal, formed from a central hole within each vertebra. The spinal cord is part of the central nervous system that supplies nerves and receives information from the peripheral nervous system within the body. The spinal cord consists of grey and white matter and a central cavity, called the central canal. Adjacent to each vertebra emerge spinal nerves, which provide sympathetic nervous supply to

the body. The spinal canal follows the different curves of the spine: large and triangular in those parts of the spine which experience the greatest freedom of movement (that is, the cervical and lumbar regions) and small and rounded in the thoracic region, where motion is more limited.

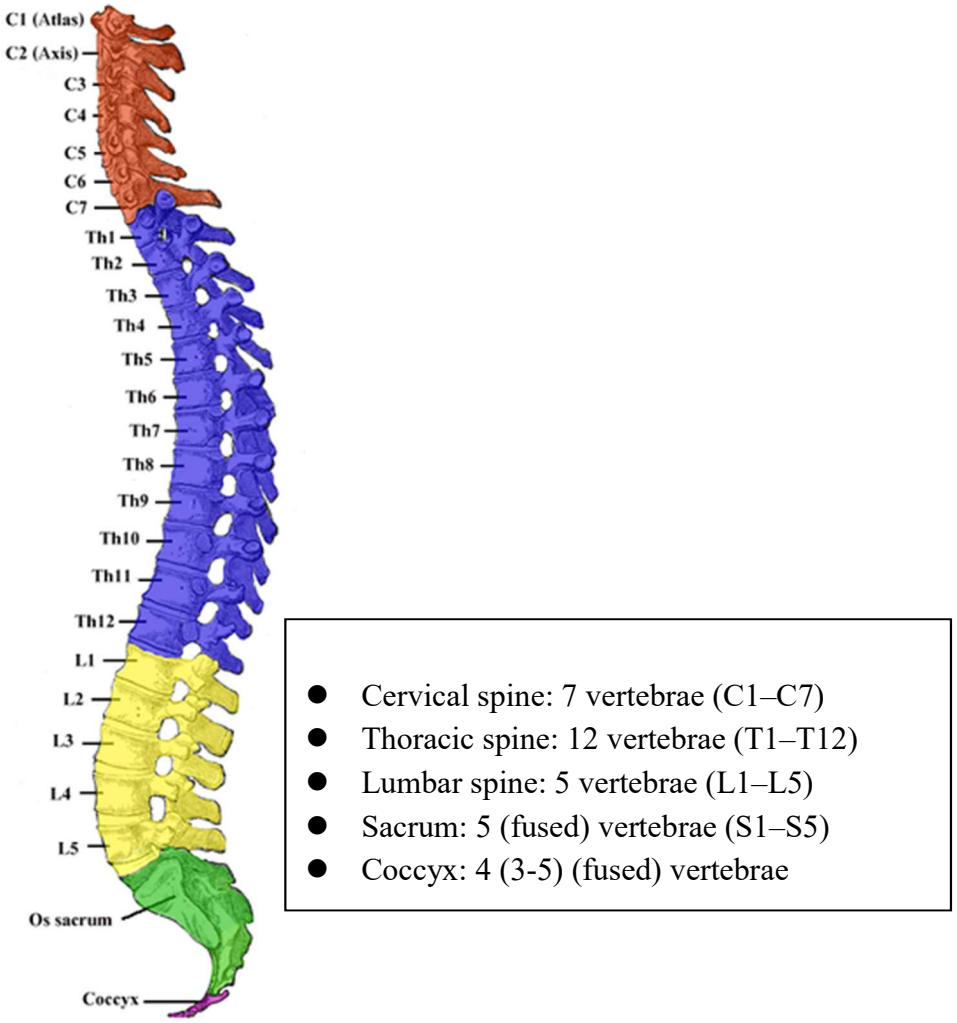

Figure 2.1. Schematic drawing of the spine [2].

2.2. Function of the spine

The spine has many functions that allow a person to be able to perform a wide variety of activities of daily living.

2.2.1. Strength and support

The spine provides strength and support for the remainder of the body, with particular attention to the heavy bones of the skull. The thoracic region of the spine is responsible for the task of offering strength and stability to the body. The lumbar region carries most of the body's weight and allows flexion but not rotation.

The spine provides the body the ability to distribute its weight, and adapts to changes in the body, such as weight gain or pregnancy. During times of carrying extra weight, the curves of the spine become more marked in order to for the body to find its center of gravity and maintain it. The array of muscles, ligaments, and tendons assists the spine in providing this flexibility.

2.2.2. Movement

The intricate design of the spine and its accompanying structures of muscles, tendons, ligaments permit the body to move in many different ways, such as bending, stretching, rotating,

and leaning. The cervical spine is responsible for allowing movement and rotation of the head and neck, due to the presence of the first two cervical vertebrae, called the atlas and the axis.

2.2.3. Protection of nerves and spinal cord

The spine provides reliable protection of the delicate nerves and the spinal cord, without which a human could not function, as certain nerve impulses control the functions of the major internal organs, such as the kidney and the bladder. The design and placement of the vertebrae and certain ligaments form a network of protection that keeps the spinal cord from getting injured.

2.2.4. Blood supply

The vertebrae provide plenty of bone to produce red blood cells and minerals from within the hollow interior chamber of the bone, known as bone marrow. There are two types of bone marrow; namely, red and yellow. Red bone marrow is responsible for the production of red blood cells, platelets, and white blood cells, while yellow bone marrow contains high levels of fat cells and also produces some amounts of white blood cells.

2.2.5. Protection of major internal organs

The skeleton allows a base for the ribs to attach, which surround and protect the major internal organs. The rib cage is the combination of the sternum (breast bone), 12 pairs of ribs, and the 12 thoracic vertebrae. The ribs attach to the spine, but only the upper 7 pairs attach to the sternum. The ribs form the cage of protection around the heart and lungs.

2.2.6. Absorption of impact

Except for the top two vertebrae in the cervical spine called the atlas and the axis, each of the pairs of the articulating vertebrae is separated by an intervertebral disc (or, simply, disc). In the central part of the disc, called the nucleus fibrosus, is a substance that absorbs forceful motions, thus preventing the impact from being transferred to the next vertebra, it is much like a shock absorber in an automobile function.

2.3. Anatomy of the cervical spine

2.3.1. Cervical spine vertebra

A typical vertebra consists of two parts: the vertebral body and the vertebral arch (Figure 2.2). The vertebral arch is posterior (meaning it faces the back of a person), is formed by a pair of pedicles and a pair of laminae, and supports seven processes (four articular, two transverse, and one spinous). The transverse processes and the spinous process are posterior to (behind) the vertebral body. The spinous process comes out the back and, thus, can be felt through the skin. One transverse process comes out the left, and the other the right.

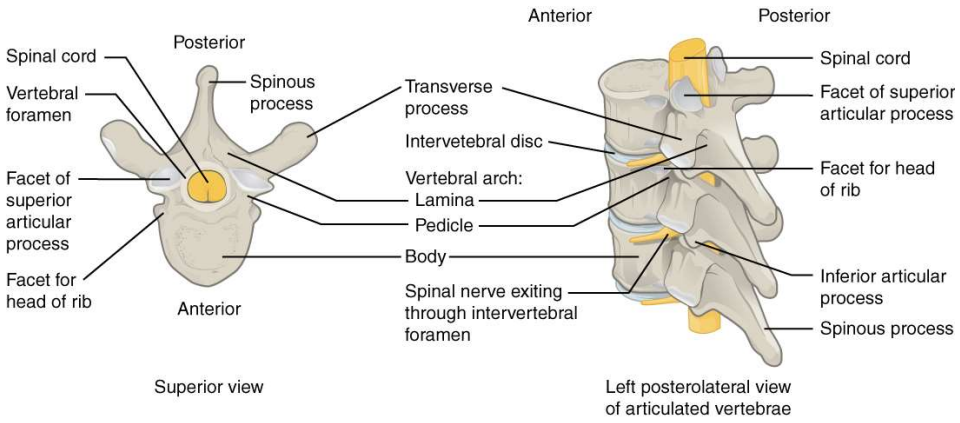

Figure 2.2. Anatomy of a cervical vertebra [2].

2.3.2. Cervical spine ligaments

Ligaments are fibrous bands or sheets of connective tissue linking two or more bones, cartilages, or structures together. One or more ligaments provide stability to a joint during rest and movement. Excessive movements, such as hyper–extension or hyper–flexion, may be restricted by the ligaments. Furthermore, some ligaments prevent movement in certain directions. Three of the more important ligaments in the cervical spine are the ligamentous flavum (LF), the anterior longitudinal ligament (ALL), and the posterior longitudinal ligament (PLL). [3] LF forms a cover over the dura mater: a layer of tissue that protects the spinal cord. This ligament connects under the facet joints to create a small curtain over the posterior openings between the vertebrae. ALL attaches to the front (anterior) of each vertebra and runs up and down the spine (vertical or longitudinal). PLL runs up and down behind (posterior) the spine and inside the spinal canal. (Figure 2.3)

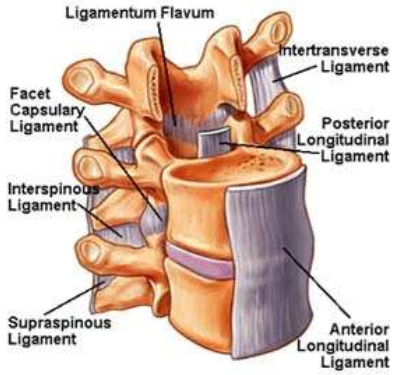

Figure 2.3. Ligaments in the cervical spine [3].

2.3.3. Cervical spine discs

In the cervical spine, each disc is made up of a tough outer zone (annulus fibrosus (AF) and a soft, jelly-like inner zone (nucleus pulposus (NP)). AF, which consists of a matrix in which collagen fibers are embedded, distributes pressure and force on the cervical spine. NP is a loose, fibrous network suspended in micro-protein gel that is sealed by AF and needs to be well-hydrated in order to maintain its strength and softness. As a person ages, the cervical discs lose water, stiffen, and become less flexible in adjusting to compression. Such degenerative changes may result in NP extruding through the outer core and coming in contact with the spinal nerve root, a condition known as a herniated cervical disc (Figure 2.4). In other instances, a cervical disc may degenerate as a result of direct trauma or gradual changes. With no blood supply and very few nerve endings, a cervical disc cannot repair itself.

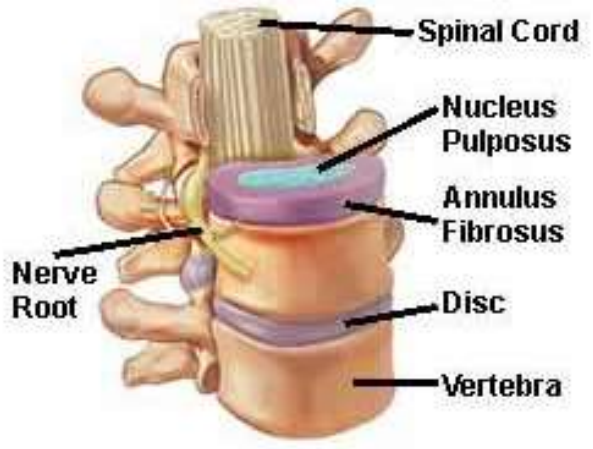

Figure 2.4. Human cervical spine discs [5].

2.3.4. Cervical spine muscles

Muscles are named according to their shape, location, or a combination. They are further categorized according to function such as flexion, extension, or rotation. Muscles and ligaments work together to support the spine, hold it upright, and control movement during rest and activity. The muscles in the cervical spine and the upper thoracic spine, together with their functions (Figure 2.5).

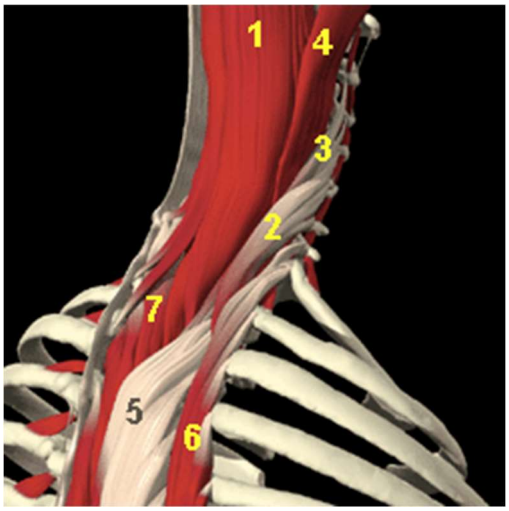

Figure 2.5. Muscles of the posterior cervical spine and upper thoracic spine [4].

1: Semispinalis capitus (involved in head rotation/pulls backward)

2: Iliocostalis cervicis (extends cervical vertebrae)

3: Longissimus Cervicus (extends cervical vertebrae)

4: Longissimus capitus (involved in head rotation/pulls backward)

5: Longissimus thoracis (involved in extension/lateral flexion of the spine, rib rotation)

6: Iliocostalis thoracis (involved in extension/lateral flexion of the spine, rib rotation)

7: Semispinalis thoracis (extends/rotates vertebral column).

2.4. Normal kinematics of the cervical spine

The cervical spine may be considered to comprise four units, each with a unique morphology that determines its kinematics and its contribution to the functions of the whole cervical spine. In anatomical terms, the units are the atlas (C1), the axis (C2), the C2-C3 junction, and the remaining vertebrae (that is, C3-C7). In functional terms, these units can be referred to as the cradle, the axis, the root, and the column. There are many literature reports of the range of motion at various levels in the cervical spine (Tables 2.1-2.3).

Table 2.1. Mean values and ranges of axial rotation of cervical motion segments as determined by CT scanning [30]

Segment	Range of motion (deg)	
	Mean	Range
Occ–C1	1.0	−2–5
C1–C2	40.5	29–46
C2–C3	3.0	0–10
C3–C4	6.5	3–10
C4–C5	6.8	1–12
C5–C6	6.9	2–12
C6–C7	2.1	2–10
C7–T1	2.1	−2–7

Table 2.2. Normal ranges of motion of cervical spine in axial rotation, and ranges of coupled motions, as determined by bi-planar radiography [31]

Segment	Coupled movement		
	Axial rotation mean degrees (SD)	Flexion/ extension mean degrees (SD)	Lateral flexion mean degrees (SD)
Occ–C2	75 (12)	−14 (6)	−2 (6)
C2–3	7 (6)	0 (3)	−2 (8)
C3–4	6 (5)	−3 (5)	6 (7)
C4–5	4 (6)	−2 (4)	6 (7)
C5–6	5 (4)	2 (3)	4 (8)
C6–7	6 (3)	3 (3)	3 (7)

SD: standard deviation.

Table 2.3. Results of studies of cervical flexion and extension (mean and standard deviation given in parentheses).

Source	Number	ROM				
		C2-C3	C3-C4	C4-C5	C5-C6	C6-C7
Aho et al. [32]	15	12(5)	15(7)	22(4)	28(4)	15(4)
Bhalla and Simmons [33]	20	9(1)	15(2)	23(1)	19(1)	18(3)
Lind et al. [34]	70	10(4)	14(6)	16(6)	15(8)	11(7)
Dvorak et al. [35]	28	10(3)	15(3)	19(4)	20(4)	19(4)

2.5. Minor injuries of the cervical spine

Minor injuries of the cervical spine are defined as injuries that do not involve a fracture. The most common minor injury is the whiplash injury [36]. There is lack of agreement that an injury to the neck can occur in a whiplash accident [36]. In pursuit of the injury mechanism, mathematical modeling, cadaver studies, and human volunteer studies have been used to

determine the kinematics of the neck under the conditions of whiplash [36]. Particularly illuminating have been cinephotographic and cineradiography studies of cadavers and of normal volunteers [50, 37]. It was shown that during whiplash, the motions of the head and the neck do not exceed normal physiological limits, but the cervical spine undergoes a sigmoid deformation very early after impact. During this deformation, lower cervical segments undergo posterior rotation around an abnormally high axis of rotation, resulting in abnormal separation of the anterior elements of the cervical spine, and impaction of the zygapophysial joints. The demonstration of a mechanism for injury of the zygapophysial joints complements results of postmortem studies that reveal lesions in these joints, and results of clinical studies that have demonstrated that zygapophysial joint pain is the single most common basis for chronic neck pain after injury [38].

2.6. Pathologies of the cervical spine

Common pathologies are degenerative disc disease (DDD), herniated nucleus pulposus (HNP) (Figure 2.6), symptomatic cervical disc disease (SCDD), internal disc disruption (IDD), and cervical radiculopathy (CRP).

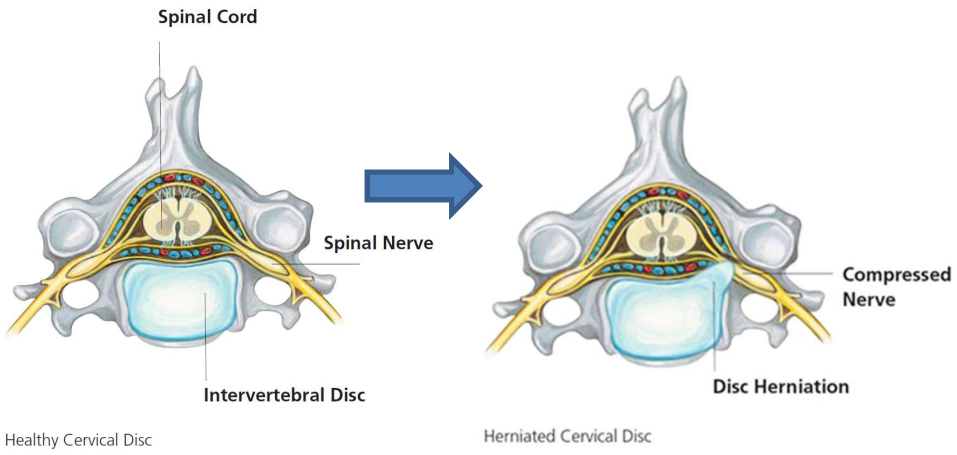

Figure 2.6. Disc herniation compress spinal nerve [7].

DDD involves a combination of reduction of disc height, development of tears in the AF, and degradation of the NP. HNP is localized displacement of the NP, cartilage, fragmented apophyseal bone, or fragmented annular tissue beyond the disc space (Figure 2.6). SCDD occurs when the normal functions of a disc are lost due to, for example, wear or injury, causing the vertebral body to compress or lose height, and to press on the nerves or the spinal cord. IDD is annular fissuring of the disc without external disc deformation. CRP results from nerve root injury in the presence of disc herniation or stenosis, leading to sensory, motor, or reflex abnormalities in the affected nerve root distribution.

In a serious case of any of the above-mentioned conditions, spine nerve compression occurs, with common symptoms being tingling pain or weakness in the neck, shoulder, elbow and/or hand, dizziness, severe headache, and insomnia. There are two common causes of cervical nerve compression. The first is placing the neck in a position that causes a significant change in the

normal curvature of the cervical spine. Activities that may cause this are sleeping on a pillow that is too high, reclining on a sofa, reading and/or watching television in bed, using the crock of the neck to rest a telephone while speaking on it, and diving. The second reason is poor posture.

2.7. Surgical treatment methods for symptomatic cervical spine pathologies

2.7.1. Overview

In cases where the pain arising from a pathological condition is persistent, severe, and unresponsive to conservative treatments, such as medication and physical therapy, it is common to employ a surgical method. The three most popular methods are anterior cervical discectomy without fusion (ACD) [6], anterior cervical discectomy followed by fusion (ACDF), [10] and implantation of total disc replacement (TDR) [7]. Use of a standalone U-shaped dynamic stabilization system is an emerging method [53].

2.7.2. Anterior cervical discectomy without fusion

The goal of ACD is to relieve pressure on the nerve roots or on the spinal cord by removing the ruptured disc. It is called anterior because the cervical spine is reached through a small incision in the front of the neck. During the surgery, the soft tissues of the neck are separated, the

anterior longitudinal ligament is cut, the disc is removed, and, then, the endplates are removed from the cartilage to induce fusion (Figure 2.7).

Figure 2.7. Schematic drawing of the ACD procedure [54].

2.7.3. Anterior cervical discectomy followed by fusion

The surgery involves all the steps used in ACD, except that the space left behind when the disc is removed is filled with either a graft or a cage (with or without supplementary member (s) such as plates and screws) (Figure 2.8). The graft could be bone taken from the patient's pelvis (iliac crest) (auto graft) or is a synthetic product (made, for example, from hydroxyapatite, calcium phosphate, or calcium sulfate). If the cage has a hole in it, the hole is filled with either an auto-graft or a synthetic product.

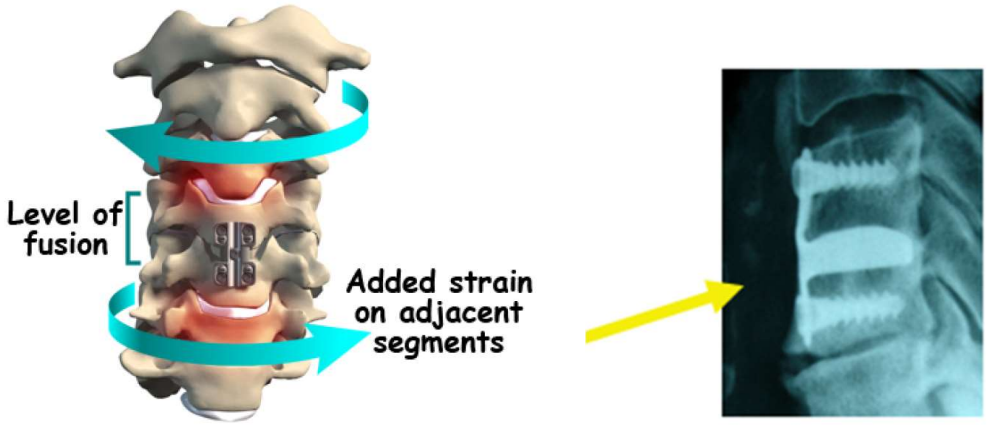

Figure 2.8. Anterior cervical discectomy and fusion [9].

2.7.4. Total disc replacement

A TDR aims to preserve the normal motion at the implanted level, and, as such, a common design is a synthetic ball-and-socket joint that comprises top and bottom endplates (usually, fabricated from cobalt-chromium-molybdenum alloy) on which a metal porous coating is deposited (to improve fixation between the endplates and the vertebral bodies between which the disc is surgically removed) and a hemispherical inlay between these parts (usually, fabricated from ultra-high-molecular-weight polyethylene) (Figure 2.9). It is to be noted, however, that geometrical, material, and other details of a TDR depend on its design.

Figure 2.9. Parts of a typical total disc replacements [7].

There are a multitude of TDR designs (Figure 2.10), although, as per December 2015, only six are approved for clinical use in the United States. These are the Bryan (Medtronic, Inc., Memphis, TN, USA)), Mobi-C (LDR Spine USA, Austin, TX, USA), PCM® (NuVasive, San Diego, CA, USA), Prestige LP (Medtronic, Inc.), ProDisc-C (Synthes, Inc., Philadelphia, PA, USA), Secure ®-C (Globus, Audobon, PA, USA) design (Figure 2.10). In each of these designs, there are porous-coated

Figure 2.10. Schematic drawings of a collection of TDR designs: (A) Prodisc-C®; (B) Prestige® LP; (C) Mobi-C; (D) Discover® (DePuy, Warsaw, IN, USA); (E) M6® (Spinal Kinetics, Union, NJ, USA); (F) ActivC® (Aesculap, Center Valley, PA, USA); (G) Discovery® (Scient'X, Carlsbad, CA, USA); (H) Bryan® [39].

Co-Mo-Cr alloy endplates and a UHMWPR inlay. One important difference between these designs is that the Bryan, unlike the ProDisc-C® and the Prestige® LP, relies on a tight fit between its designed geometry and the concavity of the vertebral bodies rather than on an explicit fixation mechanism (Figure 2.11).

A

B

C

Figure 2.11. Geometrical representations of the Bryan® (A), Prestige® LP (B), and ProDisc-C® (C) TDR designs [40].

During the surgery, the herniated disc, usually, at C4-C5 or C5-C6 [18], and the associated endplates on the vertebra above and below the disc are removed after the ligaments have been cut and, then, the TDR is implanted (Figure 2.12).

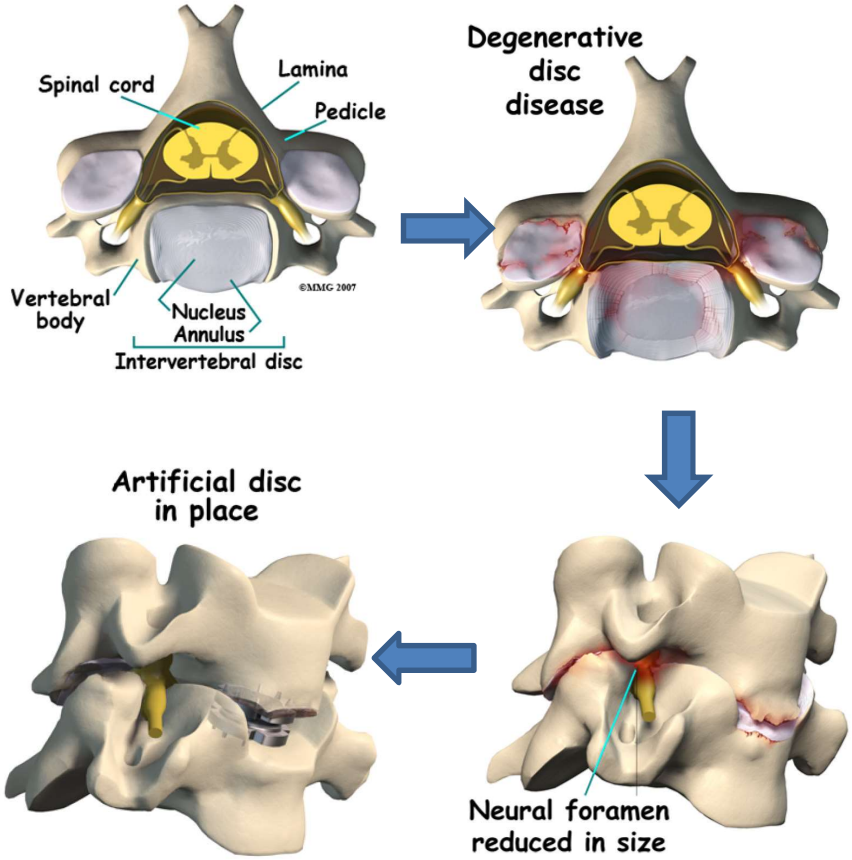

Figure 2.12. Degenerative disc disease and treatment with a total disc replacement [9].

2.7.5. Dynamic cervical implant

To prevent adjacent-level overloading induced by rigid fusion, a dynamic cervical implant is sometimes used [41, 42]. In a prospective study, satisfactory clinical outcomes were obtained when a U-shaped dynamic cervical implant was used, with improvement in neck and arm pain in a majority of patients [53]. However, biomechanical studies of this type of are lacking.

CHAPTER 3

LITERATURE REVIEW

3.1. Summaries of literature reports

Wheedon et al. [11] used a C4-C7 model and validated it against experimental data for normal cervical spines tested in flexion and extension, right and left lateral bending, and right and left axial rotation at loads of 0.33, 0.50, 1.00, 1.50, and 2.00 Nm (Figure 3.1). It was found that, in flexion, finite element (FEA) model results were within one standard deviation of the experimental results for C4–C5 and C5–C6 and, at high loading for C6–C7, the FEA model results were less than the experimental results (Figure 3.2). In lateral bending, the FEA model results were within one standard deviation of the experimental results. In axial rotation, the FEA model results for C4-C5 and C5-C6 were outside the experimental results corridors but, for C5–C6, right and left axial rotation FEA model and experimental results were close.

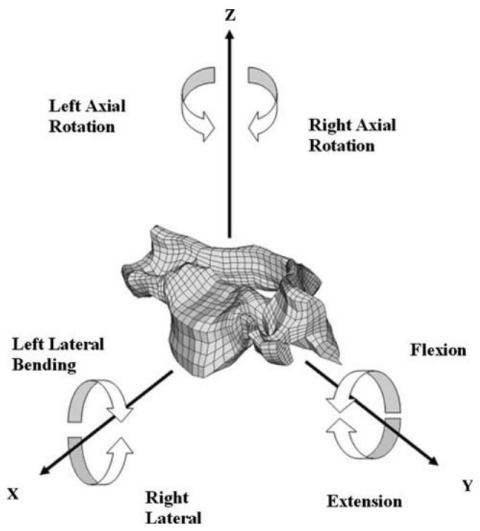

Figure 3.1. Moment directions [11].

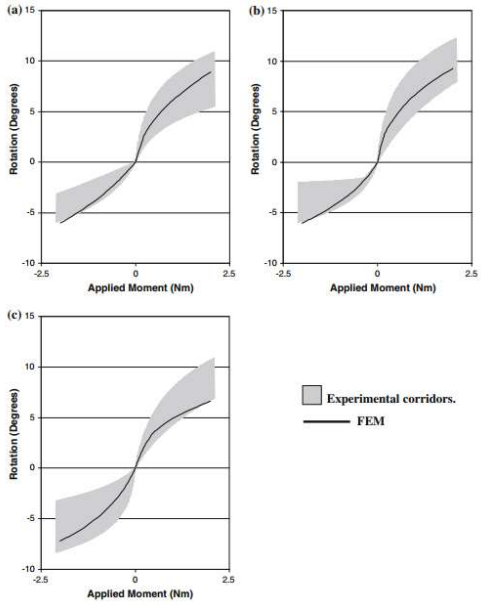

Figure 3.2. Rotation moment curves for experiments and finite element models. [11] extension/flexion. (a) C4–5, (b) C5–6, and (c) C6–7 [11].

Beltrán-Fernández et al. [12] modeled the effects due to load conditions on a C3-C5 model after an implant was used to transfer compression loads from C3 to C5 as C4 was considered to

be damaged as a result of a medical condition (Figure 3.3). For this study, three different scenarios that model common motion conditions of the head-neck system are modeled: weight head over the FEA model (Case 1), average patient weight over the FEA model (Case 2), and compression load failure of a cervical vertebra over the FEA model (Case 3) (Figure 3.4). The results for Case 1 represented the behavior of the implant when the patient was recovering from the surgery, where the movement of the head-neck system is limited by the use of a neck support.

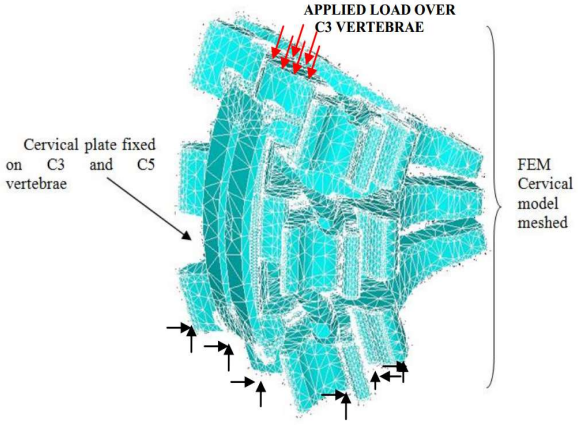

Figure 3.3. Boundary and loading conditions of the finite element model [12].

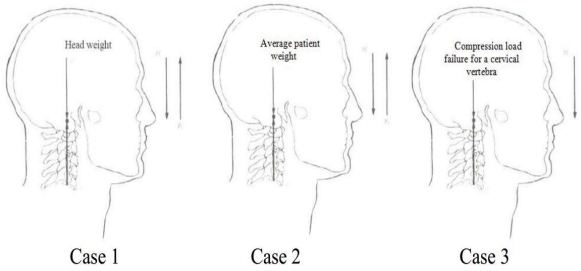

Figure 3.4. Compression loading for the three study cases [12].

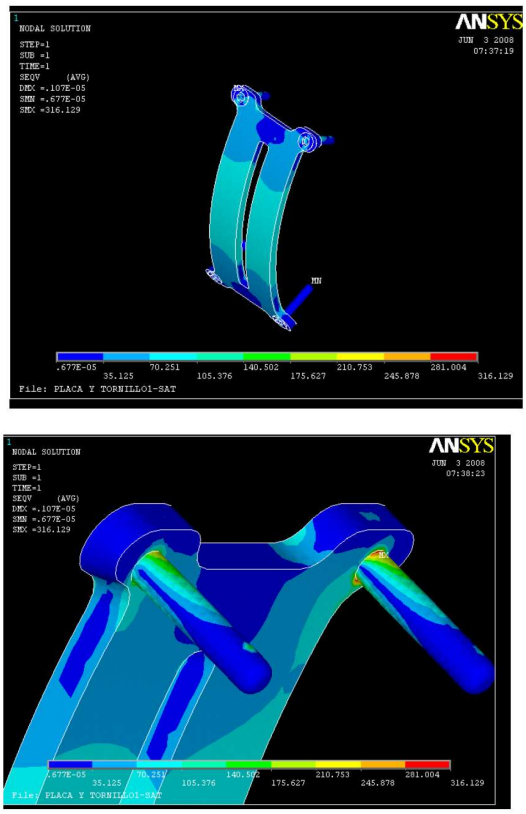

Figure 3.5. Von Mises stress distribution results for Case 1 (top) and Case 2 (bottom) [12].

The results for Case 2 can be related with the daily activities of a patient who has resumed his normal daily activities. Case 3 evaluates the stress conditions under which the head-neck system experiences a sudden movement of the head, as in a fall or an automobile accident. The von Mises stress showed that the elements work on the elastic range of the material (Figure 3.5).

Punzer and Cronin [13] developed a C4–C5 model and validated it against a wide variety of experimental data (axial rotation, flexion, extension, lateral bending, and translation loadings of different magnitudes) (Figure 3.6). For each of the modes of loading considered, except extension and higher levels of flexion, the disc was the primary load-bearing structure in the segment. At higher levels of flexion, the ligaments carried most of the load (Figure 3.7).

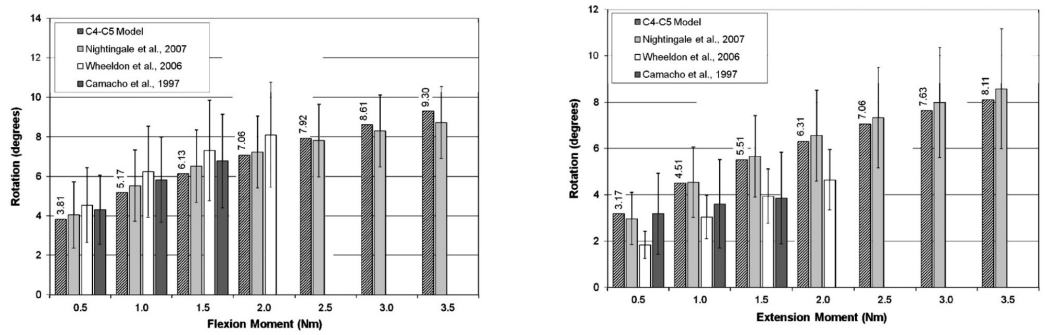

Figure 3.6. C4–C5 model response to flexion/extension loading compared with experimental data (error bars indicate standard deviation) [13].

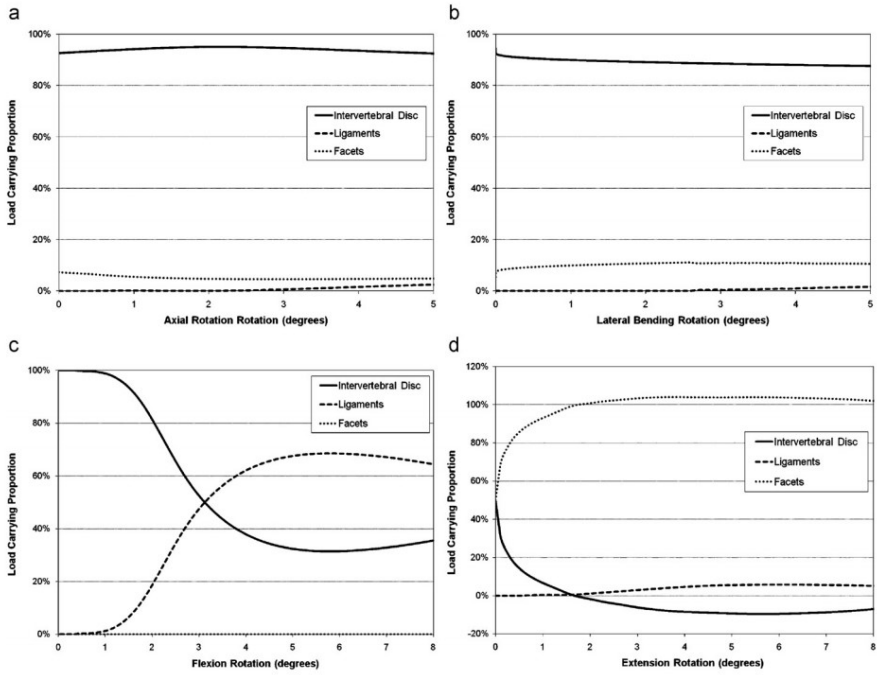

Figure 3.7. Distribution of load attributed to the intervertebral disc, ligaments, and facets for (a) axial rotation, (b) lateral bending, (c) flexion, and (d) extension [13].

Laville et al. [14] built sixteen finite (FE) models of the lower cervical spine (C3-C7) from cadaver specimens using low-dose bi-planar x-rays (Figure 3.8) and performed a preliminary evaluation using the C5–C6 functional unit and a database of results from previous experimental

tests. The responses show the influence of the geometry (Figure 3.9). It has to be noted that the mechanical properties were not changed from one model to another. As such, the observed variations in motion are caused only by geometrical changes. The simulated axial rotation and lateral bending present wide variations in terms of ranges of motion. For these motions, it can be supposed that geometry variability explains a major part of the motion variability.

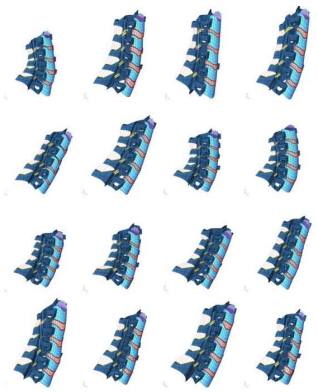

Figure 3.8. Sixteen finite element models of the lower cervical spine (C3-C7) [14].

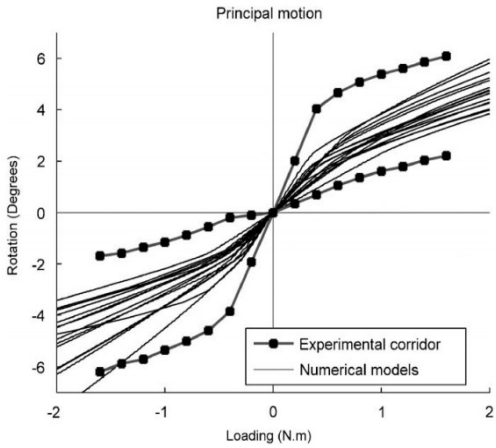

Figure 3.9. Extension/flexion curves for the simulations of the 16 C5-C7 FE models compared to experimental results (principal motion) [14].

Hussain et al. [15] constructed an FE model of an intact C3–T1 segment and, from it, a fusion model (two-level [C5, C6] anterior corpectomy) was developed and validated (Figure 3.10). After corpectomy, allograft inter-body fusion with a rigid anterior screw-plate construct was created from C4 to C7. Five additional FE models were developed from the fusion model corresponding to five different combinations of screw angulations within the vertebral bodies (C4, C7): (0°, 0°), (5°, 5°), (10°, 10°), (15°, 15°), and (15°, 0°). The last-mentioned model was designated a "hybrid fusion model". The results (Figure. 3.11 and 3.12) showed that 1) the rotational construct stability is independent of screw angulations; 2) the stresses in the bone graft, endplates, and bone near the screws is dependent on screw position with respect to the endplate; 3) with increasing screw angulations [(0°, 0°), (5°, 5°), (10°, 10°), (15°, 15°)], the construct became more of a load-sharing device than a load-bearing one; and 4) there were higher stresses at more divergent angles, particularly at the lower level of the construct. In the hybrid fusion model, there were low stresses on the bone graft, endplates, and bone-screw interface, suggesting that there was potential for failure of the construct (such as endplate fractures and screw pullout) at the inferior end.

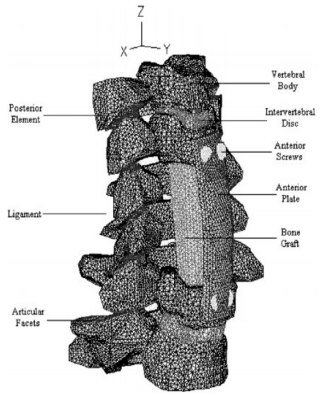

Figure 3.10. A finite element (FE) model of cervical spine with C5 and C6 anterior corpectomy reconstruction using a bone graft and a rigid screw-plate [15].

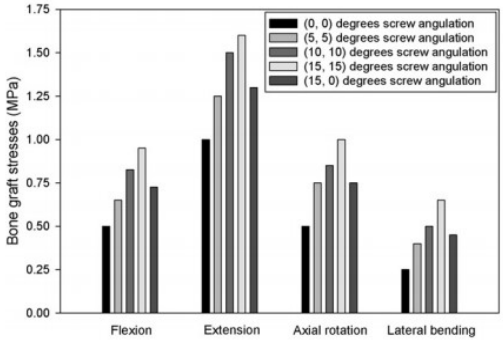

Figure 3.11. Variation of bone graft stresses with the angular position of screws [15].

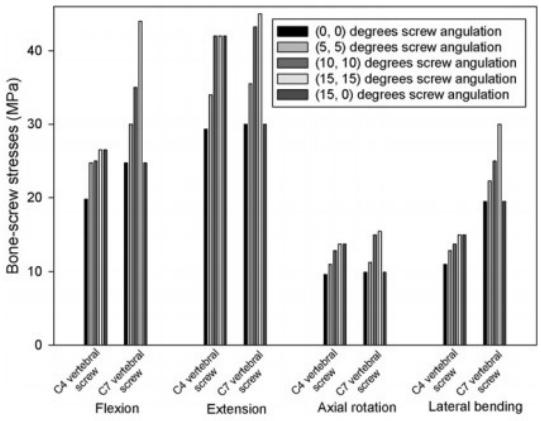

Figure 3.12. Variation of bone-screw stresses in the C4 and C7 vertebral bodies with the angular position of screws. [15].

Faizan et al. [16] used an experimentally-validated FE model of the C3-C7 spine to examine the influence of clinically relevant parameters on various responses of different variants of ball-and-socket TDR designs. The designs were: spherical-shaped with inferior and superior ball components ((a) in Figure 3.13 and SPH-I and SPH-S in Figure 3.14) and oval-shaped with inferior and superior ball components ((b) in Figure 3.13 and OVL-I and OVL-S in Figure 3.14). In each case, the TDR was placed at C5–C6 (Figure 3.13).

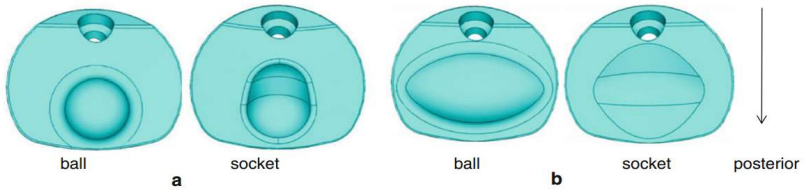

Figure 3.13. The spherical disc design components (a) and oval disc design components (b) [16].

It was found that 1) for the SPH-I and OVL-I designs, the facet loads were close to the level for the intact model (Figure 3.14), while, for OVL-I and OVL-S designs, the implant stresses were lower than the value for the intact case (Figure 3.15); 2) in all models, the implant stresses were than the yield and fatigue strengths of the material; and 3) for the OVL-1 design, capsule ligament strains were close to those for the intact model (Figure 3.15). Although the motions were similar for all four designs; the facet loading, implant stress, and ligament strain data suggest that OVL-I design may be the best. This finding may be because of the shape, larger radius, and assembly configuration of this design.

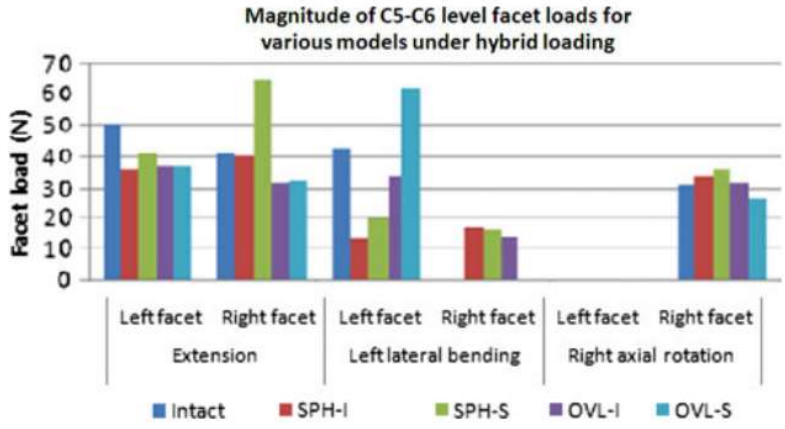

Figure 3.14. Magnitudes of FE predicted facet loads (N) in the various models [16].

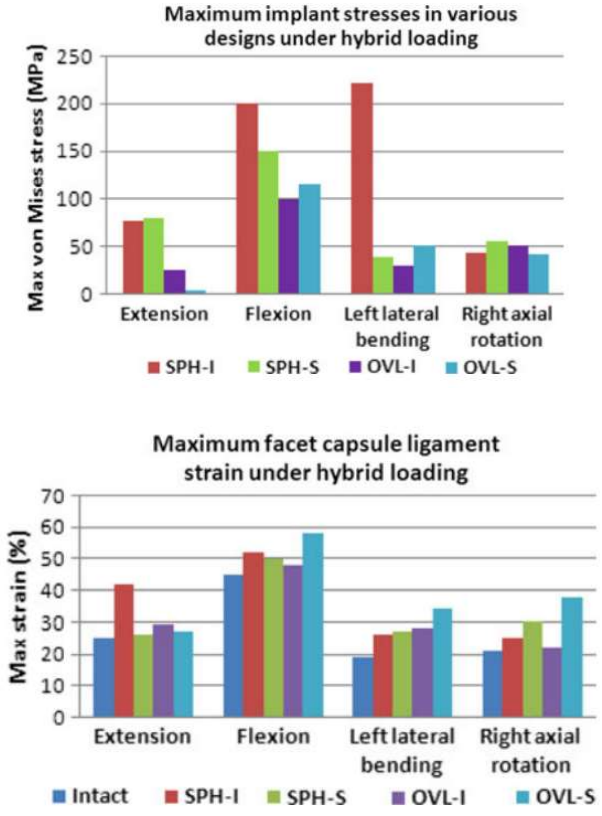

Figure 3.15. Maximum implant stresses & facet capsule ligament strains under hybrid loading [16].

Galbusera et al. [17] built an FE model of the C5–C6 spine that included an implanted ball-and-socket TDR and applied pure moments of 1.6 Nm in flexion, extension, lateral bending, and axial rotation to the upper endplate of C5. 100 simulations were conducted for the each of the loading conditions. It was found that 1) for each of the loading conditions, axial position of the center of rotation produced a significant effect on the facet force only in extension, lateral bending, and axial rotation; 2) the antero-posterior position of the center of rotation influenced the spine flexibility in flexion and extension and the facet force when lateral bending and axial rotation were applied; and 3) the lateral position of the center of rotation was not significant under any of the loading scenarios.

Li and Lewis [18] constructed a model of the full cervical spine (C1–C7) and used it to perform a FEA study of the influence of three simulated surgical methods for treating DDD at the C5-C6 level on biomechanical parameters of the model. The surgical methods simulated were ACDF, with fusion achieved using a synthetic bone graft; ACD; percutaneous nucleotomy (PN); and three variants of nucleus replacement (NR). The loading used was a combination of 1 Nm sagittal plane (extension) moment+ 73.6 N axial compression pre-load. The biomechanical parameters determined included displacement of the model, range of motion, maximum von Mises stress, and strain energy density *SED) in each of the tissues/materials, and maximum strain energy density in each of the tissues/materials. Among other things, it was found that there were markedly fewer changes (relative to the results when the intact, healthy spine model was used) e in each of the biomechanical parameters obtained above a threshold in the case of the

simulated PN and the simulated NP models, on one hand, compared to the simulated ACDF and simulated ACD models, on the other (Figure 3.16 and Figure 3.17).

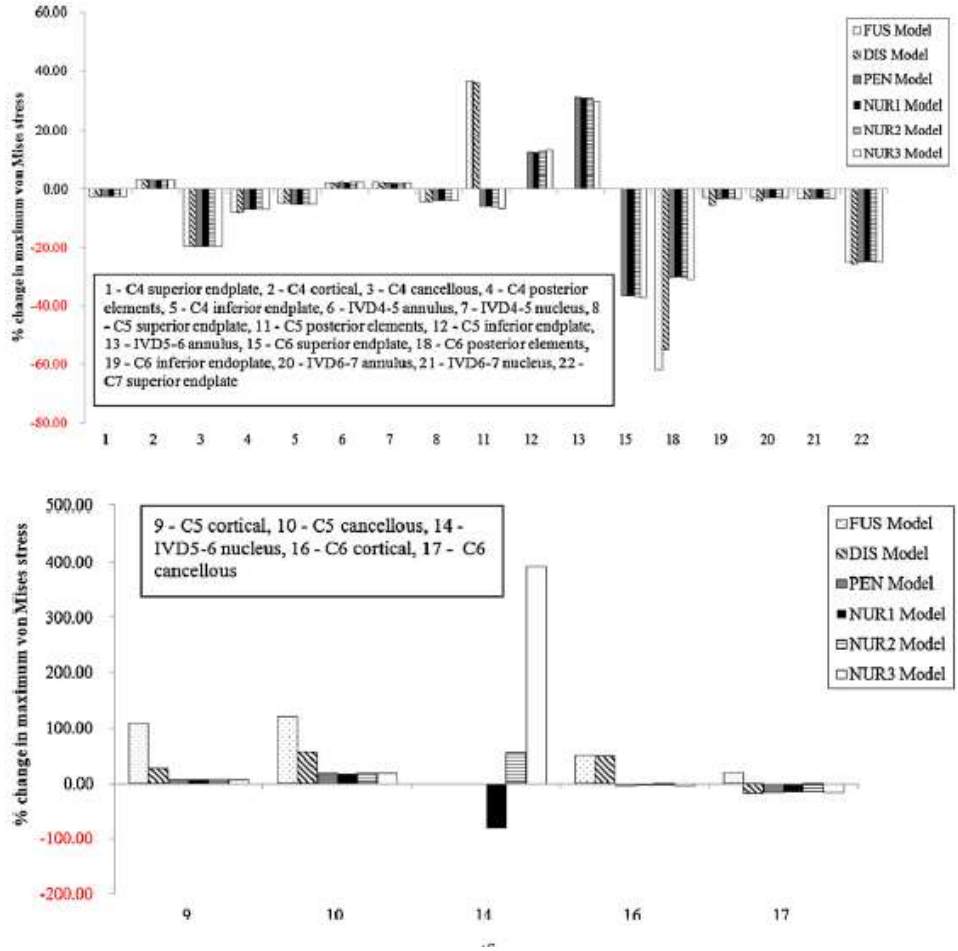

Figure 3.16. Summary of the percentage change in the maximum von Mises stress in a specified tissue in a specified simulated surgical treatment model [18].

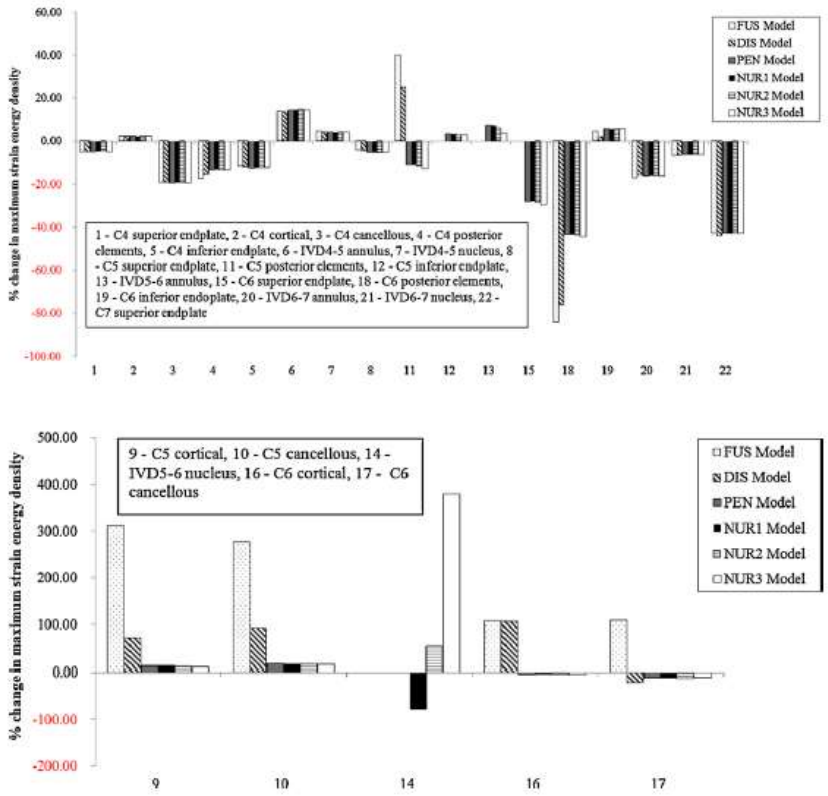

Figure 3.17. Summary of the percentage change in the maximum strain energy density in a specified tissue in a specified simulated surgical treatment model [18].

Kang et al. [19] built a model of the C5–6 spine unit based on computer tomography (CT) images acquired from a candidate patient for TDR. Models of the facet and uncovertebral joints were added and a TDR was placed in the disc space. Three different TDR designs were modeled: Bryan, Prestige LP, and ProDisc-C (Figure 3.18). Flexion, extension, and lateral bending were applied and the von Mises stress and SED was obtained. The results (Figure 3.19)showed that the Bryan design disc imposed the greatest mean von Mises stress and and SED at the facet and uncovertebral joints with flexion-extension and lateral bending, while the ProDisc-C and Prestige LP discs lower loads due to their rigid cores.

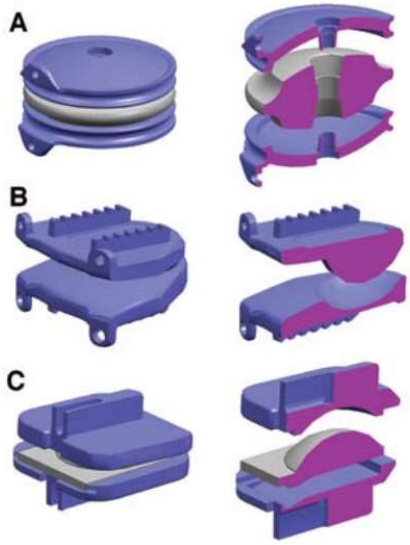

Figure 3.18. Geometrical representations of Bryan (A), Prestige LP (B), and ProDisc-C (C) artificial cervical discs [19].

However, under each of the designs, loads were increased at the joints in lateral bending, which may be attributed to direct impinging contact force. It is worth noting that with unconstrained/semi-constrained TDRs that have different core rigidities, the shared loads at the joints differ, and greater flexibility may result in greater joint loads. With Bryan, load sharing was highest and was closest to the normal in a normal disc, but the Prestige LP and ProDisc-C carried more load through their rigid core, resulting in decreased load transmission to the facet and uncovertebral joints (Figure 3.19).

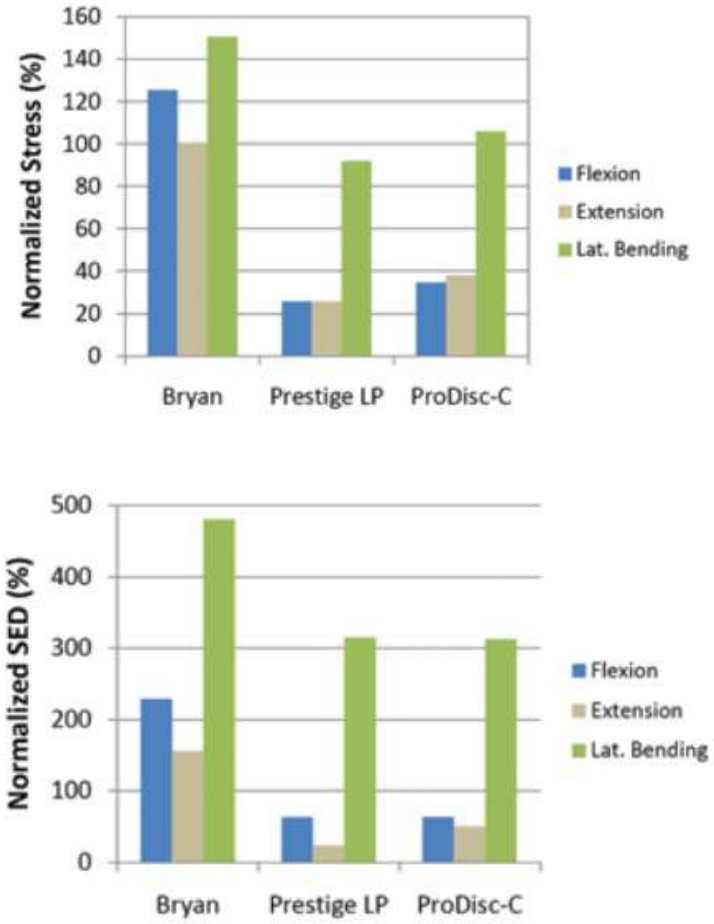

Figure 3.19. Comparison of average von Mises stresses/SED at uncovertebral joints of C5–6 spine segment with Bryan, Prestige LP, and ProDisc-C prostheses, normalized to the von Mises stress/SED in the intact disc [19].

Kallemeyn et al. [20] presented a specimen-specific C2–C7 cervical spine model that was developed using multi-block meshing techniques. The model was validated using in-house experimental flexibility data obtained from the cadaveric specimen used for the mesh development. The model was subjected to pure continuous moments, up to ±1.0 N m in flexion, extension, lateral bending, and axial rotation. Motions at each of the levels were obtained. Some of the findings were that 1) with a few exceptions, the experimental and FEA results were close

(Figure 3.20 and Figure 3.21; 2) removal of the CL caused the greatest increases in motion as compared to the case when either IS or LF removed.; 3) for both LB and AR, removal of CL at C4–C5 CL caused more of an increase in motion compared when either IS or LF was removed (Figure 3.22); and 4) in axial rotation, the highest difference in ROM between the FEA results and experimentally-obtained ones was obtained at C5-C6, (Figure 3.22).

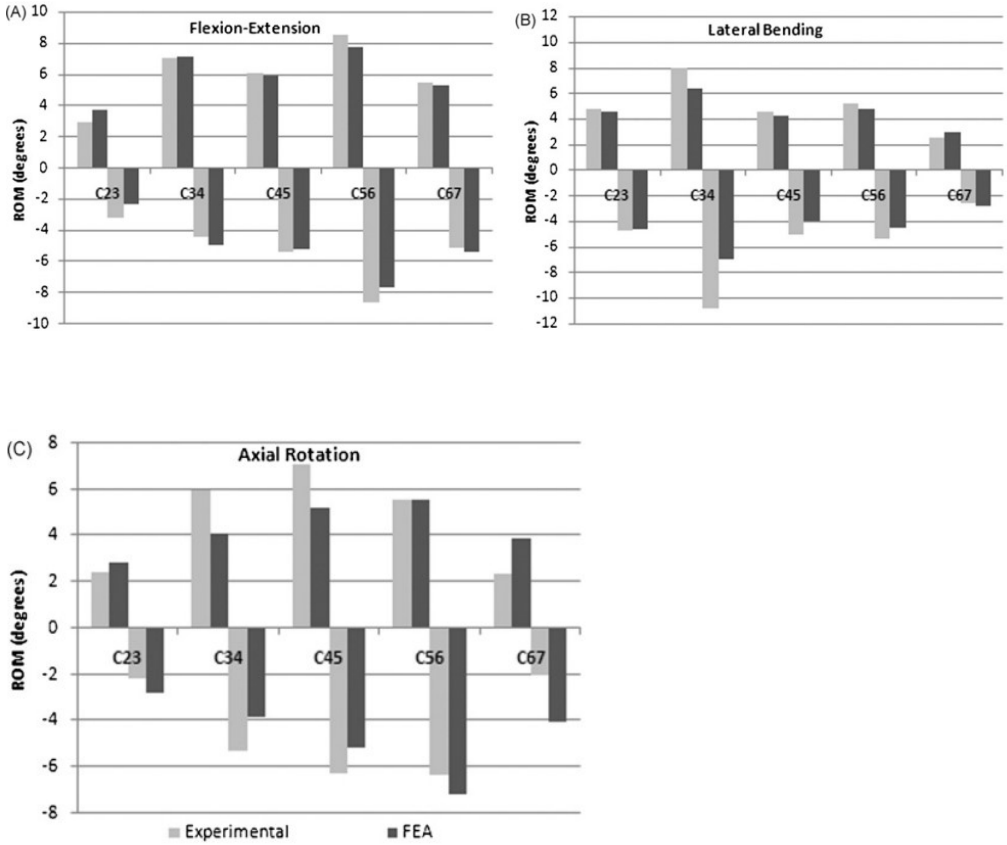

Figure 3.20. Summary of the experimental and FEA results: (A) Flexion (+) and extension (−), (B) right (+) and left (−) lateral bending, (C) right (−) and left (+) axial rotation [20].

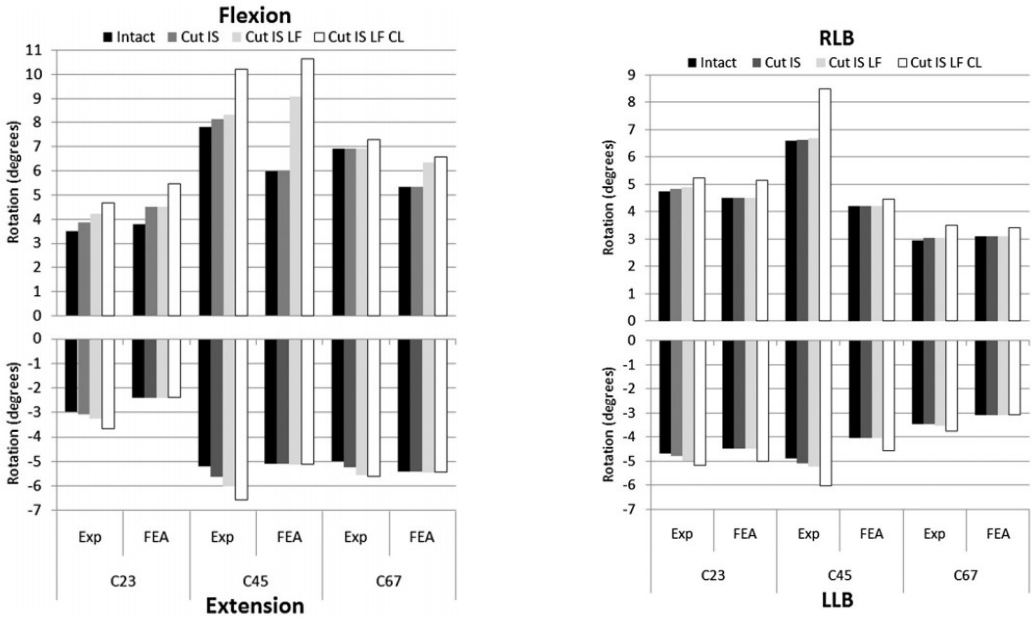

Figure 3.21. Summary of the experimental and FEA results, under flexion extension/lateral bending [20].

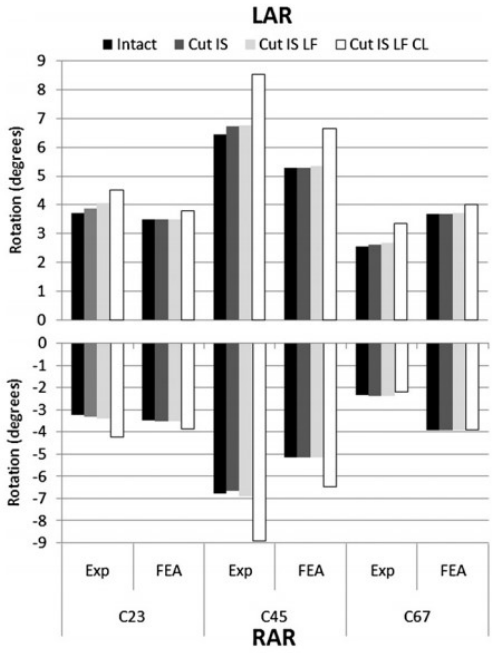

Figure 3.22. Summary of the experimental and FEA results, under axial rotation FSU results [20].

Faizan et al. [21] compared the adjacent-level biomechanics of four variants of a model of the C3-C7 spine: intact, bi-level disc replacement (Bi-TDR), bi-level fusion (Fusion), and a construct having a combination of adjoining-level disc replacement and fusion system (Hybrid). The applied load was a combination of moment + 73.6 N compression force on C3. The results showed that 1) the Fusion movement was moment more than twice that of the intact model during flexion-extension, lateral bending and axial rotation (Figure 3.23); 2) the movement of the Hybrid model was 10–25% more than that of the intact model, except in extension. (Figure 3.23); 3) adjacent-level motions, facet loads, and endplate stresses increased substantially in the Fusion model (Tables 3.1 and 3.2); 4) adjacent-level motions, facet loads, and endplate stresses for the Bi-TDR model were similar to the corresponding values for the intact model (Tables 3.1 and 3.2); and 5) in the Hybrid model, adjacent-level motions, facet loads, and endplate stresses were very close to the corresponding values for the intact model (Tables 3.1 and 3.2).

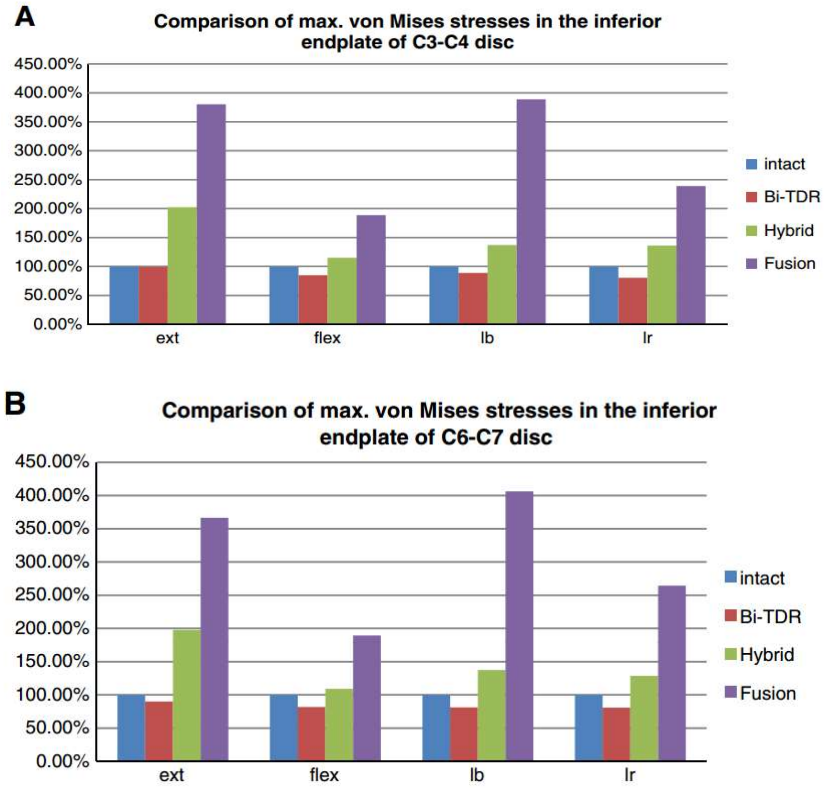

Figure 3.23. (A) FEA predicted adjacent-level (C3–C4) endplate stresses in various models under hybrid loading conditions; (B) FEA predicted adjacent-level (C6–C7) endplate stresses in various models under combination loading conditions [21].

Table 3.1. FE predicted implant-level facet loads (N) for various models under combination loading conditions [21].

	C4–C5 facet load (N)				C5–C6 facet load (N)			
	Intact	Bi-TDR	Hybrid	Fusion	Intact	Bi-TDR	Hybrid	Fusion
Ext	87	26	0	0	145	36	53	0
Flex	0	81	0	0	0	38	68	0
Lb	36	19	0	0	58	19	70	0
Rb	19	17	0	0	18	0	0	4
Lr	30	43	0	2	67	34	86	0
Rr	28	37	0	4	45	36	68	0

Table 3.2. FE predicted adjacent level facet loads (N) for various models under combination loading conditions [21].

	C3-C4 facet load (N)				C6-C7 facet load (N)			
	Intact	Bi-TDR	Hybrid	Fusion	Intact	Bi-TDR	Hybrid	Fusion
Ext	93	98	192	288	60	76	170	190
Flex	0	0	0	0	0	0	0	0
Lb	19	16	28	67	18	22	31	36
Rb	8	7	10	24	6	6	9	28
Lr	26	19	35	48	36	26	50	70
Rr	31	20	51	135	24	20	40	72

Toosizadeh and Haghpanahib [22] studied a nonlinear and validated FE model of C0–C7, which was created using CT images of the cervical spine. This model was used to derive the moment–rotation responses of the cervical spine, under physiological moments of 0.33, 0.50, 1.00, 1.50 and 2.00 Nm for flexion/extension in the sagittal plane, lateral bending in the frontal plane, and axial rotation applied to C0 (the head). According to the results, more risk of tissue injury exists under the lateral bending than under flexion or extension. Also, although the estimated internal forces were lower than the failure tolerance of the tissues, repetition and prolonged bending (and, consequently, reduction in tissue tolerance) or inflammation of muscles and ligaments might lead to injury, but this issue needs further study.

Haghpanahi et al. [23] created a model of the lower cervical spine and validated it by comparing the FE results obtained using the model with experimental data from a previous literature report and another FEA model used in a previous literature report. The match was good

(Figure 3.25), with the small differences seen being a consequences of some features of and assumptions used in the present model.

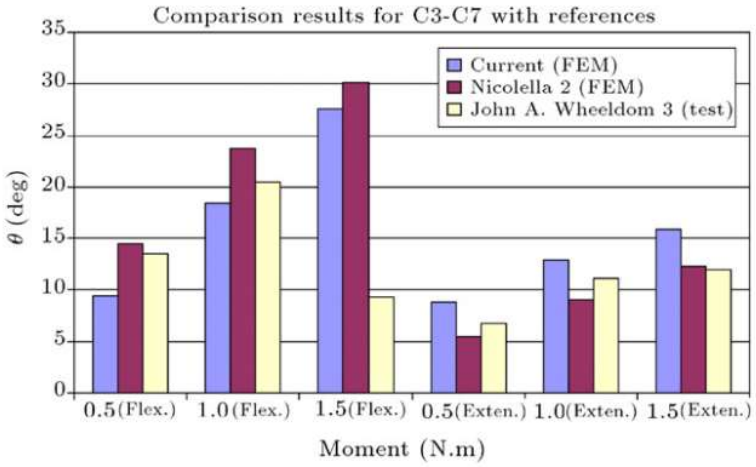

Figure 3.24. Comparison of normalized values for the complete model; flexion & extension [23].

Galbusera et al. [24] created an FE model of a healthy C4–C7 segment and placed a TDR (Bryan design) at C5-C6 and, then, used this model to investigate the influence of the arthroplasty on the biomechanics of the cervical spine. An important point to note is that interactions between the TDR and the adjacent tissues at C5 and C6 were taken into account. Motion patterns of the spine in flexion–extension were obtained by determining the moment–rotation curves for all levels and the location of the instantaneous center of rotation (ICR) of the implanted level. It was found that 1) the ROM at the C5–C6 level was reduced, but only by a small amount, compared to the results when the intact model was used (Figure 3.25); 2) in extension, a small reduction of the ROM occurred but the mobility at C5-C6 was globally

preserved. (Figure 3.25); 3) the total ranges of motion of C4-C7 were 29.2° in flexion and 20.4° in extension (Figure 3.26); and 4) the small increase in facet force at C5-C6 (Figure 3.27) may be related to the different motion pattern imposed by implantation of the disc prosthesis.

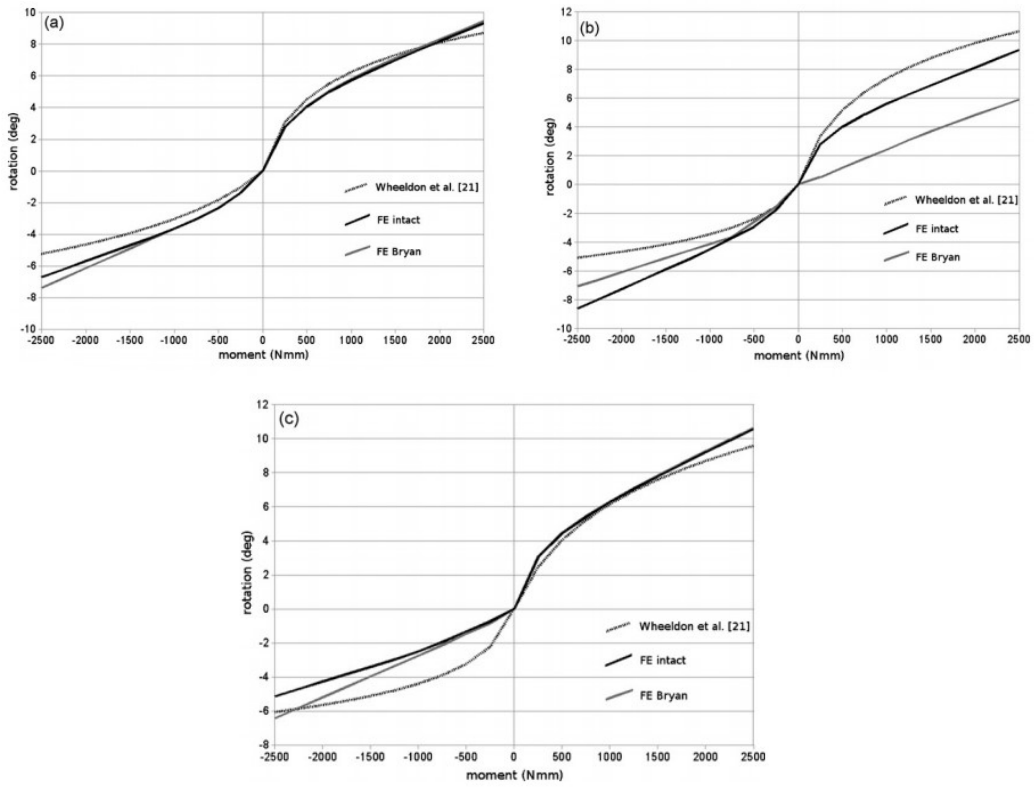

Figure 3.25. Moment–rotation curves obtained with the models of the intact and the implanted segment at C4–C5 (a), C5–C6 (b) and C6–C7 level (c) in flexion and extension, compared with experimental results [24].

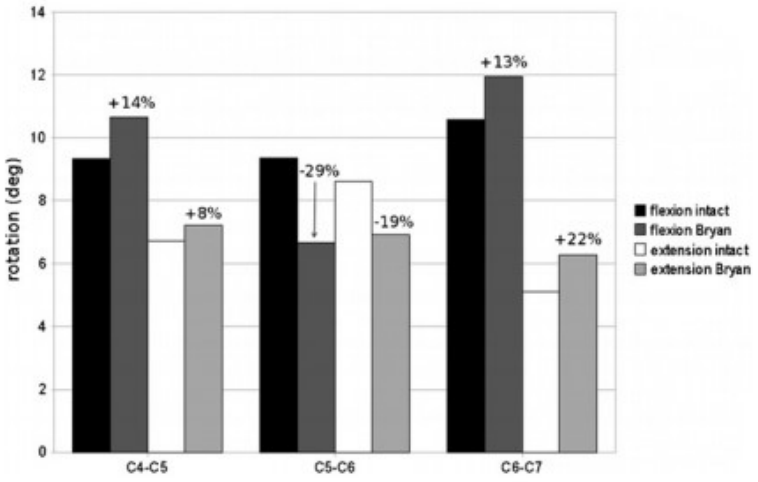

Figure 3.26. Segmental motion compensation induced by the disc prosthesis, by using the hybrid load protocol, for the three considered levels (C4–C5, C5–C6 and C6–C7) [24].

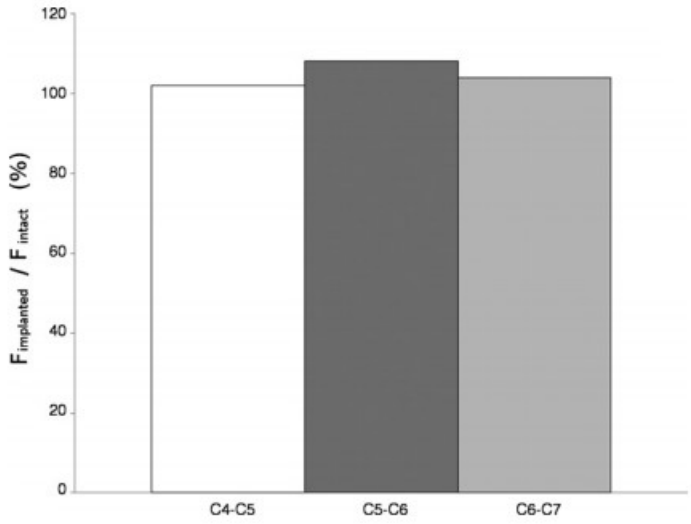

Figure 3.27 The bar chart of ratios between the forces transmitted through the facet joints calculated with the FE model of the implanted segment (Fimplanted) and those calculated with the FE model of the intact segment (Fintact), in extension. [24].

DeWit et al. [25] set out to verify and validate an enhanced C4-C5 FE model and, then, used the model to predict tissue-level failure under three load conditions: tension, flexion, and

extension. Some of the findings were that 1) the extension simulated results fell outside the results for the failure force and just inside those for ultimate failure displacement (Figure 3.28); 2) the injuries observed in the simulations show good agreement with the injuries described in the results of the experimental testing; 3) the flexion simulation results showed failure initiating with the ISL and LF at the posterior end of the segment (Figure 3.29); 4) in extension, failure started with the onset of fracture at the posterior pedicles of the facets in the upper vertebral body (Figure 3.30); and 5) in compression, failure occurred in the cortical and cancellous bones of the middle vertebral body (Figure 3.31).

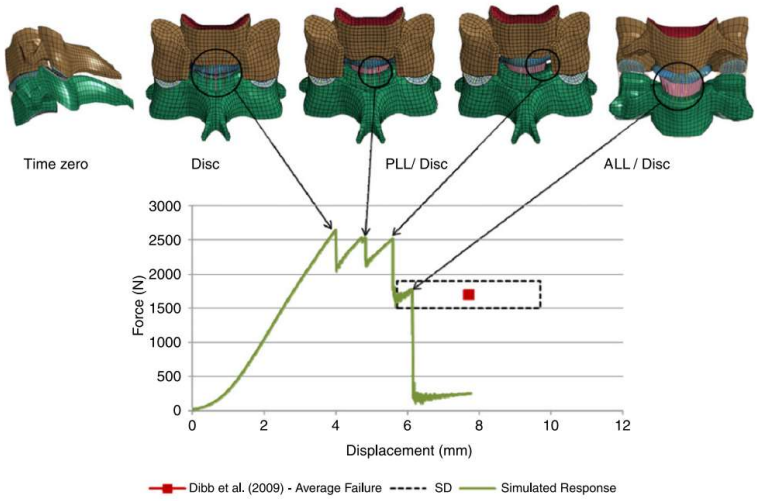

Figure 3.28. Simulated response in tension (C4 spinous process removed for clarity) [25].

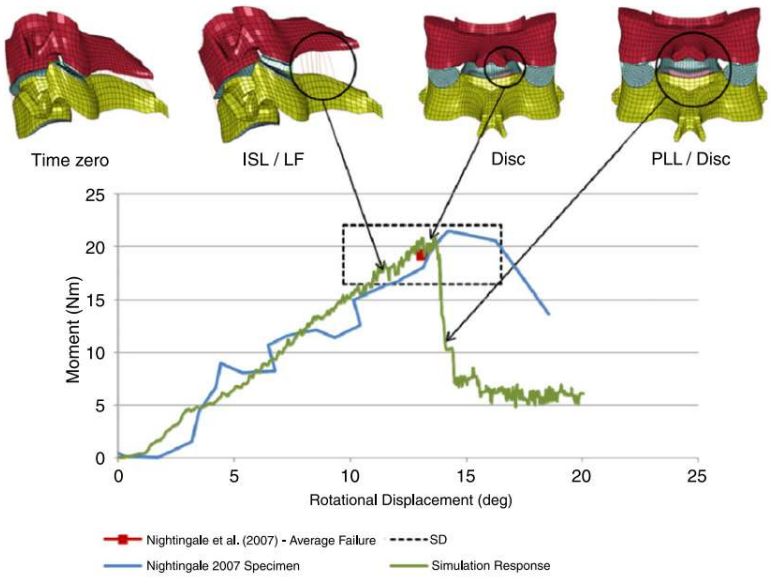

Figure 3.29. Simulated responses in flexion [25].

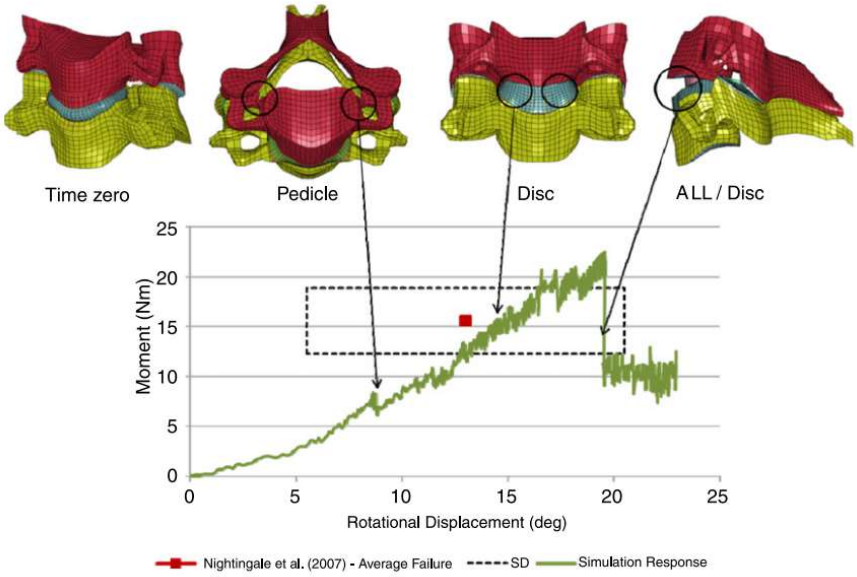

Figure 3.30. Simulated responses in extension [25].

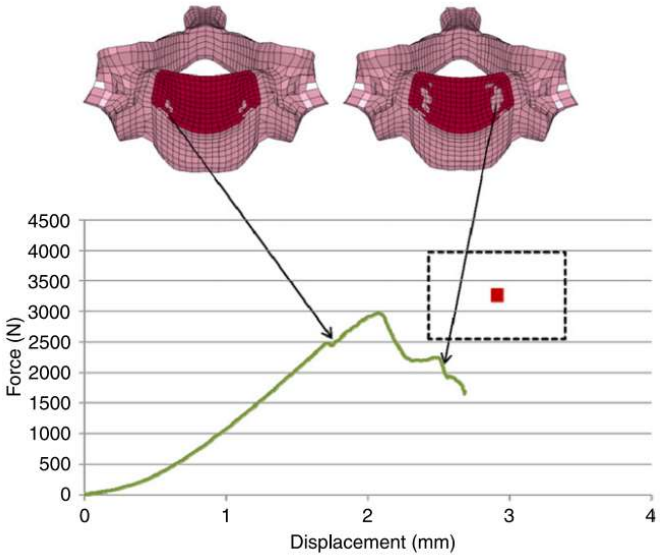

Figure 3.31. Simulated responses in compression [25].

Hussain et al. [26] used a previously validated C3–T1 intact finite FEA model but modified it to build three anterior C4–C7 fusion models: a two-level corpectomy alone (one graft and four screws), a corpectomy-discectomy (two grafts and six screws) (Figure 3.32), and a three-level discectomy alone (three grafts and eight screws). Two unicortical screws were placed parallel to the endplates at 1) C4 and C7, for the corpectomy model; 2) C4, C6, and C7, for the corpectomy-discectomy model; and 3) C4, C5, C6, and C7, for the discectomy model. Range of motion, graft stresses, plate stresses, and bone-screw stresses were determined. It was found that 1) although total construct motion decreased with an increasing number of bone grafts and screws, this was not significantly different between reconstruction technique (Figure 3.33); and 2) stresses in the bone grafts, endplates, and bone near screws decreased as a result of increasing the number of bone grafts and screws (Figure 3.34).

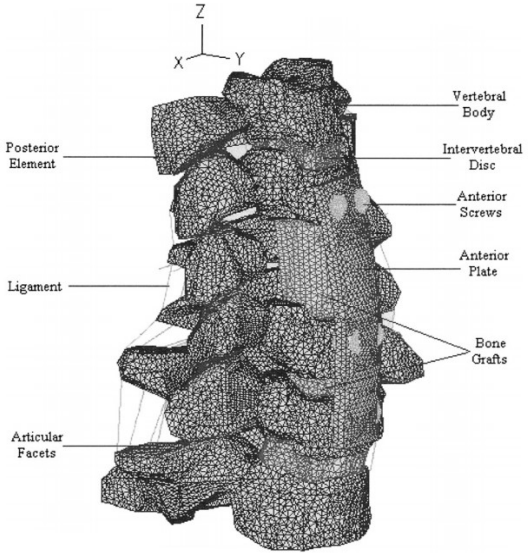

Figure 3.32. Finite element model of a corpectomy-discectomy model [26].

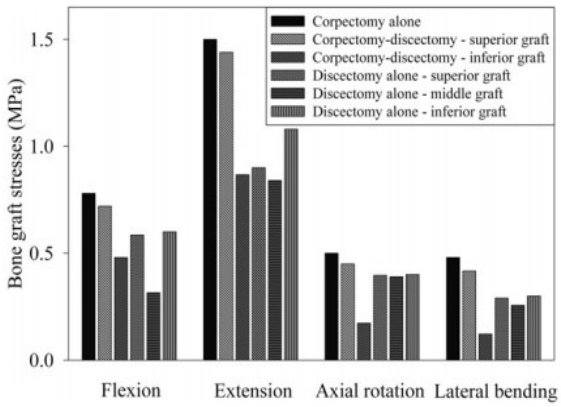

Figure 3.33. Effect of different reconstruction techniques on stresses in the bone grafts [26].

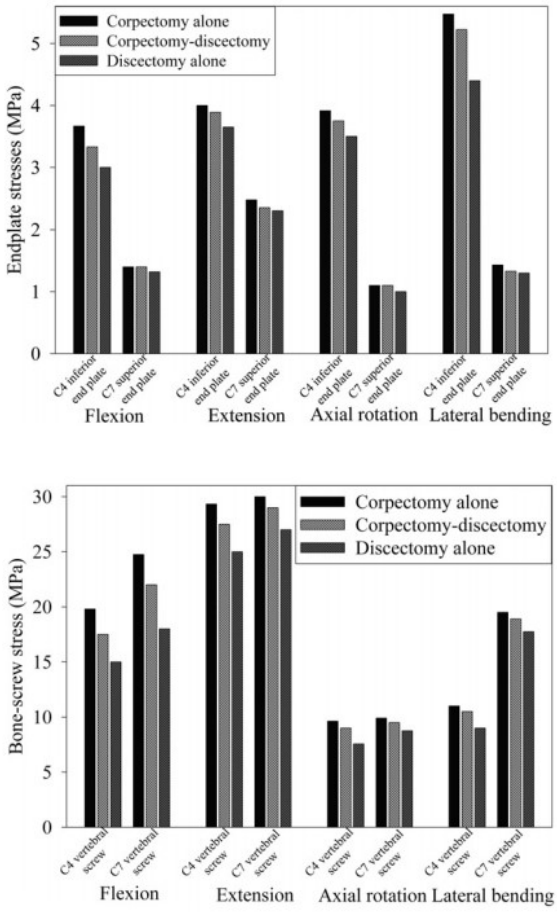

Figure 3.34. Influence of reconstruction techniques on stresses in the end plates superior and inferior/ bone near screws at cephalad (C4) and caudal (C7) levels to the fusion construct [26].

Hussain et al. [27] used a previously validated FE model of an intact C3–T1 segment and constructed three additional models of techniques; anterior (using a rigid screw-plate), posterior (using a rigid screw-rod), and combined anterior-posterior fixation techniques after a C4–C7 corpectomy and fusion (Figure 3.35). Motion patterns, disc stresses, and posterior facet loads at the levels cephalad and caudal to the fusion were determined. Among the findings (Figures 3.36-38) were 1) range of motion, disc stresses, and posterior facet loads increased at the adjacent segments; 2) posterior fixation, whether alone or in combination with anterior fixation, causes

higher changes in segmental motion, disc stresses, and posterior facet loads at adjacent segments compared with the case when anterior fixation alone was used; 3) the superior C3–C4 motion was most affected during lateral bending, the inferior C7–T1 motion was most affected during flexion, and both the superior C3–C4 and inferior C7–T1 motions were least affected during extension; and 4) disc stresses and facet loads were most affected under extension.

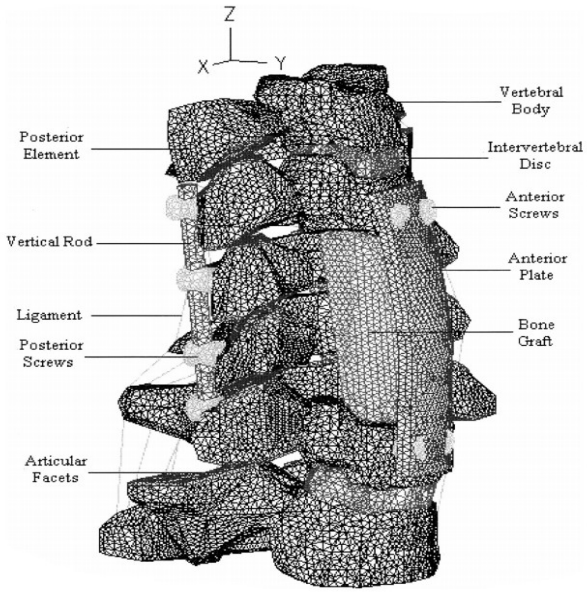

Figure 3.35. A two-level C4–C7 corpectomy model with combined anterior screw-plate and posterior screw-rod instrumentations [27].

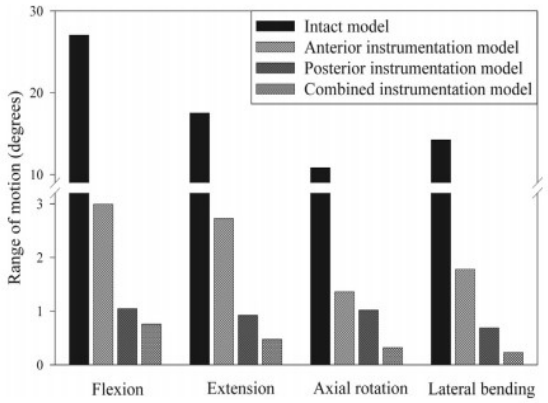

Figure 3.36. Range of motion of the C4–C7 corpectomy construct. [27].

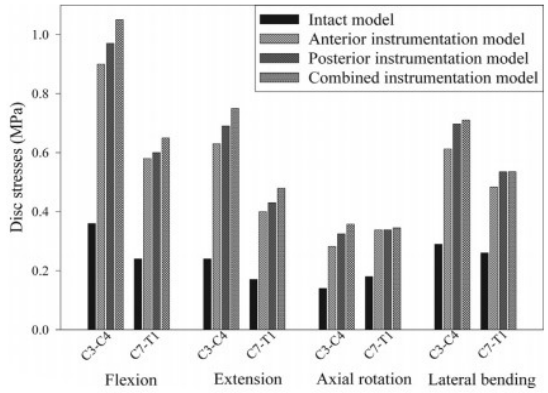

Figure 3.37. Stresses inside the superior C3–C4 and inferior C7–T1 discs after a C4–C7 corpectomy fusion with three instrumentation techniques [27].

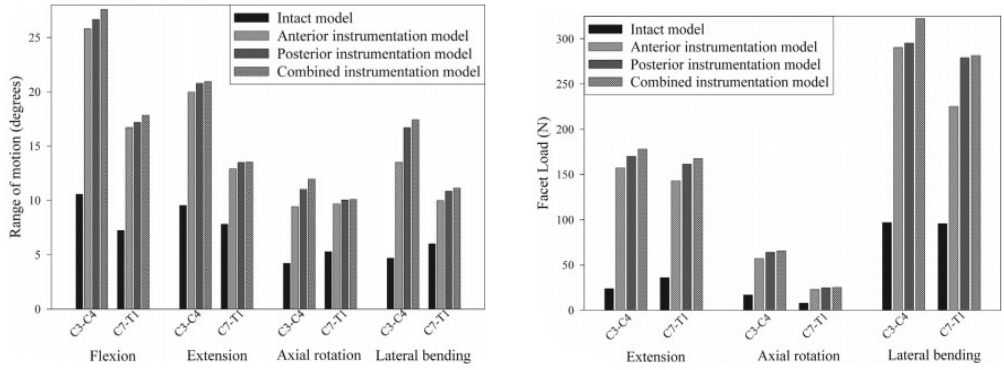

Figure 3.38. Range of motion and facet load for an adjacent level segment [27].

Erbulut et al. [28] considered asymmetry in an FE model of the full cervical spine in their investigation of the influences of ligaments, facet joints, and the nucleus pulposus on the stability of the model during flexion and extension. The model was validated against various published results of in vitro studies and FE studies for the three main loading planes. The C4-C5 level was modified to simulate different cases of the role of the soft tissues in segmental stability. The FE model predicted that excluding ISL from the index level causes excessive instability during flexion and that excluding PLL or LF would not affect segmental rotation. Additionally, 1) ISL was crucial for maintaining cervical spine stability during flexion, and the facet joints were the main contributors to stability during extension (Figure 3.39); and 2) NP provided stability under lower loads, while the ligaments provided this stability under higher loads during flexion.

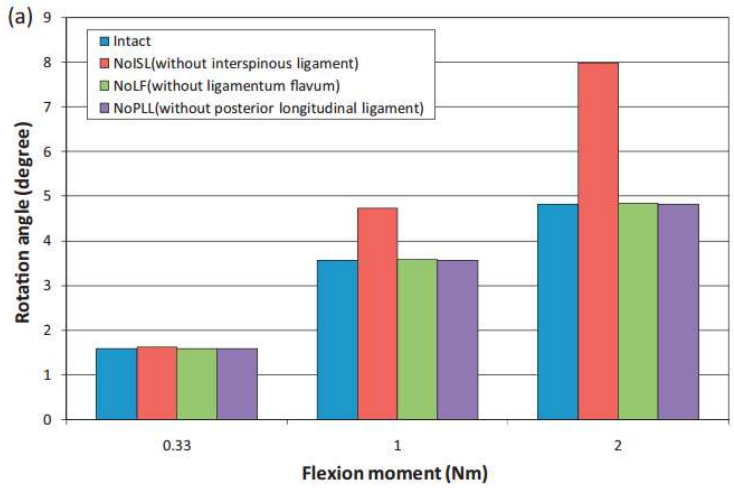

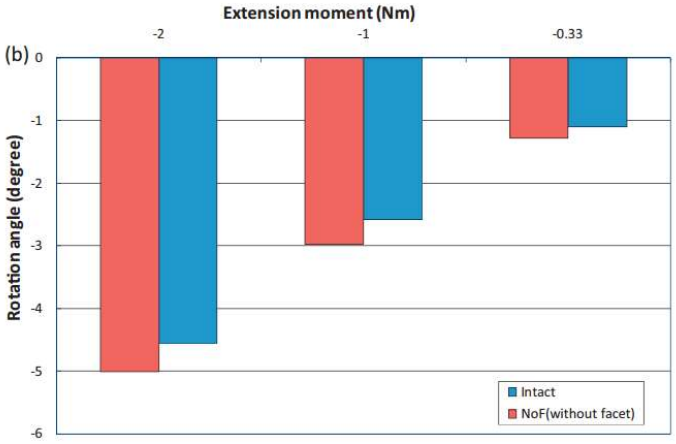

Figure 3.39. (a) Influence of interspinous ligament (ISL), ligamentum flavum (LF), and posterior longitudinal ligament (PLL) on the stability of C4-C5 under flexion loading; (b) Influence of facet joints on the stability of C4-C5 under extension loading [28].

Coelhoa et al. [29] presented a design approach to obtain a cage to enhance the fusion between adjacent vertebrae of the cervical spine. The authors used a multi-scale model for topology optimization of structures to define the cage microstructure. The cage must be able to bear large loads and be fabricated from a material that is osteoconductuive (that is, promotes bone formation within the fusion domain). The design domain was the intervertebral space that will be filled with a bone graft. The topology of the unit-cell was defined to obtain the optimal equivalent properties for stiffness and permeability, which were computed using an asymptotic homogenization method. Thus, the goal of the optimization goal was to obtain the stiffest cage structure for the local strain/stress field. A constraint on the cage microstructure permeability was assumed to obtain interconnected porosity necessary to bone cell migration and nutrient supply. The final cage design that was obtained (Figure 3.40 and Figure 3.41) displayed interconnectivity in all spatial directions and the elastic properties met the stiffness requirements.

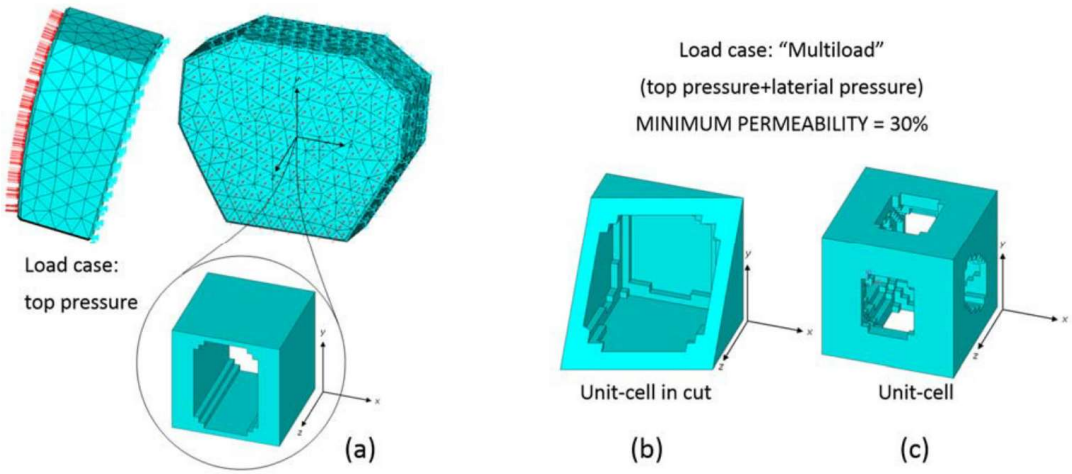

Figure 3.40. Topology optimization of the spinal cage. (a) for a top pressure load; (b) for a multi-load case comprising top pressure and lateral pressure; (c) for the multiload case considering also the constraint on permeability [29].

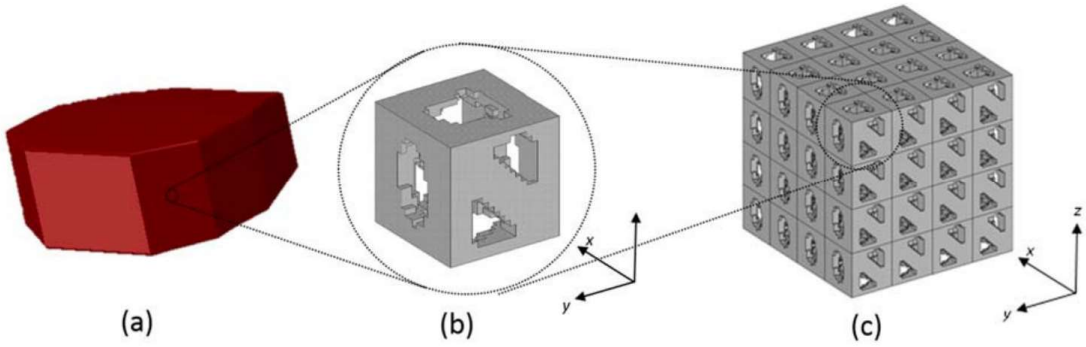

Figure 3.41. Cage design obtained with the spine multi-scale model. The scaffold microsctrute shown was obtained for a multi-load case with 50% volume fraction and 30% permeability. (a) Design domain. (b) Obtained unit cell. (c) Array of 4 x 4 x 4 unit cells [29].

3.2. Shortcomings of the literature

An examination of some key features of the literature reports reviewed in the foregoing section (Table 3.3) reveals six shortcomings of the literature. First, a number of the studies concentrate exclusively on validation of a model of a normal spine. Second, there are very few studies involving a model of spine that includes a degenerated disc. Third, some studies were on multi-level treatments although, in clinical practice, single-level treatments are more common. Fourth, with a few exceptions, all of the studies have been on models that include three or fewer motion segments. Fifth, kinematics results were not given in any study. Sixth, there are no comparisons of models of ACD, ACDF, and TDR, the three methods that are most often used in clinical practice.

Table 3.3. Summary of some features of studies reported in the literature

Spine section	Level of disc problem （s）	Surgical method (s)	Applied loading	Reference
C3-C5	C3-C5	Cervical plate implant	C	Beltran-Fernandez et al. [12]
C3-T1	C3-T1	Fusion, anterior cervical corpectomy fusion	C, F-E, LB	Hussain et al. [15]
C3-C7	C5-C6	TDR(SPH-S/SPH-I/ OVL-S/OVL-I)	C, F-E, LB	Faizan et al. [16]
C4-C7	C5-C6	TDR (ball-and-socket)	F-E, LB	Galbusera et al. [17]
C1-C7	C5-C6	ACDF vs. ACD vs. PEN vs. nucleus replacement vs. intact model	C+(F/E/LB/AR)	Li and Lewis [18]
C5-C6	C5-C6	TDR (Bryan vs. Prestige LP vs. ProDisc-C) vs. intact model	73.6 N C+(1.5N F/E/LB	Kang et al. [19]
C3-C7	C4-C6	TDR (bi-level) vs. ACDF (bi-level) vs. hybrid (TDR+ ACDF) vs. intact model	73.6 N + varying moment (F/E/LB/AR)	Faizan et al. [21]
C4-C7	C5-C6	TDR (Bryan) vs. intact	F-E	Galbusera et al. [24]
C3-T1	C4-C7	Fusion (discectomy vs . corpectomy)	73.6 N C+(1.5 N F/E/LB/AR)	Hussain et al. [26]
C3-T1	C4-C7	Corpectomy, Fusion (anterior fixation, Posterior fixation, anterior-posterior fixation)	F/E/LB/AR	Hussain et al. [27]

Note: C is compression, F is flexion, E is extension, LB is lateral bending and AR is axial rotation.

CHAPTER 4

FINITE ELEMENT MODELING

4.1. Overview

In this chapter, details of the steps used to create the five FE models studied are given. These models are of the intact full cervical spine (C1-C7) (INTACT Model), a spine of a patient who suffers from degeneration disc disease (DDD) at the C5-C6 level (DEGEN Model), a spine of a patient who suffers from DDD at C5-C6 and is surgically treated for this disease using anterior cervical discectomy only (ACD Model), a spine of a patient who suffers from DDD at C5-C6 and is surgically treated for this disease using anterior cervical discectomy followed by fusion (ACDF Model), and a spine of a patient who suffers from DDD at C5-C6 and is treated for this disease by implantation of a notional total disc arthroplasty (TDR Model). The INTACT Model was used for validation purposes; that is, for comparison of FEA results to relevant experimental results given in literature reports. It is emphasized that ACD, ACDF, and TDR Models were all built as modifications of INTACT Model.

4.2. The INTACT Model

4.2.1. Construction of solid model

Because of the irregular shape of the vertebral bodies at each of the levels, a solid model of each of its parts (cortical bone, cancellous bone, and posterior elements) was built. This involved using 1) a 3D scanning software package (Mimics® Version 8.1; Materialise, Inc., Leuven, Belgium), to import digitized quantitative axial computed tomography (CT) scans/images of that part from an adult male cadaver from the Visible Human Project® dataset (National Library of Medicine, Bethesda, MD, USA); 2) a commercially-available 3D medical image processing and editing software package (RapidForm® Version 2006; INUS Technology, Inc., Seoul. South Korea) to transfer these scans/images to a parametric format; and 3) a commercially-available computer-aided drawing software package (ProEngineer® Wildfire 5.0; Parametric Technology Corporation, Needham, MA, USA) to edit and assemble the solid models of the individual parts (Figure 4.1 and Figure 4.2).

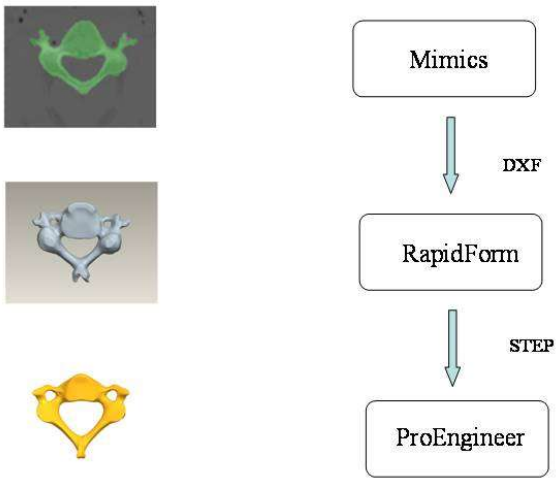

Figure 4.1. Schematic drawing of the steps used to build the solid mode of a vertebral body.

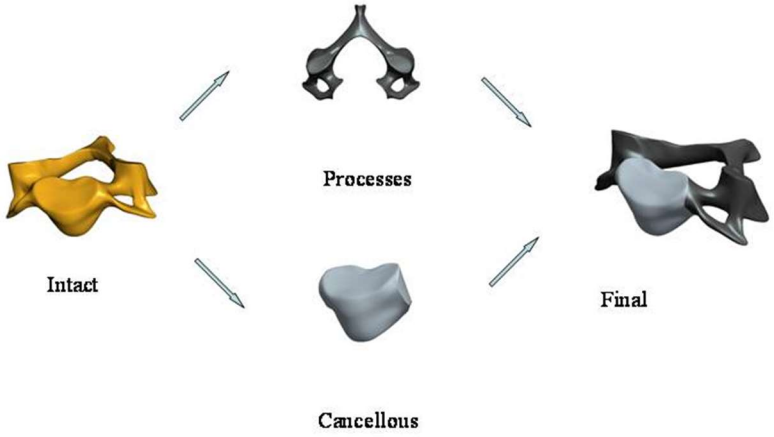

Figure 4.2. Exploded view of the built solid model of a vertebral body.

These steps are illustrated using by providing some details in the case of building the solid model of C4 (Figures. 4.3 - 4.5). These steps are: create the objective reference plane (DTM 1-4), insert the sketch on the base plane, create two different radius cycles, extrude the cycle, make intersect or subtract the bones, separate the anterior and the posterior parts, edit, and then re-assemble.

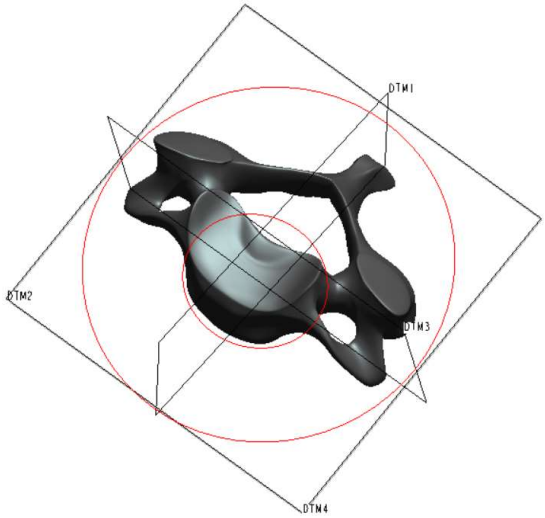

Figure 4.3. Single intact vertebra (C4).

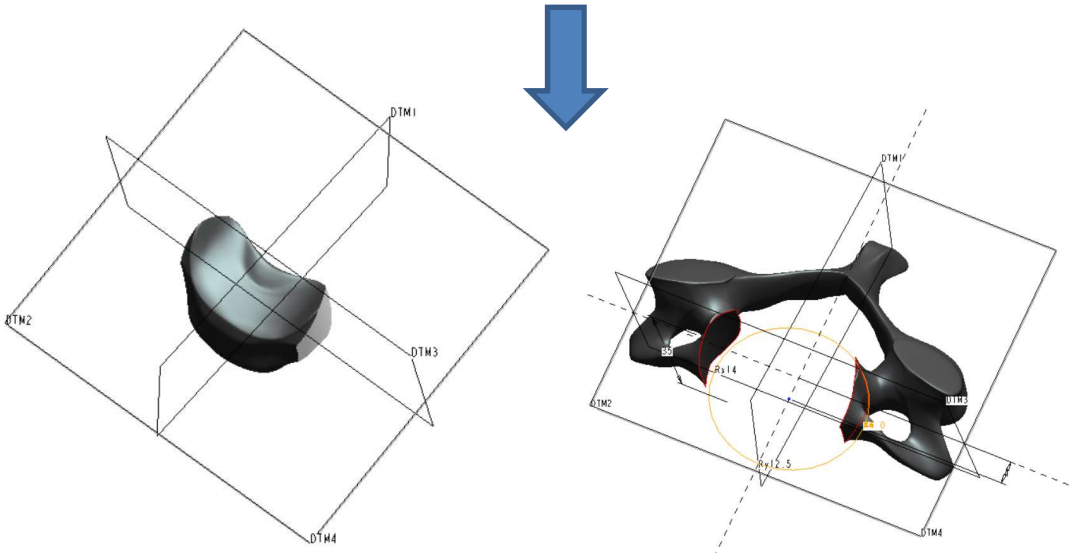

Figure 4.4. Separated anterior and posterior parts of C4.

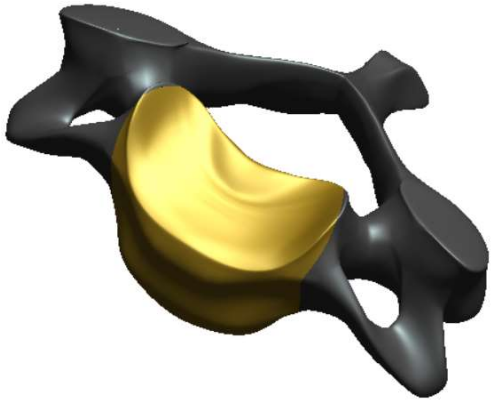

Figure 4.5. Assembled model of C4.

As with each vertebral body, the solid model of the disc was constructing by, first, building models of each of the individual parts (annulus fibrosus (AF), nucleus pulposus (NP), top endplate, and bottom endplate) and then assembling them (Figure 4.6).

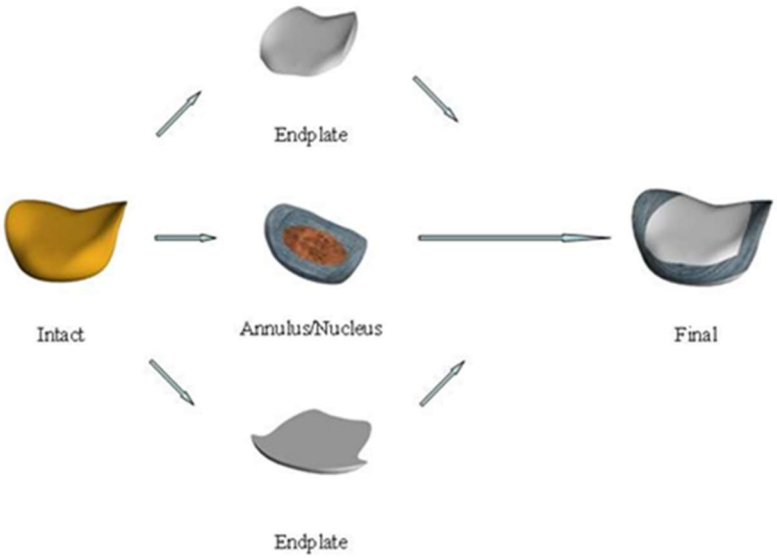

Figure 4.6. Schematic drawing of the steps used in building the solid model of a disc.

For example, for the C5-C6 disc, the steps are: create the objective reference plane (DTM 1-6), insert the sketch on the top plane and bottom plane, create two different radius cycles, extrude the cycle, subtract the original disc body, separate AF, NP, the upper endplate, and the lower endplate, and then edit and re-assemble (Figures 4.7 - 4.10).

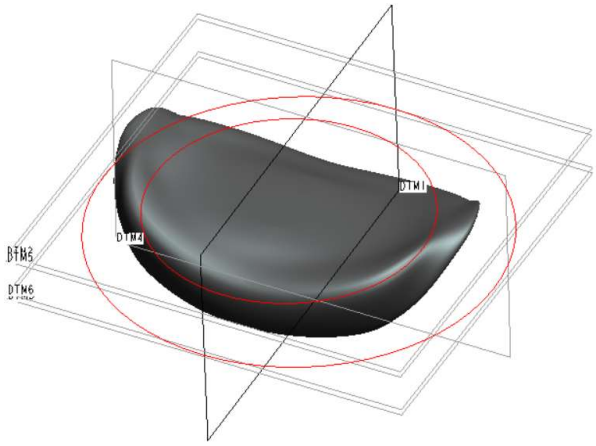

Figure 4.7. Drawing of the C5-C6 disc.

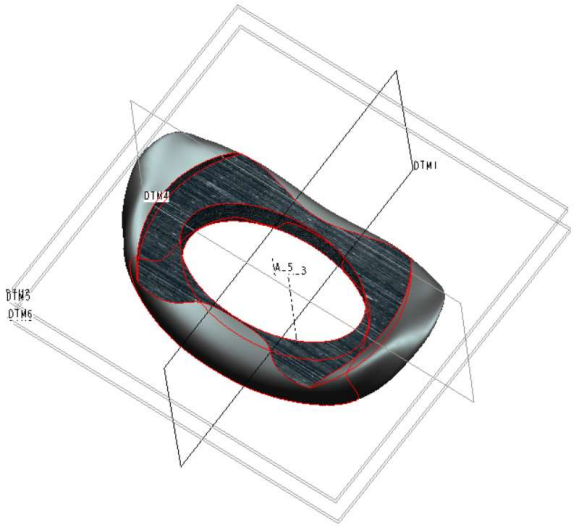

Figure 4.8. Drawing of the annulus fibrosus of the C5-C6 disc

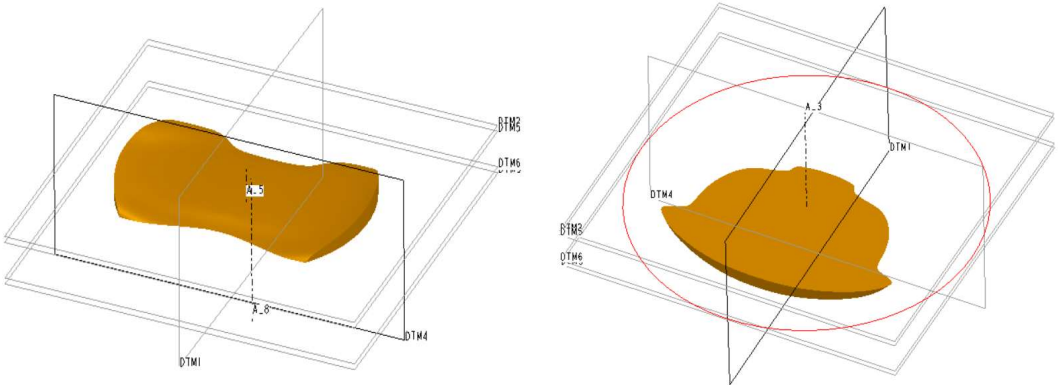

Figure 4.9. Drawings of the upper and lower endplates on the C5-C6 disc.

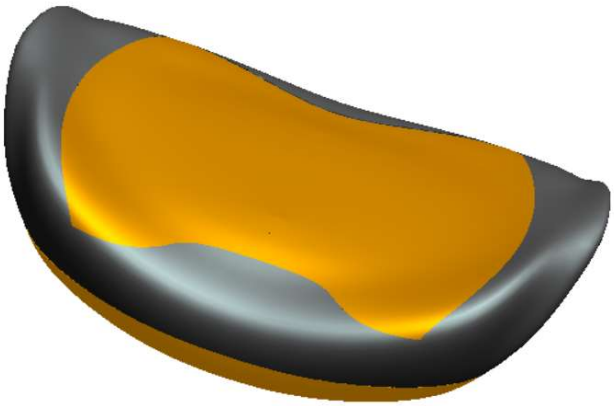

Figure 4.10. Drawing of the assembled C5-C6 disc.

After the solid models of the vertebral body and the disc at each level were built, they were assembled to obtain the solid model of the full cervical spine (Figure 4.11).

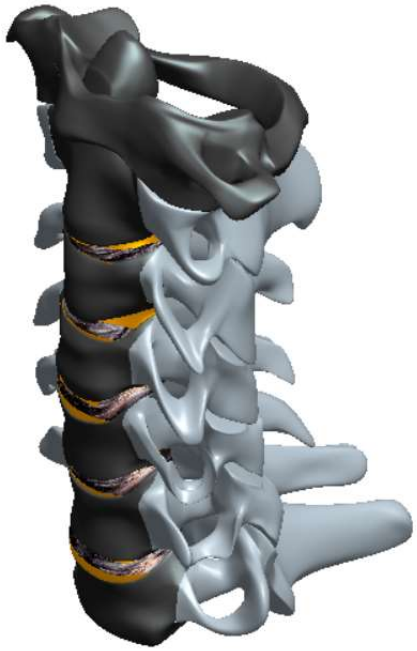

Figure 4.11. Solid model of the full normal cervical spine (C1-C7).

4.2.2. Finite element analysis

4.2.2.1 Steps

This involved five steps. In the first step, the SAT files of each tissue of the solid model were exported into a commercially-available FEA software package (ABAQUS®, Version 6.13; Abaqus, Inc., Providence, RI, USA) and meshed using element types in the library. After that, the meshes were refined through tie-up of parts, in some cases, and assembled to give the final mesh of the whole model. An illustration of tie-up is shown in Figure 4.12 and Figure 4.13.

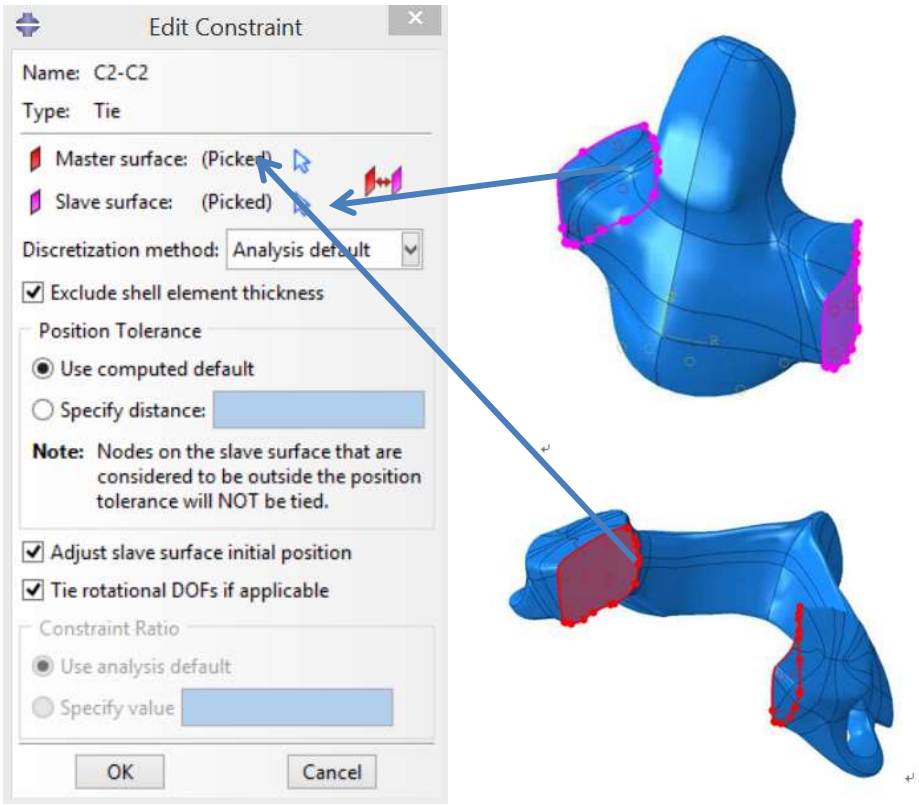

Figure 4.12. Illustration of selection of pair surface for setup constraint.

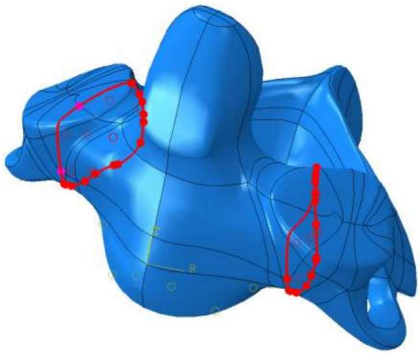

Figure 4.13. Illustration of tie-up of anterior and posterior parts.

Compared to cortical bone, cancellous bone has a higher surface area-to-mass ratio because it is less dense (Figure 4.14). Thus, each of these bones was meshed using shell elements.

Considered as a single unit, each of these bones may be described in terms of three coordinate axes: radial, tangential, and longitudinal (Figure 4.14),

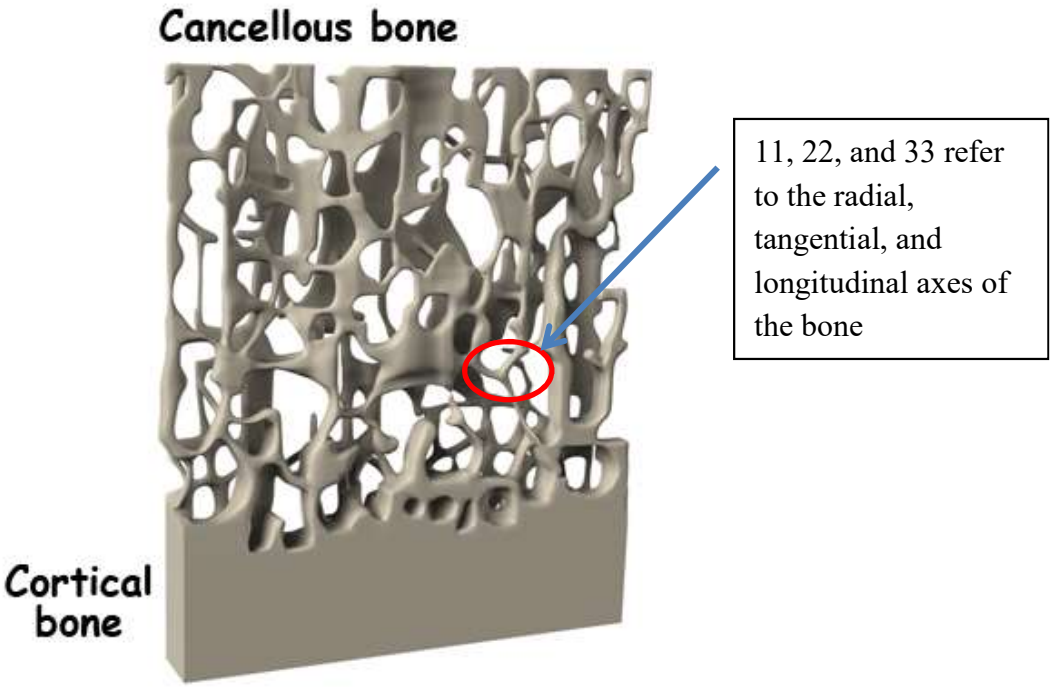

Figure 4.14. Sketch of the macrostructures of cancellous and cortical bones.

The cervical spine ligaments are anterior longitudinal ligament (ALL), posterior longitudinal ligament (PLL), supraspinous ligament (SSL), interspinous ligament (ISL), ligamentum flavum (LF), capsular ligament (CL), alar ligament (AlL); transverse ligament (TL), and apical ligament (APL). In ABAQUS, the ligaments were modeled as nonlinear tension-only spars. The following steps were used in building the FE model. First, build the wire that connects two points from the upper and lower vertebrae; give this wire a material property obtained from the literature.

Because of the tension-only characteristic, it also has to be setup as an initial length. If the ligament bears a compression force, which means the length will become less than the initial length, we let it fail. If the ligament bears a tension force, which means the ligament length will elongate under load, set it up so it works (Figure 4.15).

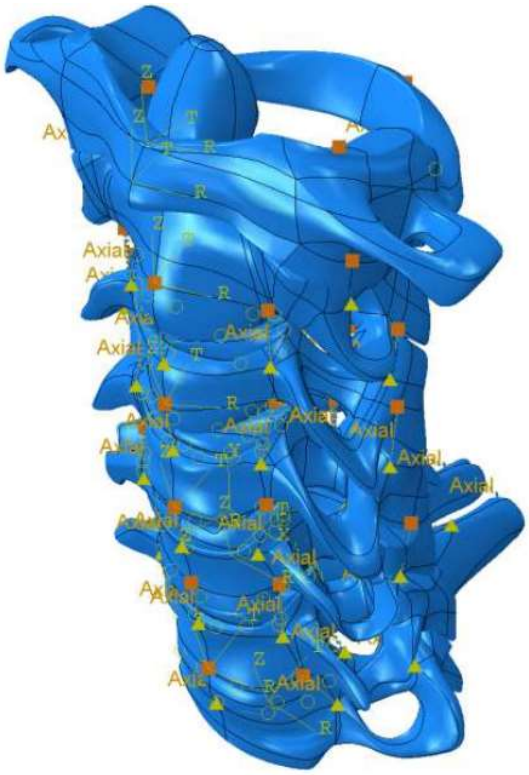

Figure 4.15. Schematic drawing showing the ligaments.

In the second step, the constraint of the model was specified (fixation at the bottom of the lower endplate on C7 in all positions and directions). In the third step, the applied loading and its point of application on the model (top surface of the upper endplate on C1) were inputted (Figure 4.16). The fourth step was to input the values of the materials. The fifth step was running of the

FEA, and, then, extracting all the results of interest (post-processing phase) (Figure 4.17).

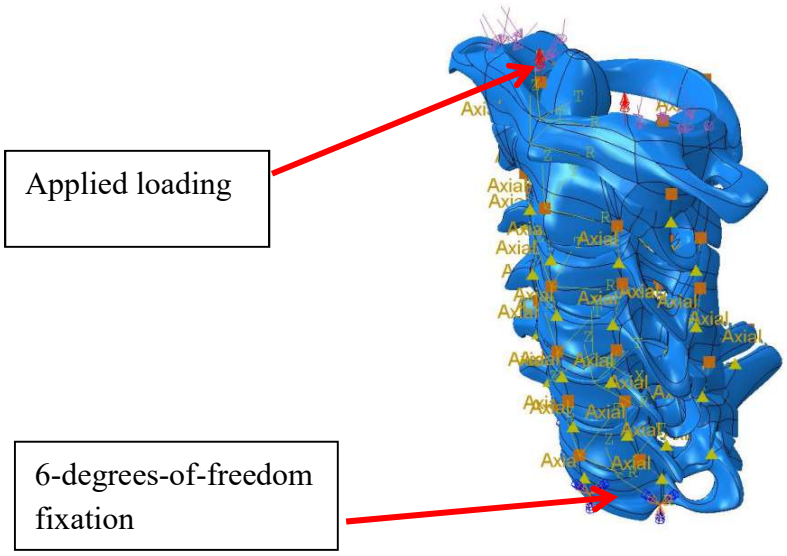

Figure 4.16. Constraints and point of application of applied loading.

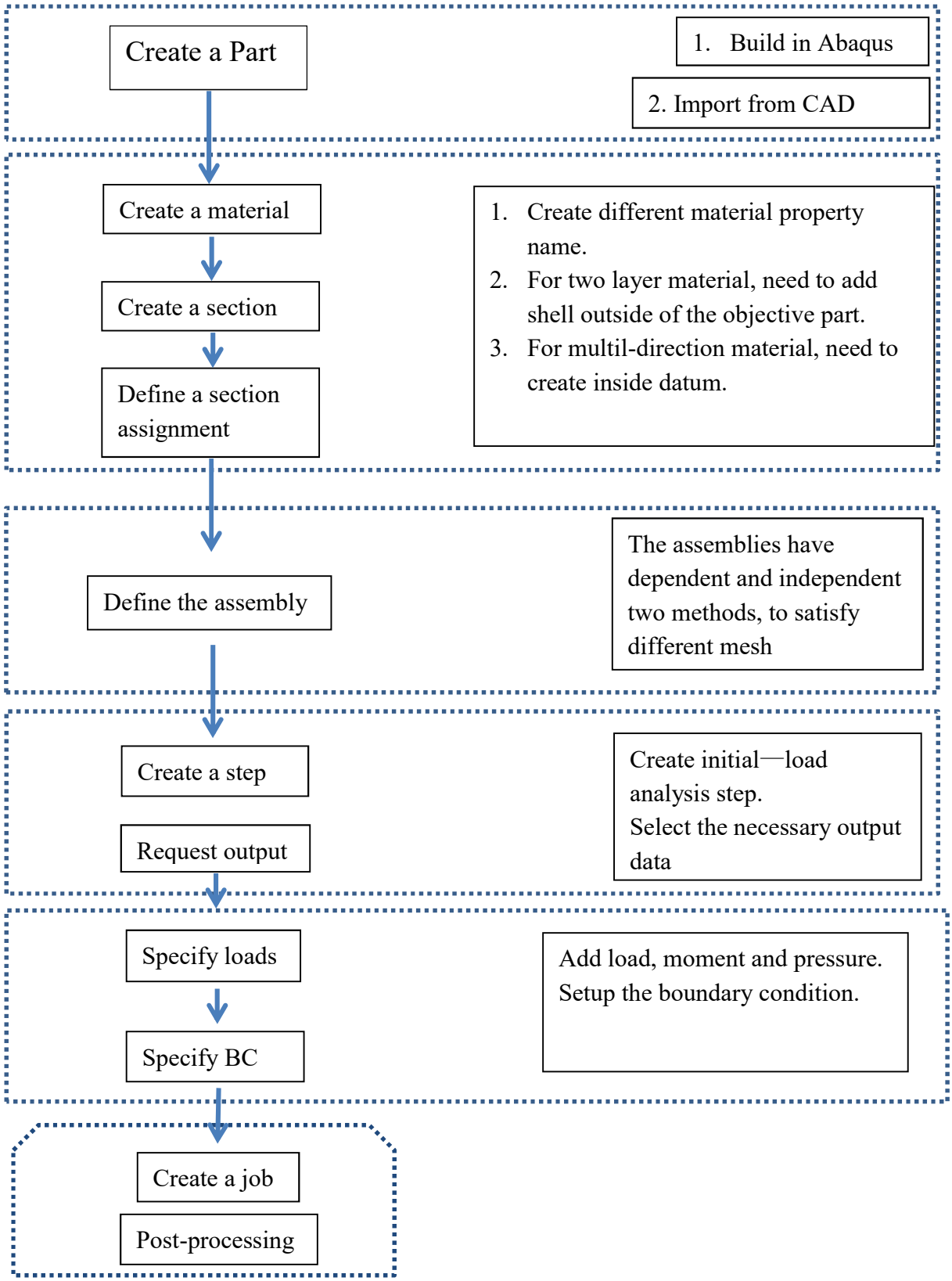

Figure 4.17. Detailed schematic drawing of the steps used in the finite element analysis.

4.2.2.2. Details of applied loadings

Six different loadings were applied, these being 1) 1 Nm sagittal plane (flexion) moment + 73.6 N axial compressive pre-load; 2) 1Nm sagittal plane (extension) moment + 73.6 N axial compressive pre-load; 3) 1 Nm left lateral bending moment + 73.6 N axial compressive pre-load; 4) 1 Nm right lateral bending moment + 73.6 N axial compressive pre-load; 5) 1 Nm clockwise-acting axial torsional moment + 73.6 N axial compressive pre-load; and 6) 1 Nm counter-clockwise-acting axial torsional moment + 73.6 N axial compressive pre-load. The magnitude of each of these applied loadings is physiologically relevant, with the axial compressive pre-load simulating the weight of the head and the magnitudes of both the moments and the axial compression force being within the range measured during a variety of activities of daily living.

4.2.2.3. Details of material properties

The values of the properties of the various materials in the model are presented in Table 4.1. It is seen that the material constitutive models are a mixture of isotropic elastic (for example, endplate and ALL)) and transversely isotropic elastic (cortical and cancellous bones).

Table. 4.1. element type and elastic properties of the tissues/materials in the finite element model

Tissue	Element type	Elastic property	Reference(s)
Cortical bone	3-noded triangular general-purpose shell	E_{11} = 9,600 MPa; E_{22} = 9,600 MPa E_{33} = 17,800 MPa; G_{12} = 3,097 MPa G_{13} = 3,510 MPa; G_{23} = 3,510 MPa ν_{12} = 0.55; ν_{13} = 0.30; ν_{23} = 0.30	Rho (43); Cowin (44)
Cancellous bone	4-noded tetrahedral	E_{11} = 144 MPa; E_{22} = 99 MPa E_{33} = 344 MPa; G_{12} = 53 MPa G_{13} = 45 MPa; G_{23} = 63 MPa ν_{12} = 0.23; ν_{13} = 0.17; ν_{23} = 0.11	Ulrich et al. (45)
Posterior elements	4-noded tetrahedral	E = 3,500 MPa; ν = 0.29	Kumaresan et al. (46)
Annulus fibrosus	4-noded tetrahedral	Ground substance: E = 4.2 MPa; ν = 0.45 Elastic fibers: E = 450 MPa; ν= 0.30	Ha et al. (47)
Nucleus pulposus	8-noded brick	E = 1.0 MPa; ν =0.499	Ha et al. (47) Brolin and Halldin (48)
Endplates	4-noded tetrahedral	E = 500 MPa; ν= 0.40	Yoganandan et al. (49)
ALL	2-noded tension-only link	E = 30.0 MPa; ν= 0.30	Zhang et al. (50)
PLL	2-noded tension-only link	E = 20.0 MPa; ν= 0.30	Zhang et al. (50)
ISL, LF (C1-C2)	2-noded tension-only link	E = 10.0 MPa; ν= 0.30	Zhang et al. (50)
SSL, ISL, LF (C2-C7)	2-noded tension-only link	E = 1.5 MPa; ν= 0.30	Zhang et al. (50)
CL (C1-C3)	2-noded tension-only link	E = 10.0 MPa; ν= 0.30	Zhang et al. (50)
CL (C3-C7)	2-noded tension-only link	E = 20.0 MPa; ν= 0.30	Zhang et al. (50)

TTABLE 4.1. ((CONTINUED)- ELEMENT TYPE AND ELASTIC PROPERTIES OF THE TISSUES/MATERIALS IN THE FINITE ELEMENT MODEL

Tissue	Element type	Elastic property	Reference(s)
A1L	2-noded tension-only link	E = 5.0 MPa; ν = 0.30	Zhang et al. (50)
TL	2-noded tension-only link	E = 20.0 MPa; ν=0.30	Zhang et al. (50)
ApL	2-noded tension-only link	E = 20.0 MPa; ν= 0.30	Zhang et al. (50)

Note that the references are for the values of the elastic properties.

E: modulus of elasticity; ν : Poisson's ratio.

11, 22, and 33 refer to the radial, tangential, and longitudinal axes of the bone, respectively.

ALL: anterior longitudinal ligament; PLL: posterior longitudinal ligament; ISL: interspinous ligament; LF: ligamentum flavum;

SSL: supraspinous ligament; CL: capsular ligament; AlL: alar ligament; TL: transverse ligament; ApL: apical ligament.

4.2.2.4. Convergence exercise

This involved obtaining the rotation of INTACT Model (ROMA), under a loading of 1 Nm axial flexion moment + 73.6 N compressions, using different mesh densities (ranging from 320,147 elements and 35,476 nodes to 617,230 elements and 120,572 nodes). Mesh convergence was obtained when there was minimal change in ROMA with increase in mesh density (Figure 4.18). The converged FE mesh of INTACT Model is presented in Figure 4.19, the final mesh density (density of the converged mesh) comprised 421,000 elements and 89,161 nodes. For the five FE models are summarized in Table 4.2.

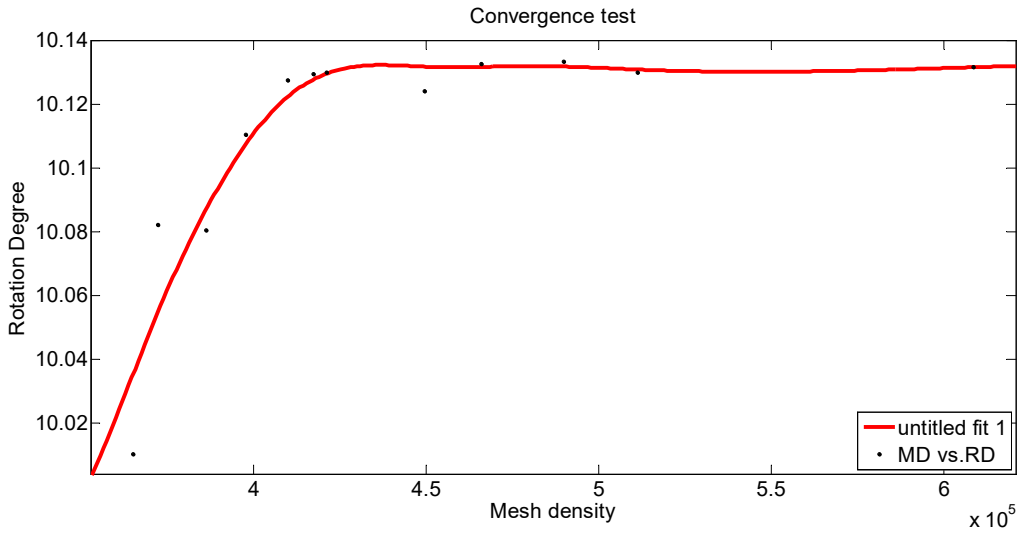

Figure 4.18. Summary of the convergence exercise results.

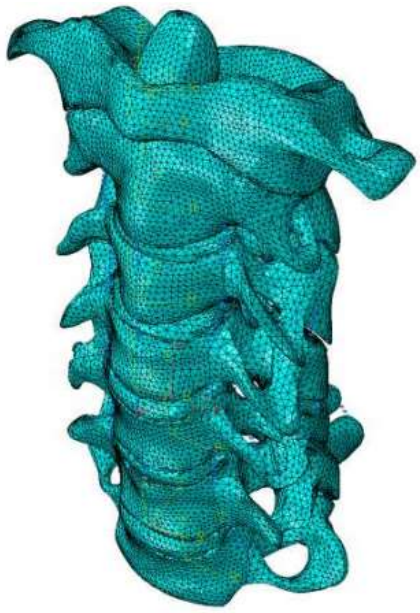

Figure 4.19. The meshed and converged intact model.

4.2.2.5. Validation exercise

This involved a comparison of FEA results, obtained using the INTACT Model (that is, converged FE model, constraints, and materials described in the foregoing sub-sections), and a specific applied loading, on the one hand, and experimental results, as given in relevant literature reports (Table 4. 2), on the other.

Table 4.2. Summary of some features of relevant experimental studies reported in the literature

Reference	Test medium	Number of specimens	Age range	Method of apply load
Panjabi Et al. [51]	In vitro	16 (1 C0-C5 5 C0-C6 2 C0-C7 8 C2-C7)	NA	The loading fixture is designed to apply pure moments to the specimens via three round discs: two vertically oriented and one horizontally oriented. The vertical pulleys are used to apply moments of flexion, extension and bilateral bending. The horizontal pulley is used to apply axial torque.
Wheeldon Et al. [52]	In vitro	7	20-51	Pure moment loads were applied to the superior end of the specimen through the use of a system of wires, pulleys and dead weights
Kallemeyn Et al. [53]	In vitro	1	74	The spine was tested using a biaxial servo-hydraulic materials testing machine (858 Mini Bionix 2, MTS Corporation, Eden Prairie, MN) retrofitted with a spine gimbal and XZ table capable of applying pure continuous moments in flexion-extension, lateral bending, and axial rotation.
Yoganandan Et al. [54]	In vitro	9	23-44	The specimen were attached to an inferiorly placed load cell (model 3803; Robert A. Denton, Rochester Hills, Michigan) that was capable of recording on-axis and off-axis moments and forces in the three planes; physiological equal and opposite forces were applied to the superior vertebra with use of a loading frame that created pure moment loading in the right and left lateral bending modes.
Yoganandan N, et.al [55]	In vitro	10	23-44	The specimen was attached to a load cell placed beneath the distal end of the column. It was capable of recording on and off-axis moments in the axial, and coronal and sagittal planes, torsion, and lateral bending and flexion-extension. To induce axial twisting moments, equal and opposite forces were applied to the superior vertebra using a loading frame.

The results of this exercise are presented in Figures 4.20 to 4.25. Considering the differences between the FE model and the conditions used in the experimental work (Table 4.2), it is concluded that the two sets of results are reasonably close. Furthermore,

the present FEA results are comparable to FEA results reported in previous relevant literature reports; that is, studies in models of C0-C7 or C1-C7 were used. Thus, the INTACT Model is considered validated.

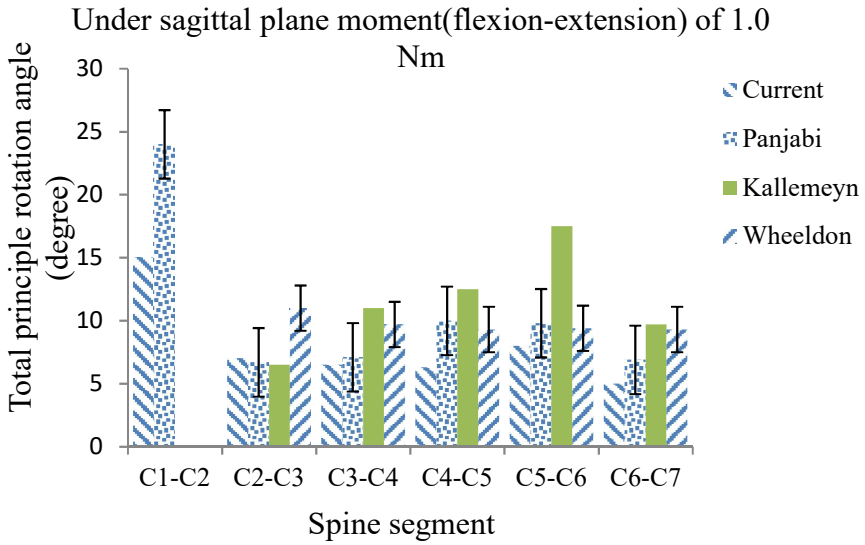

Figure 4.20. Comparison between current FEA results and experimental results under flexion-extension moment.

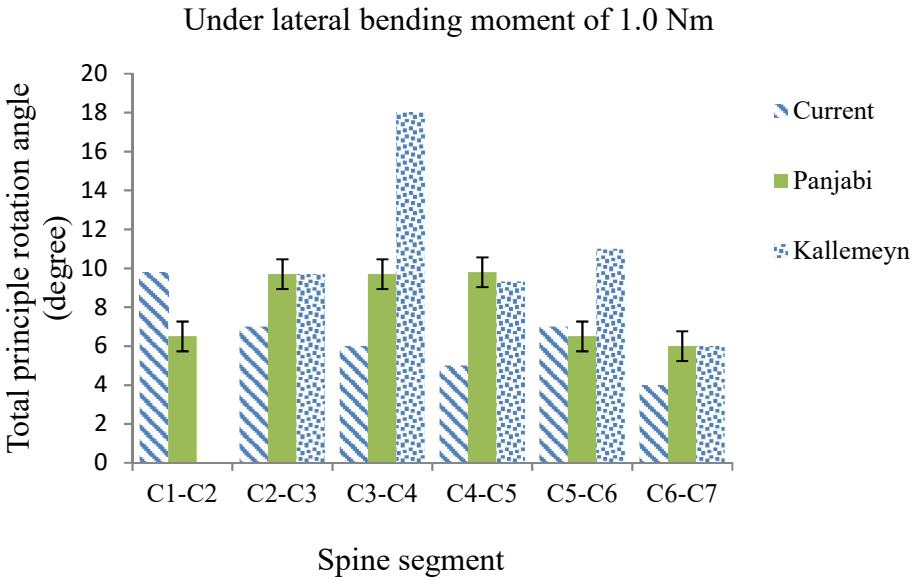

Figure 4.21. Comparison between current FEA results and experimental results under lateral bending moment.

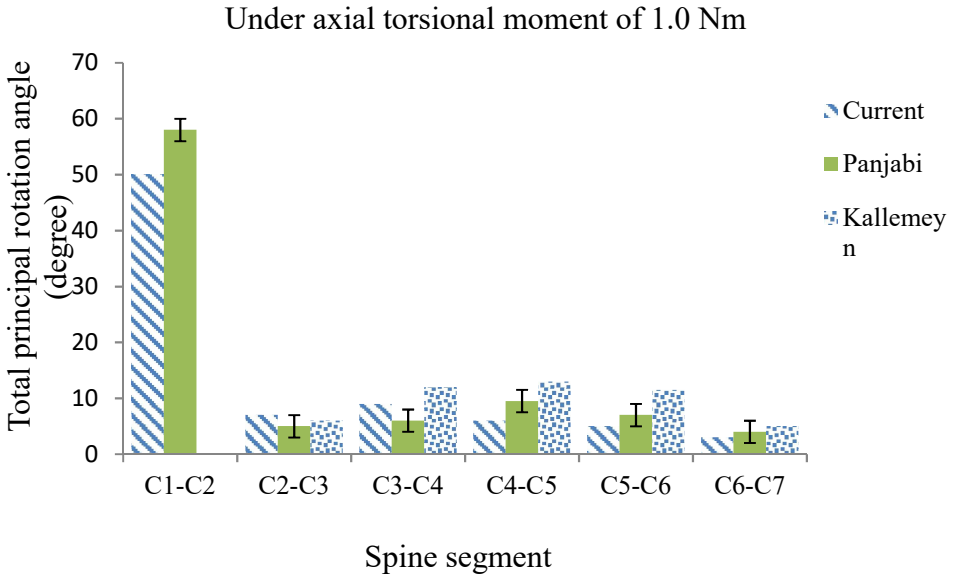

Figure 4.22. Comparison between current FEA results and experimental results under axial torsional moment.

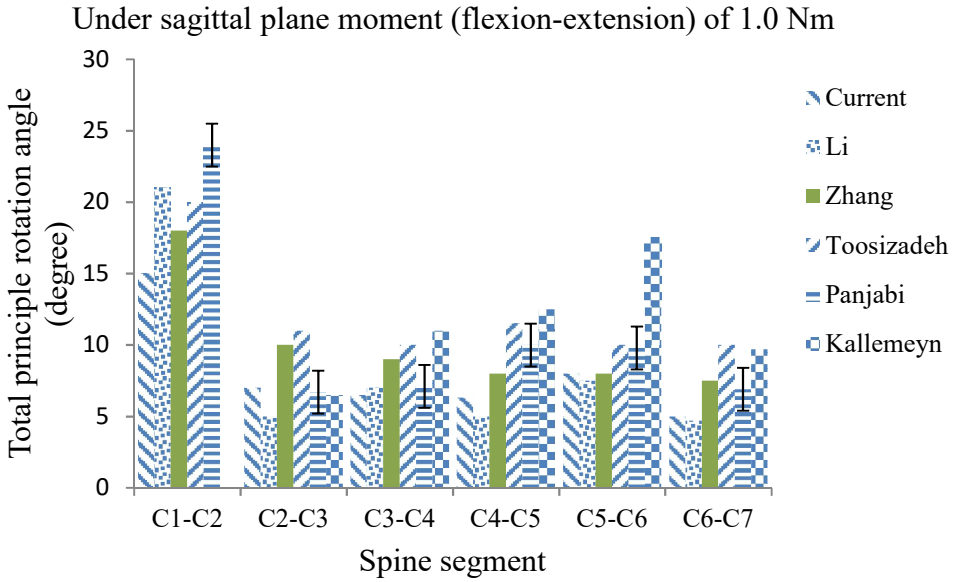

Figure 4.23. Comparison between current FEA results, literature FEA results, and experimental results under flexion-extension moment.

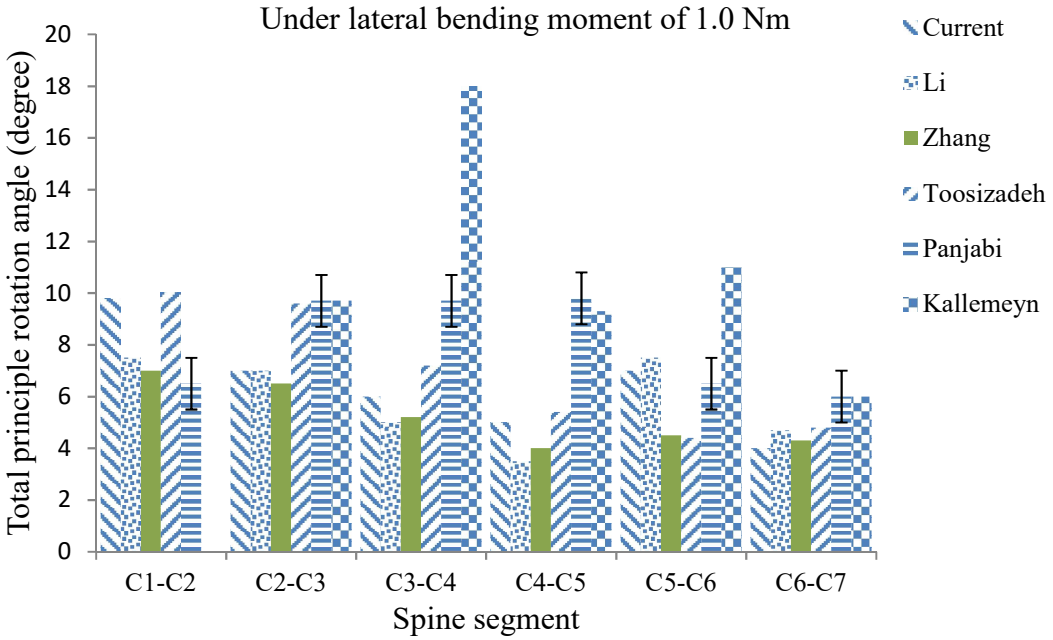

Figure 4.24. Comparison between current FEA results, literature FEA results, and experimental results under lateral bending moment.

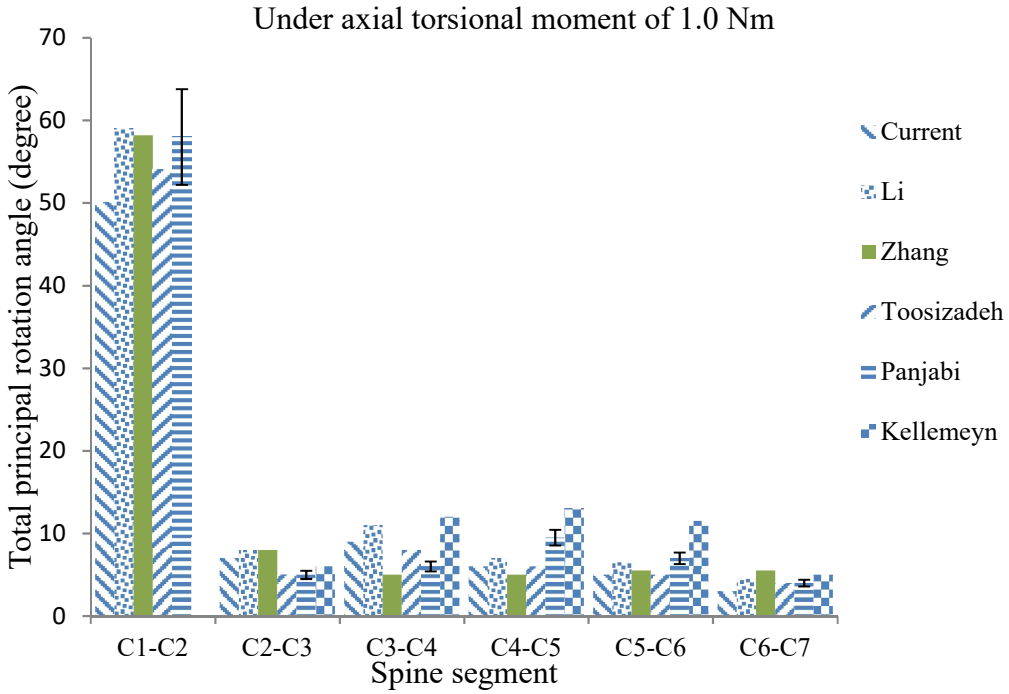

Figure 4.25. Comparison between current FEA results, literature FEA results, and experimental results under axial torsional moment.

4.3. DEGEN Model

4.3.1. Solid geometry

In a spine in which DDD presents, all the tissues in the spine are assumed to be in the same state as those in a normal spine, except for the disc that is affected by this pathology. Thus, in the present work, the first step in building the solid model was to build a degenerated disc at C5-C6 and then to assemble it with the solid models of the other tissues as taken from the INTACT Model (Figure 4.26). With moderate DDD, the changes in the disc are: 1) 30% reduction in the anterior height and 2) 41% reduction in the posterior height [18]. The solid model of the disc was built using these reduced heights (Figure 4. 27-Figure 4.30). Comparison of the heights in a degenerated and healthy disc at C5-C6 is shown in Figure 4.31.

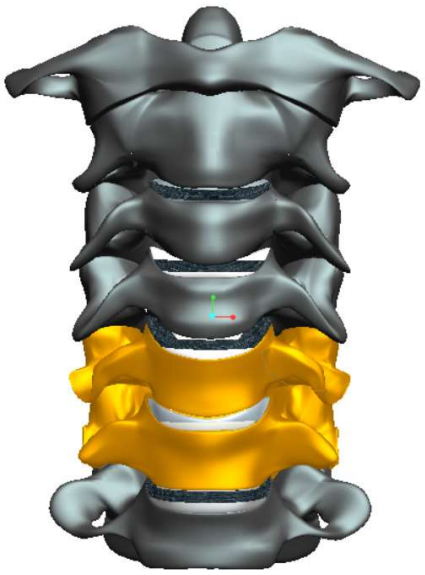

Figure 4.26. Solid model of Degenerated Model.

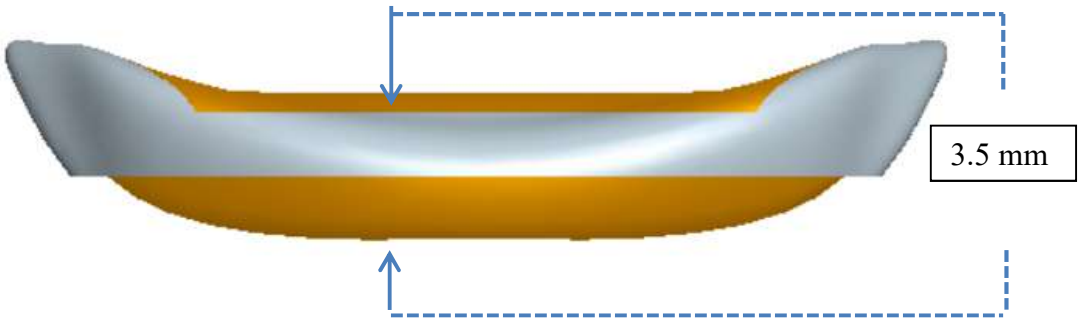

Figure 4.27. Anterior view of degenerated disc at C5-C6.

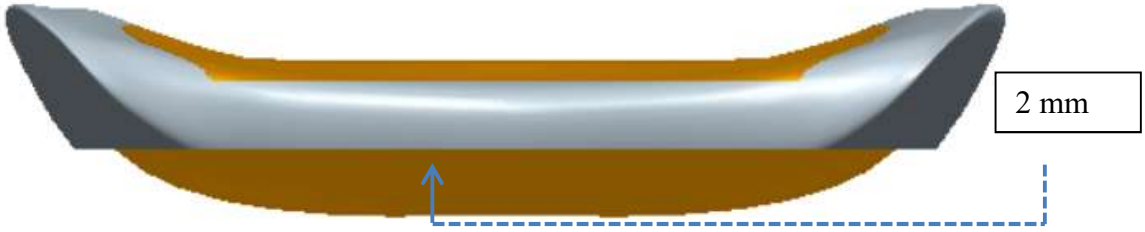

Figure 4.28 Posterior view of degenerated disc at C5-C6.

Figure 4.29. Left view of degenerated disc at C5-C6.

Figure 4.30. Left view of healthy disc at C5-C6.

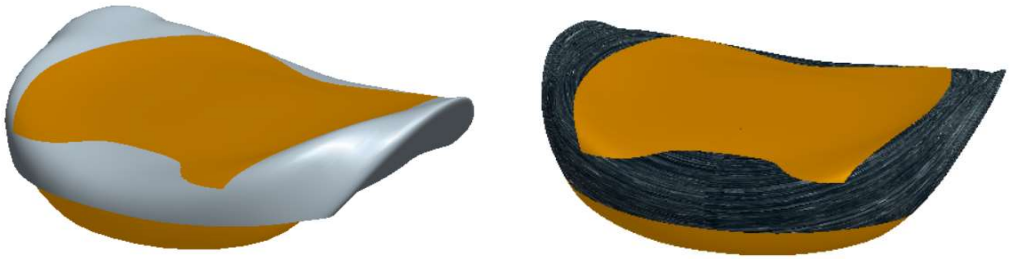

(a) (b)

Figure 4.31. 3D solid models of disc at C5-C6: degenerated (a) and healthy (b).

After the final solid model of the spine that included the degenerated disc at C5-C6 was built, it was meshed, using the same method as was done for INTACT Model. Comparison between the final meshed INTACT Model, in which the disc at C5-C6 is not degenerated, and the final meshed DEGEN Model, in which the C5-C6 is degenerated is shown in Figure 4.32 and 4.33.

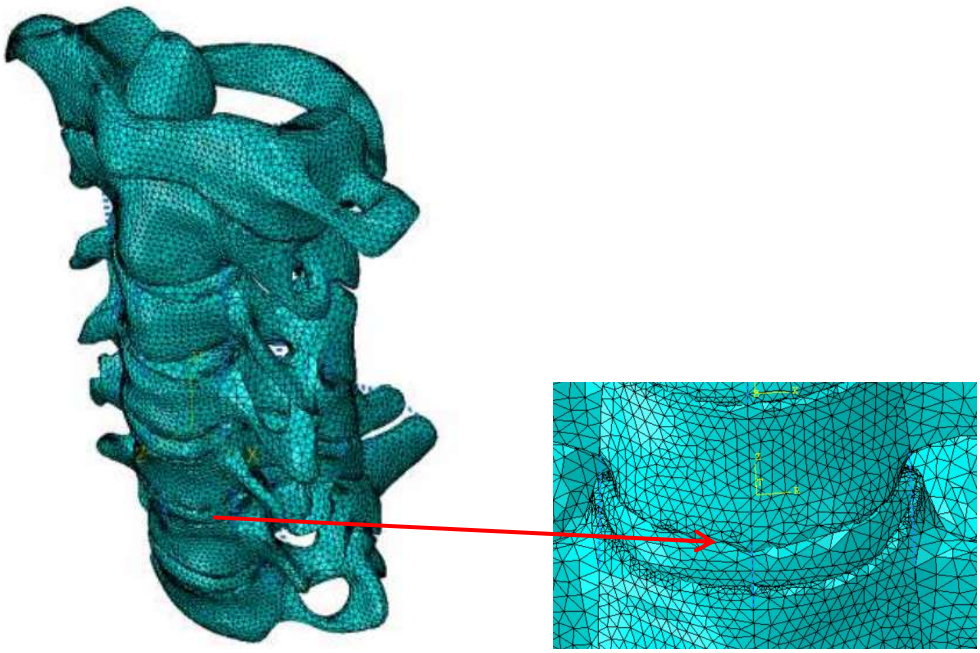

Figure 4.32. C5-C6 disc in the final meshed INTACT Model.

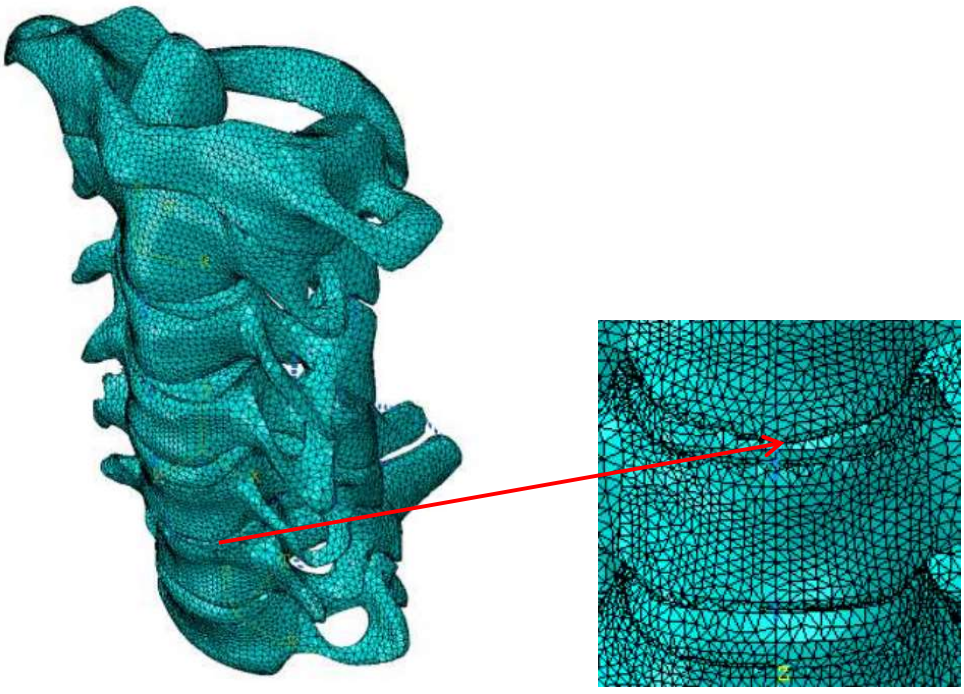

Figure 4.33. C5-C6 disc in final meshed DEGEN Model.

The FEA was run using the same constraints, applied loadings, and values of materials as were used in running INTACT Model, except that the modulus of elasticity

of the ground substance was changed to 8.4 MPa and the modulus of elasticity of the nucleus pulposus was changed to 10 MPa. Both of these changes were obtained from information given in the literature [18].

4.4. ACD Model

To build the solid model, the following changes were made to the solid models of some tissues in the INTACT Model, consistent with surgical practice: ALL was cut, the disc at C5-C6 was removed, and the endplates were cut. Then, the solid models of the remaining tissues were re-assembled, to obtain the final solid model (Figure 4.34). The solid model was meshed using the same method as was used for INTACT Model.

For the FEA, the constraint, applied loadings, and material properties were all the same as those used in the analysis of INTACT Model, except for the deletion of the material properties for ALL, the endplates at C5-C6, the annulus fibrosus at C5-C6, and the nucleus pulposus at C5-C6 (Figure 4.35).

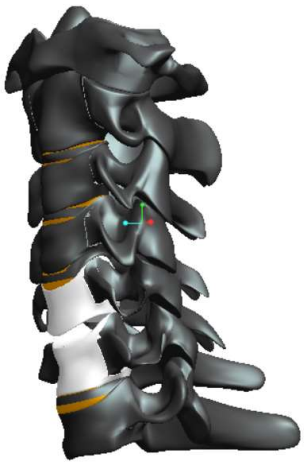

Figure 4.34. Schematic drawing of ACD solid model.

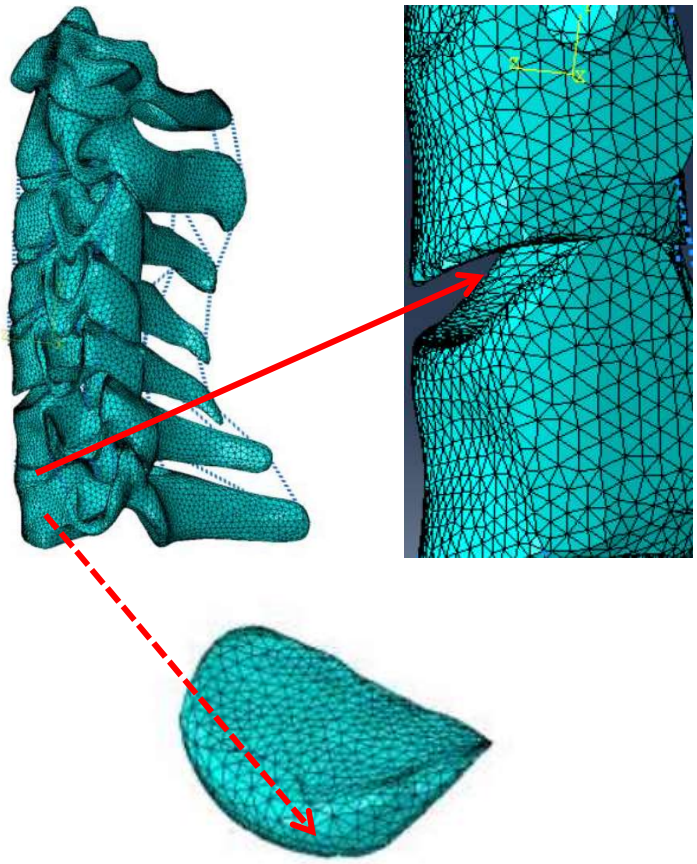

Figure 4.35. The meshed ACD solid model.

4.5. ACDF Model

To build the solid model, the following changes were made to the solid models of some tissues in the INTACT Model, consistent with surgical practice: ALL was cut, the disc at C5-C6 was removed, and the endplates were cut. A solid model of the bone graft was built. Then, that model and the solid models of the other tissues were re-assembled, forming the final solid model (Figure 4.36). Then, the solid model was meshed using the same method as was used for INTACT Model (Figure 4.37).

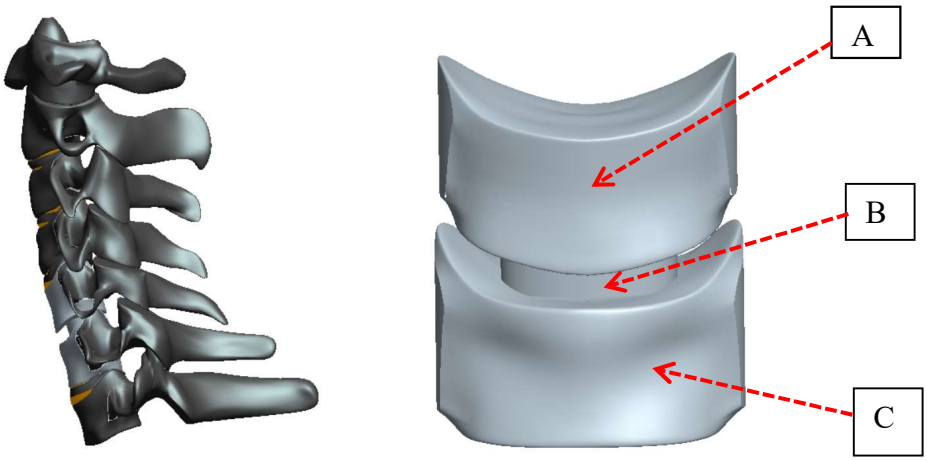

Figure 4.36. Solid model of the ACDF model.

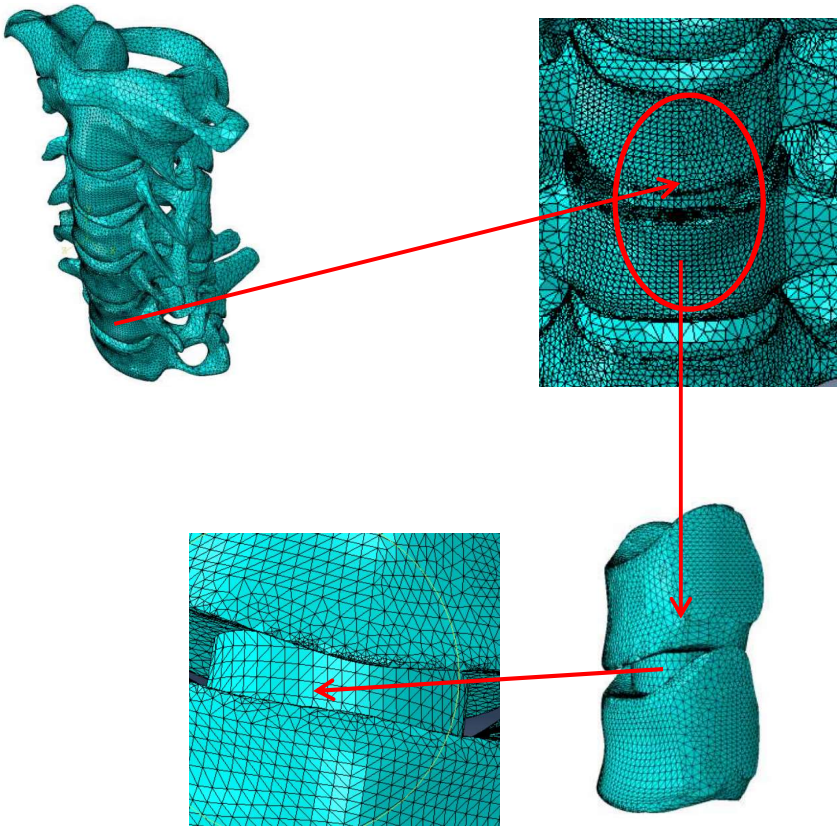

Figure 4.37. Mesh of the ACDF model.

For the FEA, the constraint, applied loadings, and material properties were all the same as those used in the analysis of INTACT Model, except for the addition of the material property values for the bone graft and deletion of the material properties for ALL, the endplates at C5-C6, the annulus fibrosus at C5-C6, and the nucleus pulposus at C5-C6.

4.6. TDR Model

In the present work, the TDR design used was a notional one, with the trays and pegs considered made of a Co-Cr-Mo alloy and the hemispherical dome considered made from ultra-high-molecular-weight polyethylene (UHMWPE) (Figure 4.38).

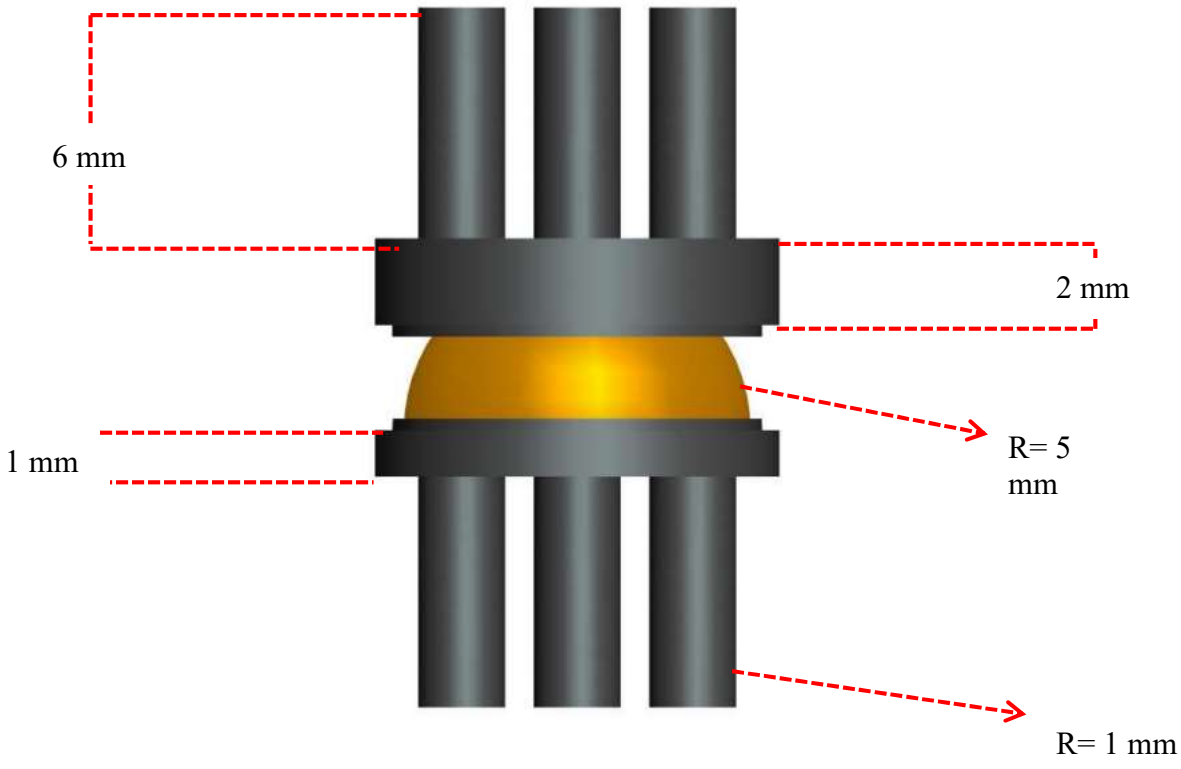

Figure 4.38. A view of the notional TDR design.

To build the solid model, the following changes were made to the solid models of some tissues in the INTACT Model, consistent with surgical practice: ALL was cut, the disc at C5-C6 was removed, and the endplates were cut. A solid model of the TDR design was built. Then, that model and the solid models of the other tissues were re-assembled, forming the final solid model (Figure 4.39 and 4.40). Then, the solid model was meshed using the same method as was used for INTACT model (Figure 4.41 and 4.42).

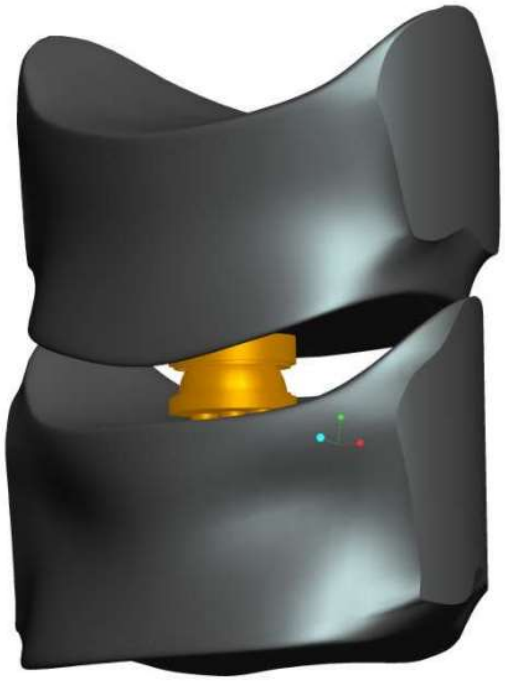

Figure 4.39. Assembled solid model of the C5-C6 notional spinal unit, with the implanted notional TDR design.

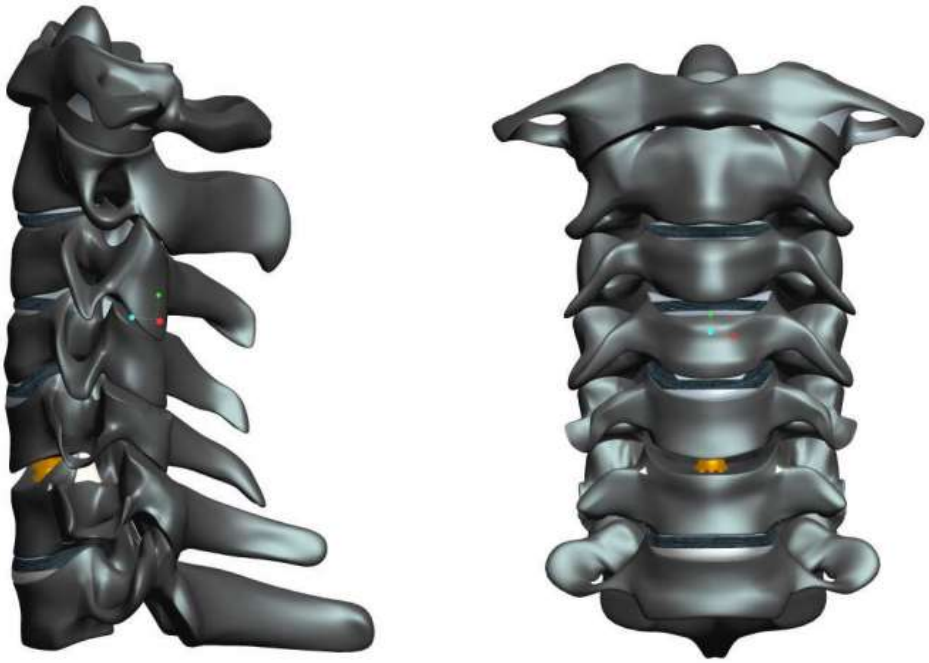

Figure 4.40. Two views of the solid TDR Model.

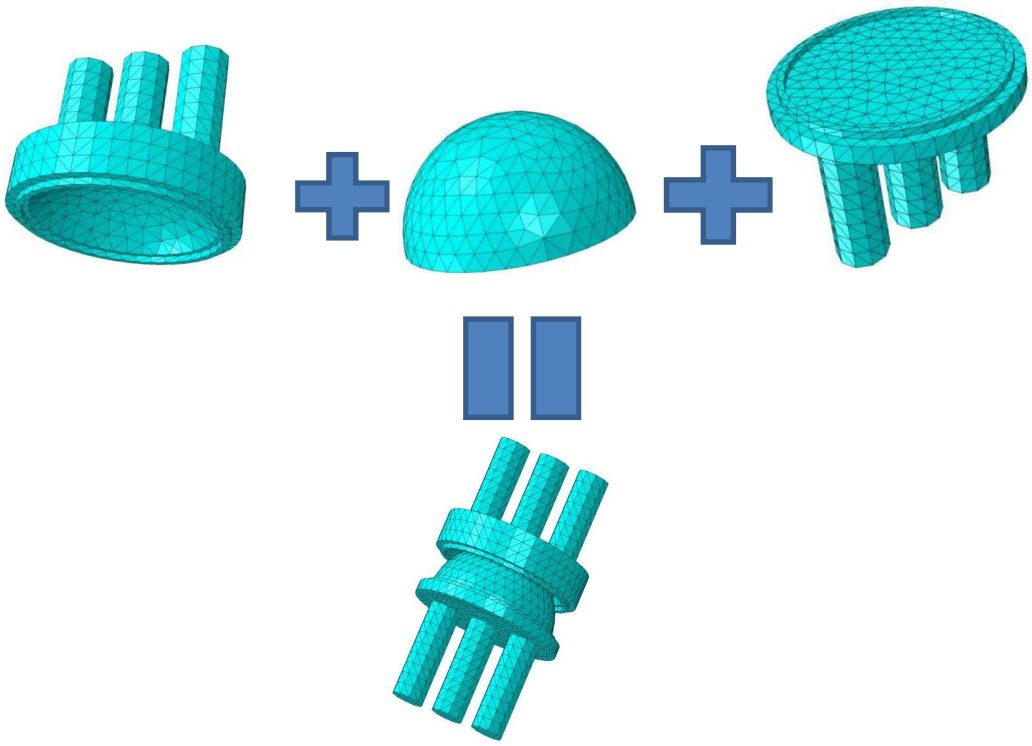

Figure 4.41. The meshed individual parts of the notional TDR design and of the assembly.

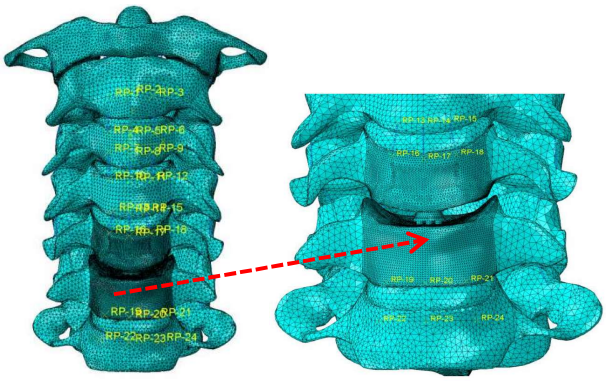

Figure 4.42. The meshed TDR Model.

A summary of the mesh densities (numbers of elements and nodes) in the final FE models is presented in Table 4.3.

Table 4.3. Summary of the final mesh densities for the finite element models

Model	Final number of elements	Final number of nodes
INTACT	421,160	89,161
DEGEN	420,801	88,021
ACD	413,107	86,868
ACDF	446,567	92,425
TDR	704,202	105,242

For the FEA, the constraint, applied loadings, and material properties were all the same as those used in the analysis of INTACT Model, except for the addition of the material property values for the parts of the TDR design (E and ν for Co-Cr-Mo alloy =

200 GPa and, 0.32, respectively, and E and ν for UHMWPE = 1 GPa and 0.49, respectively) [40] and the deletion of the material properties for ALL, the endplate, the annulus fibrosus, and the nucleus pulposus.

CHAPTER 5

RESULTS AND DISCUSSION

5.1. Compilation of results and trends in results

All of the results for all of the Models are presented in Figure 5.1- 5.6 and Tables 5.1-5.6.

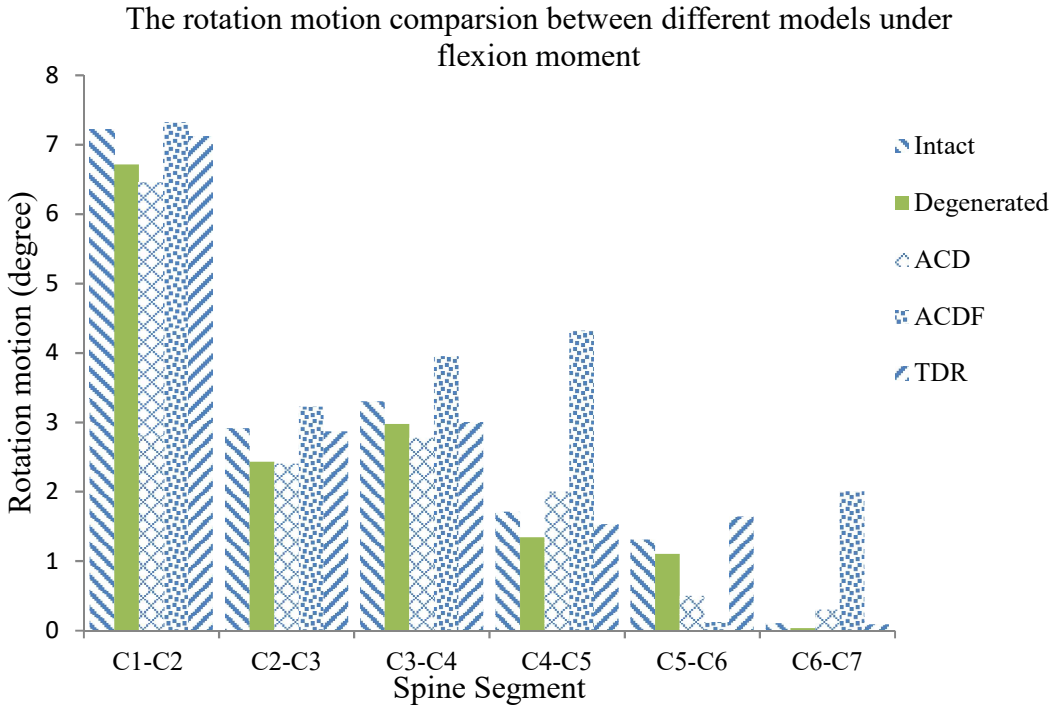

Figure 5.1. Summary the results: flexion moment.

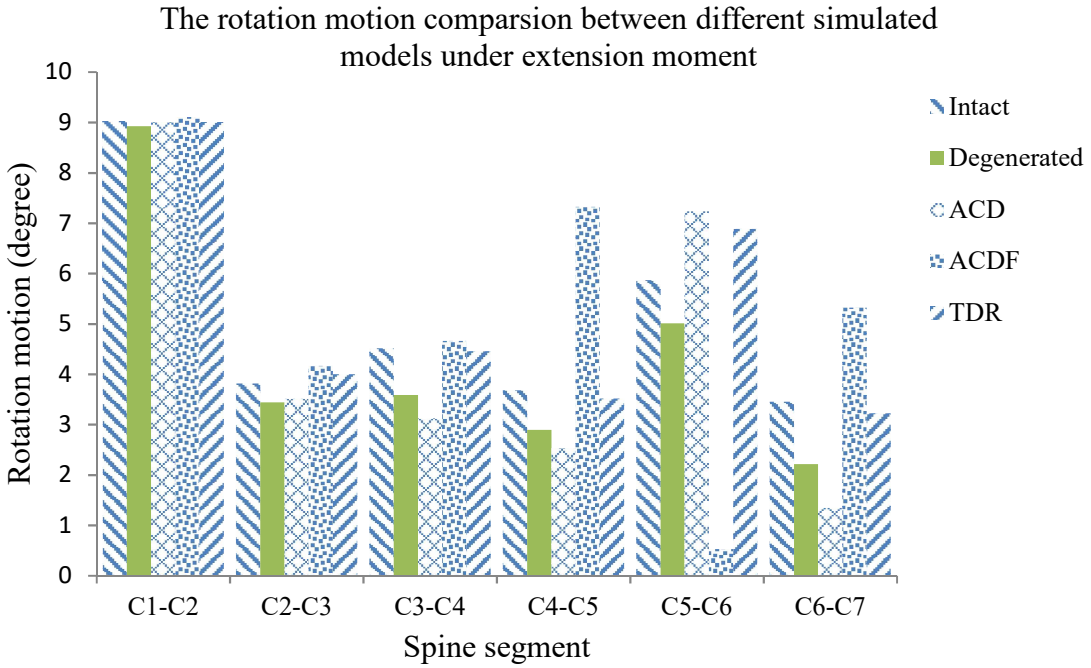

Figure 5.2. Summary of the results: extension moment.

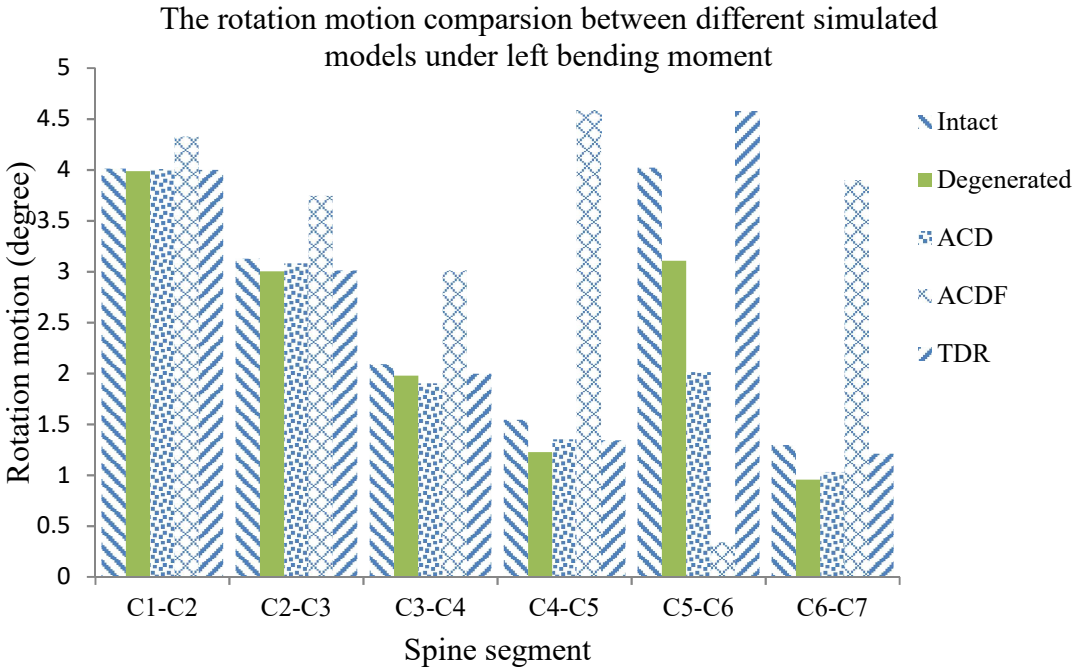

Figure 5.3. Summary the results: counter-clockwise (left) lateral bending moment.

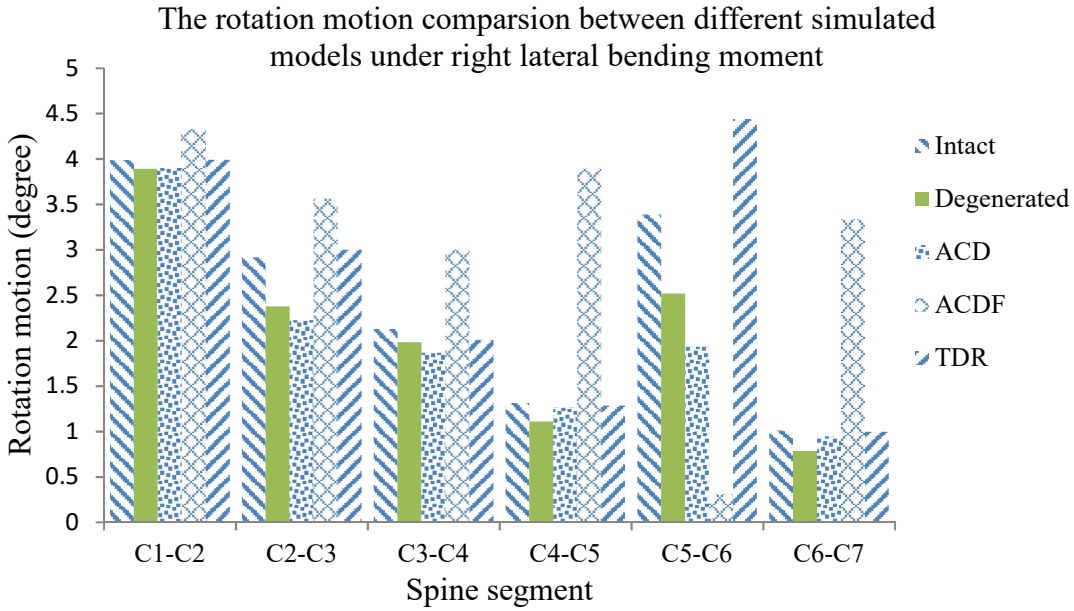

Figure 5.4. Summary of the results: clockwise (right) lateral bending moment.

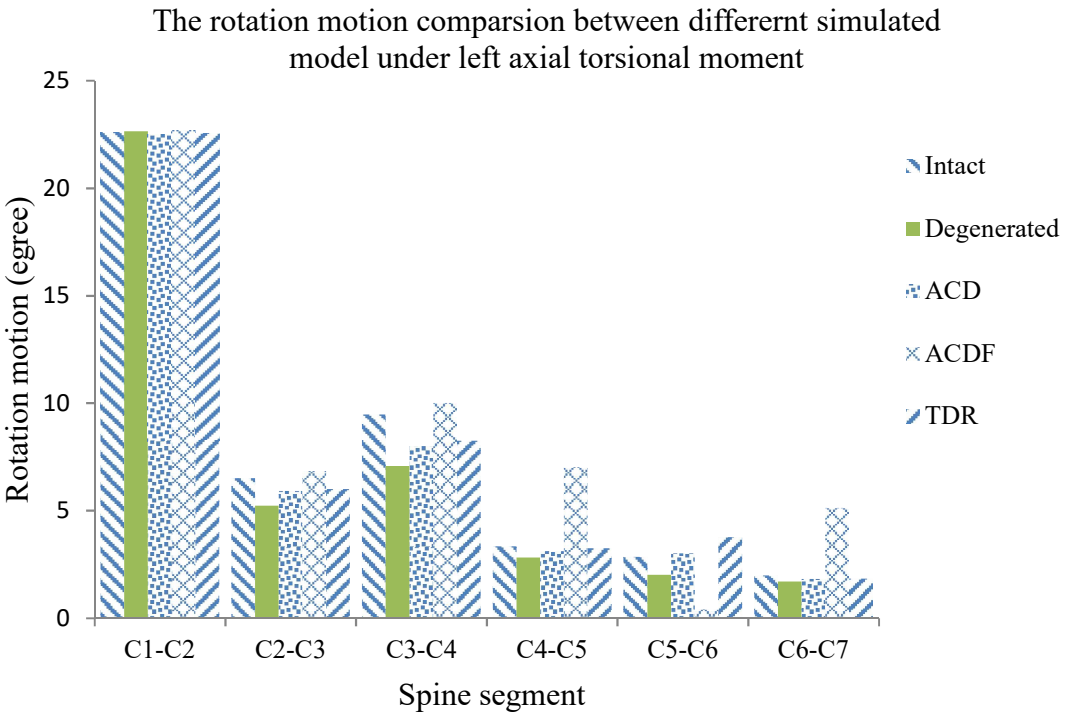

Figure 5.5. Summary the results: counter-clockwise (left) axial torsional moment.

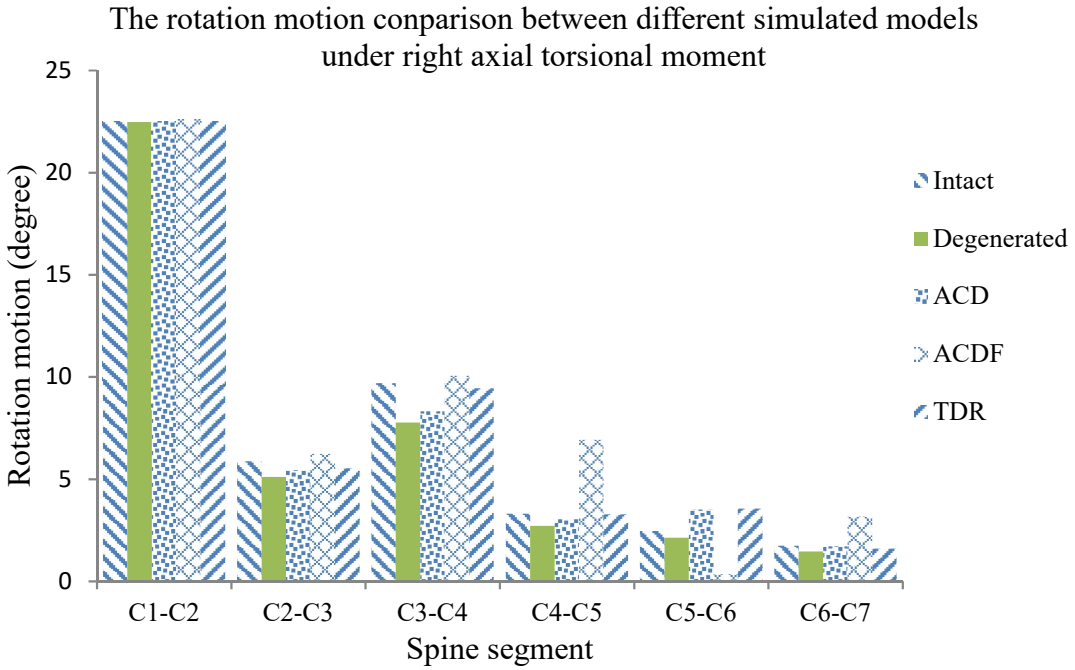

Figure 5.6. Summary the results: clockwise (right) axial torsional moment.

These results are re-presented as percentage change in rotation motion, relative to the corresponding value when INTACT Model was used (Figure 5.7 - 5.12 and Tables 5.1 – 5.6).

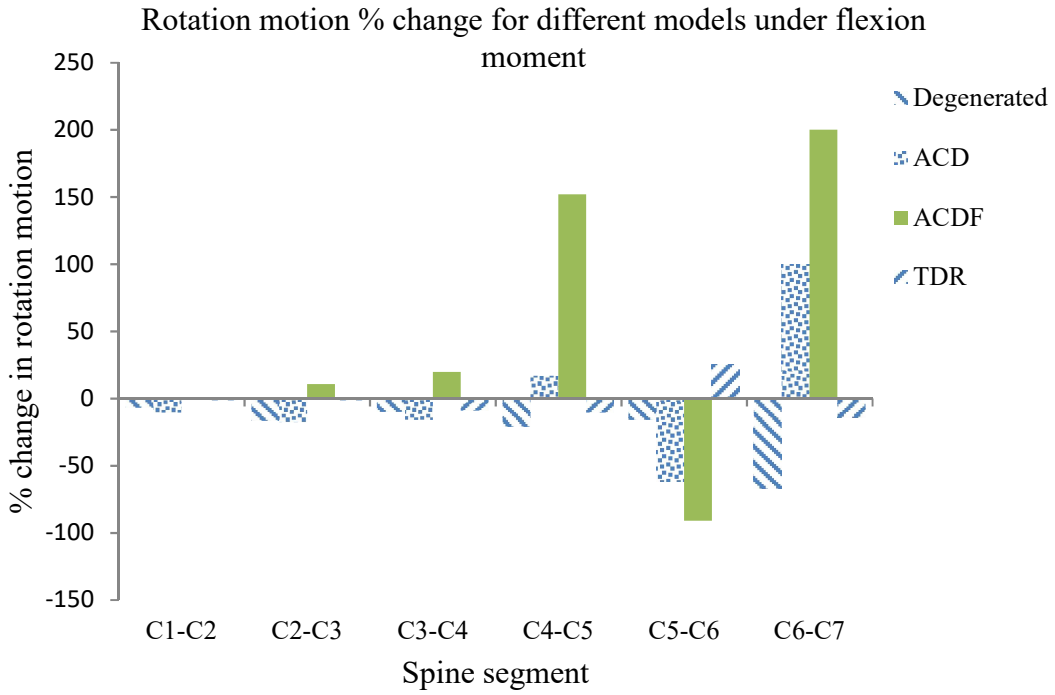

Figure 5.7. Summary of percentage change in rotation motion: combined loading of 1 Nm flexion moment + 73.6 axial compression force.

Table 5.1. Summary of % change in rotation motion results under flexion moment.

Model	C1-C2 (%)	C2-C3 (%)	C3-C4 (%)	C4-C5 (%)	C5-C6 (%)	C6-C7 (%)
Degenerated	-7	-16.6	-10	-21.3	-16	-67
ACD	-10.6	-17.6	-16	17	-62	100
ACDF	1	10.6	19.7	152	-91	200
TDR	-1.5	-1.5	-9.1	-10.4	25	-13.7

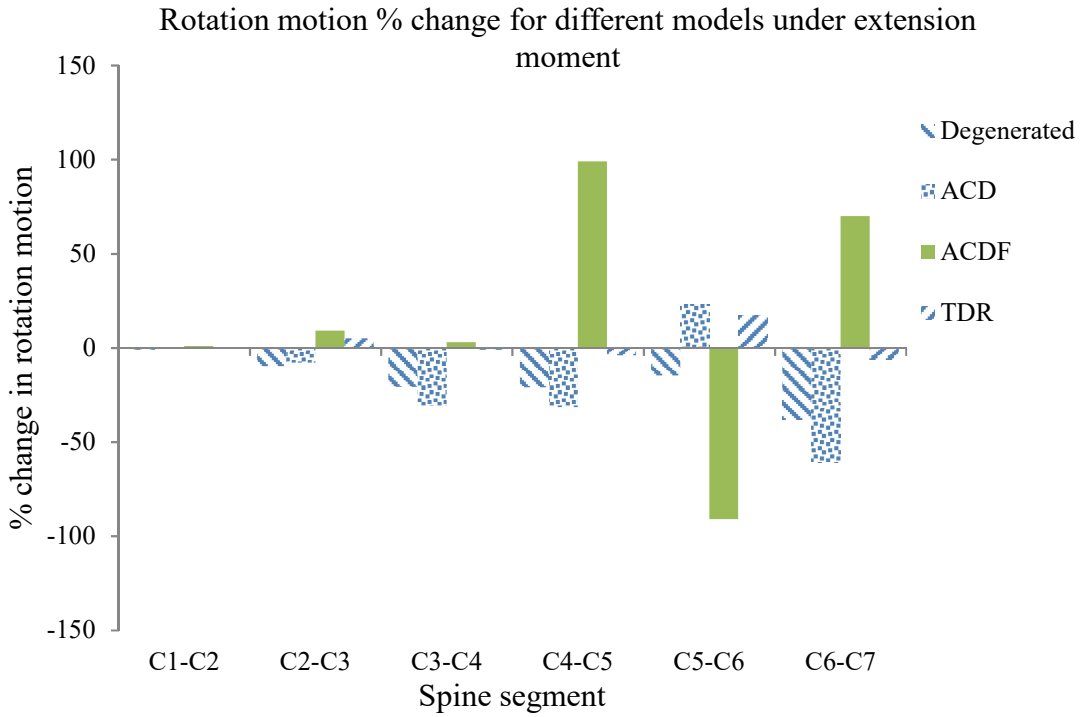

Figure 5.8. Summary of the percentage change in rotation motion: combined loading of 1 Nm extension moment + 73.6 N axial compression forces.

Table 5.2. Summary of % change in rotation motion results under extension moment.

Model	C1-C2 (%)	C2-C3 (%)	C3-C4 (%)	C4-C5 (%)	C5-C6 (%)	C6-C7 (%)
Degenerated	-1	-9.7	-20.5	-21	-14.7	-38.2
ACD	-0.1	-7.9	-30.7	-31.4	23.2	-61.1
ACDF	1	9.2	3	99	-91	70
TDR	-0.4	5	-1	-4	17.2	-6

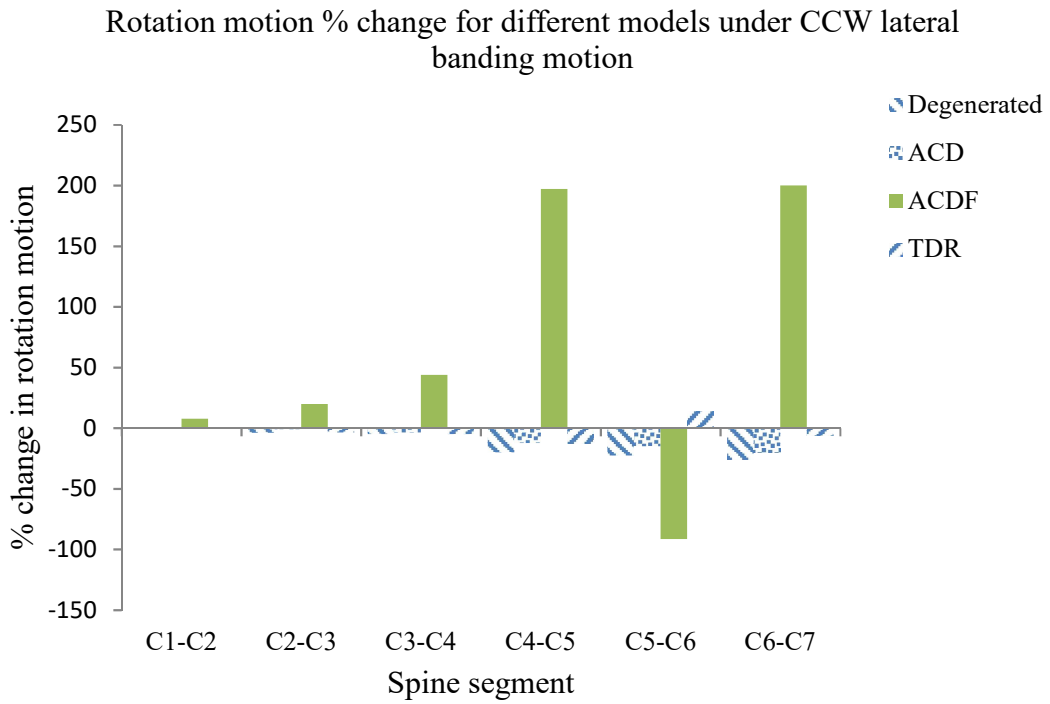

Figure 5.9. Summary of percentage change in rotation motion: combined loading of 1 Nm counter-clockwise lateral bending moment + 73.6 N axial compression forces.

Table 5.3. Summary of % change in rotation motion results under left lateral bending moment.

Model	C1-C2 (%)	C2-C3 (%)	C3-C4 (%)	C4-C5 (%)	C5-C6 (%)	C6-C7 (%)
Degenerated	-0.7	-4	-5	-20	-22.7	-26.3
ACD	-0.3	-1	-4	-12.3	-15	-20.3
ACDF	7.8	20	44	197	-91.4	200
TDR	-0.3	3.7	-5	-13	13.6	-6.5

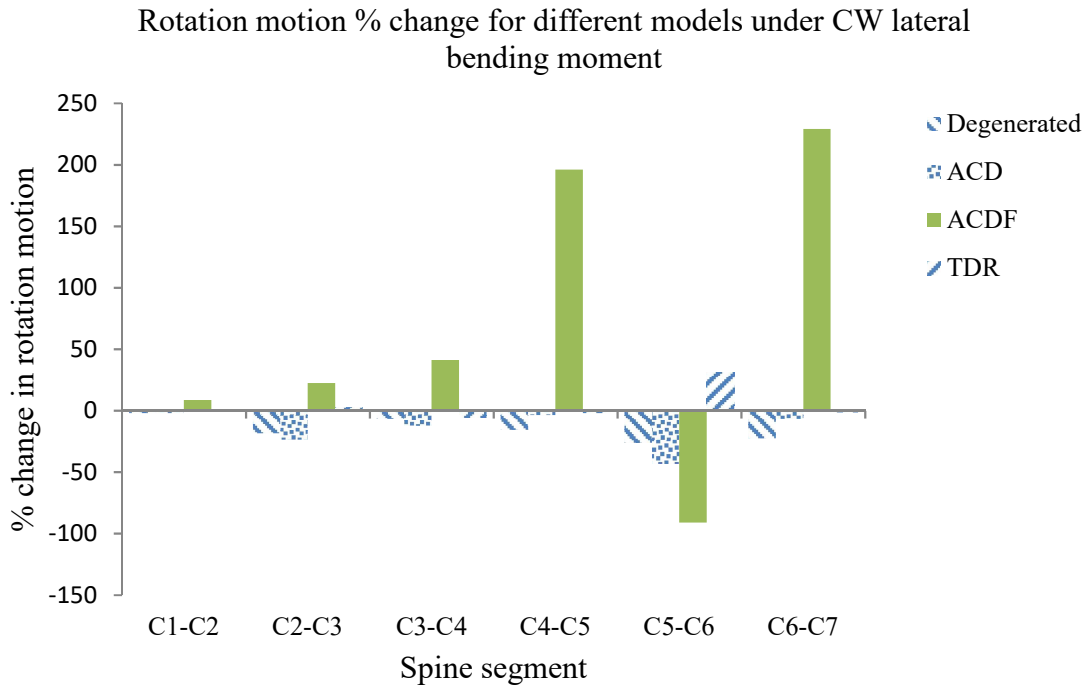

Figure 5.10. Summary of percentage change in rotation motion: combined loading of 1 Nm clockwise lateral bending moment + 73.6 N axial compression forces.

Table 5.4. Summary of % change in rotation motion results under right lateral bending motion.

Model	C1-C2 (%)	C2-C3 (%)	C3-C4 (%)	C4-C5 (%)	C5-C6 (%)	C6-C7 (%)
Degenerated	-2	-18.4	-6.7	-15.6	-25.7	-22.6
ACD	-2	-23.7	-12.2	-3.6	-43	-6.7
ACDF	8.5	22.3	41.2	196	-91	229
TDR	0.2	3	-5.6	-2	31	-1.4

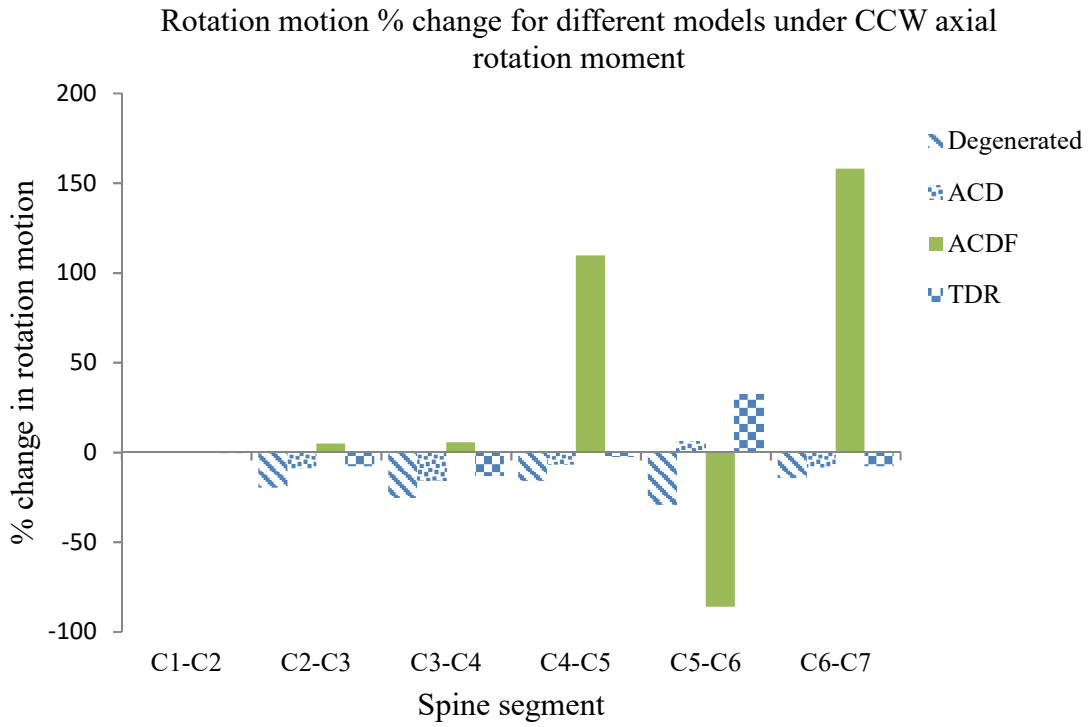

Figure 5.11 Summary of percentage change in the rotation motion: combined loading of 1 Nm counter-clockwise axial rotation moment + 73.6 N axial compression forces.

Table 5.5. Summary of % change in rotation motion results under left axial rotation motion.

Model	C1-C2 (%)	C2-C3 (%)	C3-C4 (%)	C4-C5 (%)	C5-C6 (%)	C6-C7 (%)
Degenerated	0.3	-19.7	-25.3	-15.7	-29	-14.4
ACD	-0.28	-9	-15.6	-6.8	6	-8.5
ACDF	0.46	5	5.6	109.7	-86	158
TDR	-0.35	-7.7	-12.9	-2.6	32.4	-7.8

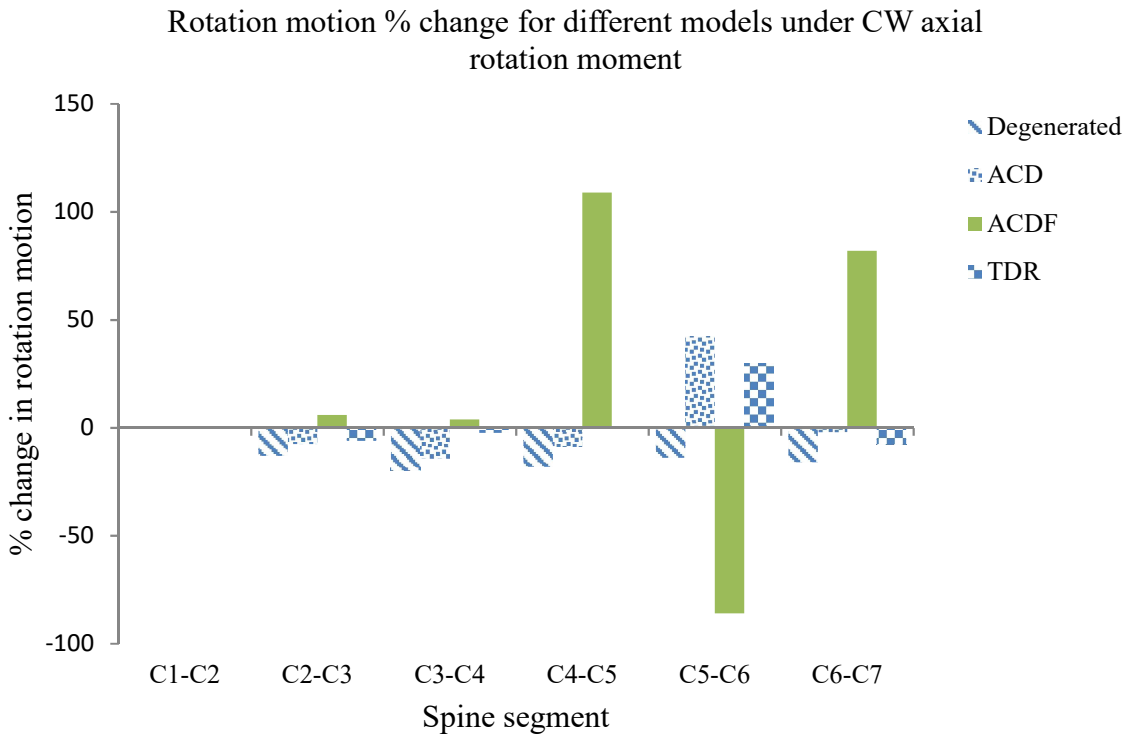

Figure 5.12. Summary of percentage change in rotation motion: combined loading of 1 Nm clockwise axial rotation moment + 73.6 N axial compression forces.

Table 5.6. Summary of % change in rotation motion results under right axial rotation motion.

Model	C1-C2 (%)	C2-C3 (%)	C3-C4 (%)	C4-C5 (%)	C5-C6 (%)	C6-C7 (%)
Degenerated	-0.3	-13.1	-19.8	-18	-13.9	-16
ACD	0.1	-7.5	-14.1	-8.9	42.1	-2
ACDF	0.5	6	3.8	109	-86	82
TDR	0.5	-6	-2.4	-0.1	30	-7.8

In Tables 5.7-5.12 are summarized, at each of the levels of the spine model, the FE model that produced the smallest percentage in rotation motion (relative to the corresponding value in the INTACT Model).

Table 5.7. The smallest rotation motion percentage change value for C1-C2 level under different models.

Loading	Model
Flexion	ACDF
Extension	ACD
Left lateral bending	ACD
Right lateral bending	TDR
CCW axial rotation	ACD
CW axial rotation	ACD

Table 5.8. The smallest rotation motion percentage change value for C2-C3 level under different models.

Loading	Model
Flexion	TDR
Extension	TDR
Left lateral bending	ACD
Right lateral bending	TDR
CCW axial rotation	ACDF
CW axial rotation	TDR

Table 5.9. The smallest rotation motion percentage change value for C3-C4 level under different models.

Loading	model
Flexion	TDR
Extension	TDR
Left lateral bending	ACD
Right lateral bending	TDR
CCW axial rotation	ACDF
CW axial rotation	TDR

Table 5.10. The smallest rotation motion percentage change value for C4-C5 level under different models.

Loading	Model
Flexion	ACD
Extension	TDR
Left lateral bending	ACD
Right lateral bending	TDR
CCW axial rotation	TDR
CW axial rotation	TDR

Table 5.11. The smallest rotation motion percentage change value for C5-C6 level under different models.

Loading	model
Flexion	DEG
Extension	DEG
Left lateral bending	TDR
Right lateral bending	DEG
CCW axial rotation	ACD
CW axial rotation	TDR

Table 5.12. The smallest rotation motion percentage change value for C6-C7 level under different models.

Loading	Model
Flexion	TDR
Extension	TDR
Left lateral bending	TDR
Right lateral bending	TDR
CCW axial rotation	TDR
CW axial rotation	ACD

To summarize, in Tables 5.7 – 5.12, the TDR Model appears 20 times, the ACD Model appears 10 times, and ACDF Model and DEG Model each appear 3 times. Thus, the TDR Model gives the best overall results.

5.2. Comparison of present results and results in relevant literature studies

Relevant literature studies are considered those that have two characteristics. First, the FEA was of a model of the intact spine section and a minimum of two of the three surgical simulation models utilized in the present work. Second, ROM results were obtained under a variety of applied loadings. By this definition, to the best of the present worker's knowledge, the only relevant literature studies are those by Mo et al. [62] and Faizan et al. [57].

Mo et al. [62] used a C3-C7 model and simulated ACDF and TDR at C5-C6 and applied a loading of 73.6 N preload + 1.8 Nm moments on C3. A comparison of Mo et al.'s ROM results and corresponding ones from the present study (Figure 5.13) shows that, at C5-C6, the two sets of results for an ACDF model are similar but the TDR model results given by Mo et al. are higher than those obtained in the present work.

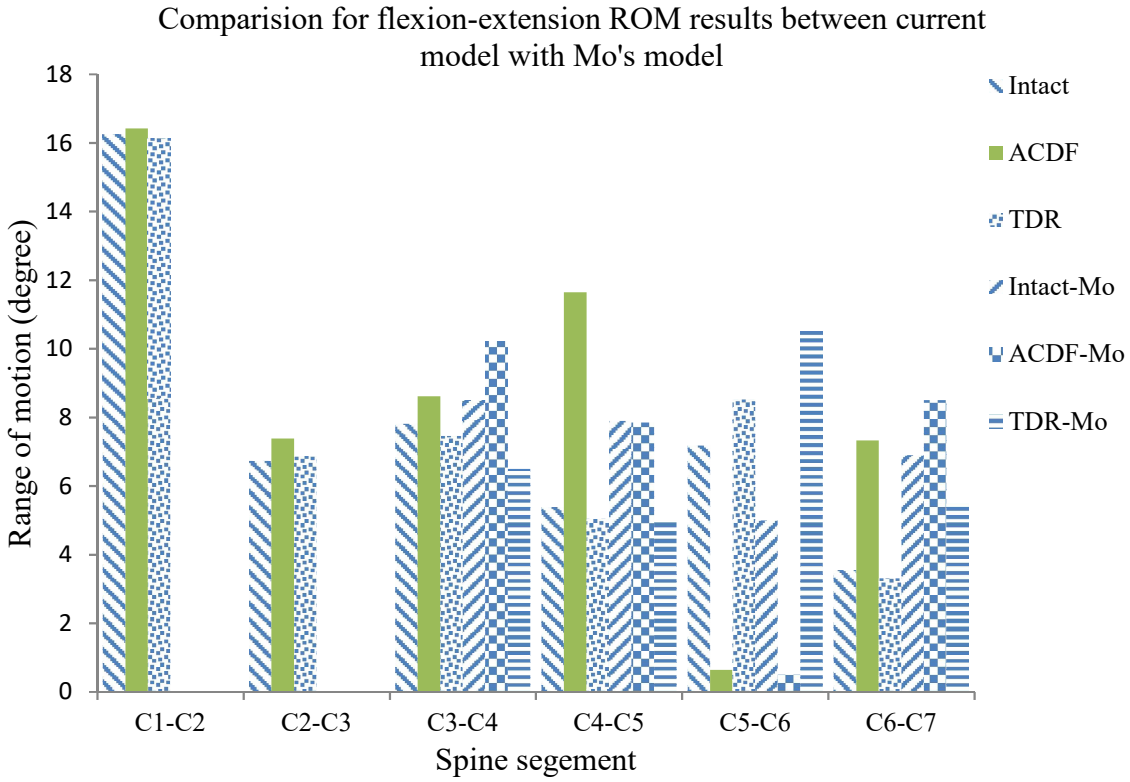

Figure 5.13. Comparison of current Intact, ACDF and TDR Model results and results of Mo et al. [40] for intact, ACDF and TDR models, under flexion-extension motion.

Fazian et al. [57] used a C3-C7 model and simulated ACDF and TDR at two levels, namely, C4-C5 and C5-C6, and applied a loading of 73.6 N + 2.0 Nm moment on C3. A comparison of Faizan et al.'s ROM results and corresponding ones from the present study (Figure 5.14) shows that, at C5-C6, Faizan et al.'s ROM results for an ACDF model are higher than those obtained in the present work, regardless of the type of applied loading. The same trend is seen for the ROM results for a TDR model. These trends are to be expected given that, in the present work, surgical treatment was simulated at one level but, in Faizan et al.'s study, simulation was at two levels.

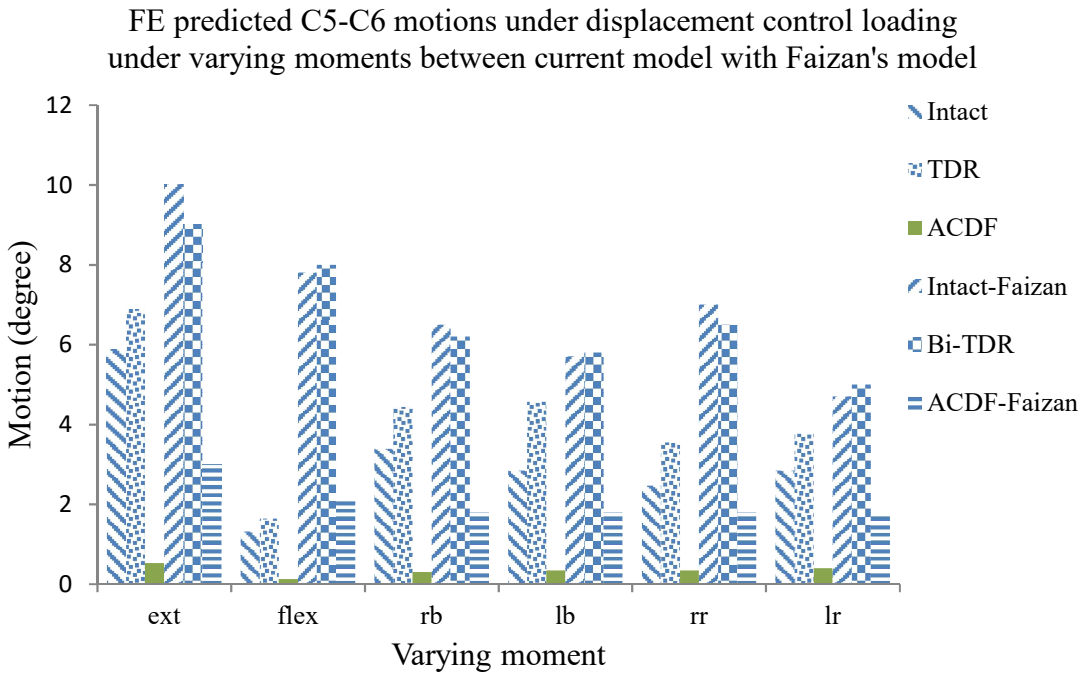

Figure 5.14. Comparison of current Intact, ACDF and TDR Model results and results of Faizan et al. [57] for intact, ACDF and TDR models, under hybrid loading motion.

5.3. Relation of results to clinical experience

The present results show that, from the perspective of kinematics, TDR is preferred to ACD and ACDF. This finding is consistent with results of clinical and patient outcomes (such as Neck Disability Index score, pain score, neurological parameters, number of secondary surgical procedures, flexion-extension range of motion, and number of adverse device-related events) from studies in which ACDF and an approved TDR design (Bryan® or Prestige® LP or ProDisc-C®) were compared in the treatment of symptomatic degenerative disc disease at one level (C3-C4 or C4-C5 or C5-C6 or C6-C7) in patient-matched cohorts [58-60].

5.4. Limitations

The present study has a number of limitations. First, the muscles of the cervical spine were not included in the solid model. The important role played by muscle forces in spinal motions is well recognized [61]. However, this aspect is particularly important when dynamic or impact loading is applied. In the present study, the loading was quasi-static. Second, in the solid model, the facet joints were included as part of the posterior bony elements, rather than as separate entities. Third, the solid model was built using data taken from one person and, as such, it is unknown if the results obtained have generality. This problem could be overcome by using a parametric modeling method [23] or a parametric and patient-specific modeling method [14]. Fourth, the FEA was carried out using quasi-static loads, rather than dynamic loads, which are imposed on the cervical spine during a number of activities of daily living.

CHAPTER 6

CONCLUSIONS AND RECOMMENDATIONS FOR FUTURE STUDY

The following are the conclusions of the study:

- The present intact full cervical spine (C1-C7) finite element model was validated. Thus, it was justified to build the solid models of each the other four cases studied from the solid model of the intact case.

- After moderate degeneration was simulated in the intervertebral disc at the C5-C6 level, the rotation motion at that level as well at each of the other levels decreased (relative to the corresponding value in the intact model), regardless of the type of applied loading used. The extent of decrease ranged from~ 0.3% to ~38%.

- When all the rotation motion results obtained at all of the applied loadings used were considered, the smallest change in rotation motion, relative to the corresponding value in the intact model, was obtained when the TDR model was used. This point to the possibility that TDR is preferable to either ACD or ACDF.

The following are the recommendations made for future study.

- The solid model of the intact case (and, hence, of each of the other four cases studied) should be modified in a number of ways, such as inclusion of all the muscles in the cervical spine and inclusion of facets as a separate entity.

- It should be recognized that the annulus fibrosus and nucleus pulposus are viscoelastic materials. As such, in the finite element analysis, the material constitutive model that should be used for each of these materials is the Mooney-Rivlin formulation.

- In the finite element analysis, dynamic loadings should be applied.

REFERENCES

[1] Lei ZP, Ji XW, Li N, Yang JZ. Simulated effects of head movement on contact pressures between head forms and N95 filtering face piece respirators-part 1: head form model and validation. Ann Occup Hyg;2014:1–11.

[2] Wikipedia, “Human vertebral Colum”. Retrieved from: http://en.wikipedia.org/wiki/Human_vertebral_column.

[3] “Ligaments”. Retrieved from: http://www.spineuniverse.com/anatomy/ligaments.

[4] Spinal Muscles: A Comprehensive Guide. Retrieved from: http://www.spineuniverse.com/anatomy/spinal-muscles-1.

[5] “Spine-health”. Retrieved from: http://www.spine-health.com/conditions/spine-anatomy/cervical-discs.

[6] Nandoe RDS, Bartels RHMA, Peul WC. Long-term outcome after anterior cervical discectomy without fusion. Eur Spine J 2007;16:1411-16.

[7] Synthes Spine. ProDisc-C total disc replacement patient information. 2008.

[8] Caruso R, Pesce A, Marrocco L, Wierzbicki L. Anterior approach to the cervical spine for treatment of spondylosis or disc herniation: Long-term results. Comparison between ACD, ACDF, TDR. Clin Ter 2014;165:263-70.

[9] Hoston Methodist Orthopedics & Sports Medicine. Cervical Artifical Disc Replacement. Retrieved from: http://www.methodistorthopedics.com/cervical-artificial-disc-replacement.

[10] “Spinal fusion”. Retrieved from: https://en.wikipedia.org/wiki/Spinal_fusion.

[11] Wheeldon JA, Stemper BD, Yoganandan N, and Pintar FA. Validation of a finite element model of the young normal lower cervical spine. Biomed Eng 2008;36: 1458–69.

[12] Beltran-Fernandez JA, Hernandez-Gomez LH, Rodriguez-Canizo RG, Merchan-Cruz EA, Urriolagoitia-Calderon G, Gonzalez-Rebatu A, Dufoo-Olvera M and Urriolagoitia-Sosa G. Modelling of a cervical plate and human cervical section C3-C5 under compression loading conditions using the finite element method. Mech & Mater 2008;13-14:49-56.

[13] Panzer MB, Cronin DC. C4-C5 segemnt finite element model development, validation, and load-sharing investigation. J Biomech 2009;42:480-90.

[14] Laville A, Laporte S, Skalli W. Parametric and subject-specific finite element modeling of the lower cervical spine, Influence of geometrical parameters on the motion patterns. J Biomech 2009;42:1409-15.

[15] Hussain M, Natarajan RN, Fayyazi AH, Braaksma BR, Andersson G, An HS. Screw angulation affects bone-screw stresses and bone graft load sharing in anterior cervical corpectomy fusion with a rigid screw-plate construct: a finite element model study. Spine J 2009;9:1016-23.

[16] Faizan A, Goel VK, Garfin SR, Bono CM, Serhan H, Biyani A, Elgafy H, Krishna M，Friesem T. Do design variations in the artificial disc influence cervical spine biomechanics? A finite element investigation. Eur Spine J 2012;21:653-62.

[17] Galbusera F, Anasetti F, Bellini CM, Costa F, Fornari M. The influence of the axial, antero-posterior and lateral positions of the center of rotation of a ball-and-socket disc prosthesis on the cervical spine biomencanics. Clin Biomech 2010;25:397-401.

[18] Li Y, Lewis G. Influence of surgical treatment for disc degeneration disease at C5-C6 on changes on some biomechanical parameters of the cervical spine. Med Eng Phy 2010;32:595-603.

[19] Kang H, Park P, Marca LF, Hollister SJ, Lin CY. Analysis of load sharing on uncovertebral and facet joints at the C5-6 level with implantation of the Bryan, Prestige LP, or ProDisc-C cervical disc prosthesis: an in vivo image-based finite element study. Neu Foc 2010;28:1-8.

[20] Kallemeyn N, Gandhi A, Kode S, Shivanna K, Smucker J ,Grosland N. Validation of a C2-C7 cervical spine finite element model using specimen-specific flexibility data. Med Eng Phy 2010;32:482-9.

[21] Faizan A, Goel VK, Biyani A, Garfin SR, Bono CM. Adjacent level effects of bi level disc replacement, bi level fusion and disc replacement plus fusion in cervical spine-a finite element based study. Clin Biomech 2012;27:226-33.

[22] Toosizadeh N, Haghpanahi M. Generating a finite element model of the cervical spine: Estimating muscle forces and internal loads. Scientia Iranica 2011;18:1237-45.

[23] Haghpanahi M, Javadi M. A three dimensional parametric model of whole lower cervical spine (C3-C7) under flexion, extension, torsion and lateral bending. Sci Ira 2012;19:142-50.

[24] Galbusera F, Bellini CM, Raimondi MT, Fornari M, Assietti R. Cervical spinebiomechanics following implantation of a disc prosthesis. Med Eng Phy 2008;30:1127-33.

[25] Dewit JA, Cronin SD. Cervical spine segment finite element model for traumatic injury prediction. J Mech Biomed 2012;10:138-50.

[26] Hussain M, Nassr A, Natarajan RN, An HS, Andersson BJ. Corpectomy versus discectomy for the treatment of multilevel cervical spine pathology: a finite elememt model analysis. Spine J 2012;12:401-8.

[27] Hussain M, Nassr A, Natarajan RN, An HS. Biomechanics of adjacent segments after a multilevel cervical corpectomy using anterior, posterior, and combined anterior-posterior instrumentation techniques: a finite element model study. Spine J 2013;13:689-96.

[28] Erbulut DU, Zafarparandeh I, Lazoglu I, Ozer AF. Application of an asymmetric finite element model of the C2-T1 cervical spine for evaluating the role of soft tissues in stability. Med Eng Phy 2014;36:915-21.

[29] Coelhoa PG, Fernandesb PC, Folgadob J, Fernandes PR. Development of a spinal fusion cage by multiscale modelling: application to the human cervical spine. Int Con Tis Eng 2015.

[30] Penning L, Wilmink JT. Rotation of the cervical spine: a CT study in normal subjects. Spine 1987;12:732-8.

[31] Mimura M, Moriya H, Watanabe T, Takahashi K, Yamagata M, Tamaki Tl. Three-dimensional motion analysis of the cervical spine with special reference to the axial rotation. Spine 1989;14:1135-9.

[32] Aho A, Vartianen O, Salo O. Segmentary antero-posterior mobility of the cervical spine. Ann Med Int Fen 1955;44:287-99.

[33] Bhalla SK, Simmons EH. Normal ranges of intervertebral joint motion of the cervical spine. Can J Surg 1969;12:181-7.

[34] Lind B, Sihlbom H, Nordwall A, Malchau H. Normal ranges of motion of the cervical spine. Arch Phys Med Reh 1989;70:692-5.

[35] Dvorak J, Froehlich D, Penning L, Baumgartner H, Panjabi MM. Functional radiographic diagnosis of the cervical spine: flexion/extension. Spine 1988;13:748-55.

[36] “Whiplash”. Retrieved from: http://www.webmd.com/back-pain/neck-strain-whiplash.

[37] Teo EC, Ng HW. Evaluation of the role of ligaments, facets and disc nucleus in lower cervical spine under compression and sagittal moments using finite element method. Med Eng Phy 2001;23:155–64.

[38] Wilke HJ, Neef B, Hinz B, Seidel H, Claes L. Intradiscal pressure together with anthropometric data: a data set for the validation of models. Clin Biomech 2001;1:111–26.

[39] Jeon TS, Chang H, Choi BW. Current concept on the operative treatment for degenerative cervical disc disease. J Korean Med Assoc 2011;54:941-50.

[40] "Artificial disc devices". Retrieved from: https://www.google.com/search?q=bryan+disc&biw=917&bih=586&source=lnms&tbm=isch&sa=X&sqi=2&ved=0CAYQ_AUoAWoVChMIovGlhdv6yAIViFcmCh1wkwRV.

[41] Wilke HJ, Drumm J, Haussler K, Mack C, Steudel W, Kettler A. Biomechanical effect of different lumber interspinous implants on flexibility and intradiscal pressure. Eur Spine J 2008;17:1049-56.

[42] Matge G, Eif M, Herdmann J, Lowery GL. Dynamic cervical implant (DCI): clinical results from an international multicenter prospective study. Par Spine 2009;1-3.

[43] Rho RY. Ultrasonic methods for evaluating mechanical properties of bone. In: An YH, Draughn RA, editors. Mechanical testing of bone and bone–implant interface. Boca Raton, FL: CRC Press; 2000.

[44] Cowin SC. Bone Mechanics Handbook. 2nd ed. Boca Raton, FL: CRC Press; 2001.

[45] Ulrich D, Rietbergen B, Laib A, Ruegsegger P. The ability of three-dimensional structural indices to reflect mechanical aspects of trabecular bone. Bone 1999;2:55-60.

[46] Kumaresan S, Yoganandan N, Pintar FA. Finite element analysis of anterior cervical spine interbody fusion. Bio-Med Mater Eng 1997;7:221–30.

[47] Ha SK. Finite element modeling of multi-level cervical spinal segments (C3–C6) and biomechanical analysis of an elastomer-type prosthetic disc. Med Eng Phys 2006;28:534–41.

[48] Brolin K, Halldin P. Development of a finite element model of the upper cervical spine and a parameter study of ligament characteristics. Spine 2004;29:376–85.

[49] Yoganandan N, Kumaresan SC, Voo L, Pintar FA, Larson SJ. Finite element modeling of the C4–C6 cervical spine unit. Med Eng Phys 1996;16:569–74.

[50] Zhang QH, Teo EC, Ng HW, Lee VS. Finite element analysis of moment–rotation relationships for human cervical spine. J Biomech 2006;39:189–93.

[51] Panjabi MM, Crisco JJ, Vasavada A, Oda T, Cholewicki J, Nibu K, Shin E. Mechanical properties of the human cervical spine as shown by three-dimensional load-displacement curves. Spine 1984;26:2692-700.

[52] Wheeldon JA, Pintar FA, Stephanite K, Yoganandan N. Experimental flexion/extension data corridors for validation of finite element models of the young, normal cervical spine. J Biomech 2006;39:375-80.

[53] Kallemeyn N, Gandhi A, Kode S, Shivanna K, Smucker J, Grosland N. Validation of a C2-C7 cervical spine finite element model using specimen-specific flexibility data. Med Eng Phy 2010;32:482-9.

[54] Yoganandan N, Pintar FA, Stemper BD, Wolfla CE, Shender BS, Paskoff G. level-dependent coronal and axial moment-rotation corridors of degeneration-free cervical spine in lateral flexion. J Bone 2007;89:1066-74.

[55] Yoganandan N, Stemper BD, Pintar FA, Baisden JL, Shender BS, Paskoff G. Normative segment-specific axial and coronal angulation corridors of subaxial cervical column in axial rotation. Spine 2008;33:490-6.

[56] DiAngelo DJ, Foley KT, Morrow BR, Schwab JS, Song J, German JW, Blair E. In vitro biomechanics of cervical disc arthroplasty with the ProDisc-C total disc implant. Neur Foc 2014;17:E7.

[57] Faizan A, Goel VK, Biyani A, Garfin SR, Bono CM. Adjacent level effects of bi level disc replacement, bi level fusion and disc replacement plus fusion in cervical spine-a finite element based study. Clin Biomech 2012;27:226-33.

[58] Rina J, Patel A, Dietz JW, Hoskins JS, Trammell TR, Schwartz DG. Comparison of single-level cervical fusion and a metal-on-metal cervical disc replacement device. Am J Orthop 2008;37:71-7.

[59] Muheremu A, Niu X, Wu Z, Muhanmode VY, Tian W. Comparison of the short- and long-term treatment effect of cervical disk replacement and anterior cervical disk fusion: a meta-analysis. Eur J Orthop Surg Traumatol 2015;25:87-100.

[60] Janssen ME, Zigler JE, Spivak JM, Delamarter RB, Darden II BV, Koplar B. ProDisc-C total disc replacement versus anterior cervicak discectomy and fusionfor single-level symptomatic cervical disc disease. J Bone Joint Surg Am 2015;97:1738-47.

[61] Kettlera A, Hartwigb E, Schultheib M, Claesa L, Wilkea H. Mechanically simulated muscle forces strongly stabilize intact and injured upper cervical spine specimens. J Biomech 2002;35:339–46.

[62] Mo ZJ, Zhao YB, Wang LZ, Sun Y, Zhang M, Fan YB. Biomechanical effects of cervical arthroplasty with U-shaped disc implant on segmental range of motion and loading of surrounding soft tissue. Eur Spine J (2014) 23: 613-621.